Cite as: ReLUIS-INGV Workgroup (2016), *Preliminary study of Rieti earthquake ground motion records V5*, available at http://www.reluis.it.

PRELIMINARY STUDY OF RIETI EARTHQUAKE GROUND MOTION DATA V5

INGV: ITACA-ESM Working Group,[1] SHAKEMAP working group.[2]

ReLUIS: Iunio Iervolino (iunio.iervolino@unina.it),[3] Georgios Baltzopoulos,[4] Eugenio Chioccarelli,[4] Akiko Suzuki.[3]

Warning: This report may be subjected to editing and revisions, check www.reluis.it, esm.mi.ingv.it and www.itc.cnr.it for updates.

INDEX

[1] The ITACA-ESM Working Group is: Lucia Luzi (lucia.luzi@ingv.it); Francesca Pacor; Rodolfo Puglia; Maria D'Amico; Emiliano Russo; Chiara Felicetta; Giovanni Lanzano. INGV-Milano, Italy.
[2] The SHAKEMAP Working Group is: Alberto Michelini (alberto.michelini@ingv.it); Licia Faenza; Valentino Lauciani. INGV-CNT, Italy.
[3] Dipartimento di Strutture per l'Ingegneria e l'Architettura, Università degli Studi di Napoli Federico II, Italy.
[4] Istituto per le Tecnologie della Costruzione ITC-CNR, URT Università degli Studi di Napoli Federico II, Italy.

1. What's New

New elements of this version are:

- Comparison between observed and predicted ground motion using the Joyner-Boore distance.
- Analysis of residuals between observed and predicted intensity measures.
- Shakemaps recalculated using the manually revised PGMs (version 15, 20160909)
- Included models for pulse-like ground motion probability of occurrence and predicted pulse durations.

2. Introduction

The Italian Accelerometric Network (RAN), managed by the Department of Civil Protection (DPC), and the Italian seismic network (RSN), managed by the Istituto Nazionale di Geofisica e Vulcanologia (INGV) have made available the records of the recent earthquake with epicenter located in the vicinity of Amatrice, central Italy (date 24/08/2016 1.36:32 AM – UTC; Mw 6.0, ref. Bollettino Sismico INGV).

About 200 accelerometric signals, manually processed using the procedure by Paolucci et al (2011), are used to evaluate the peak ground motion, acceleration and displacement spectral ordinates, integral parameters and measures of duration. **Corrected records and details of correction are available on the Engineering Strong-Motion database website (http://esm.mi.ingv.it). The unprocessed records are available at http://ran.protezionecivile.it/IT/index.php?evid=340867 for the RAN network and at the European Integrated Data Archive (http://www.orfeus-eu.org/data/eida/) for the RSN, that also distributes local networks (University of Genova, University of Trieste, OGS, AMRA, among others).**

In order to analyze peak values and spectral acceleration (Sa or PSA), data have been processed and compared to the Ground Motion Prediction Equation (GMPE) by Bindi et al (2011) for rock and soil. The geometric mean of the horizontal components are used in the analysis. As a function of epicentral distance and for fixed spectral ordinate, the average attenuation law (and its standard deviation) have been compared with the points corresponding to the values recorded at the various stations.

Moreover, *Peak Ground Acceleration* (PGA), *Peak Ground Velocity* (PGV) and *Peak Ground Displacement* (PGD) are calculated for the three components and they are reported in Tables 1. *Arias Intensity* (I_A) and Housner Intensity (or spectral intensity - SI) are the integral parameters computed for each record. Durations is computed for each record as *Significant Duration* estimated between 5% and 95% (D_{5-95}) and between 5% and 75% (D_{5-75}) of the I_A. In Tables 2 are reported integral parameters and duration for the three directions of each record.

3. Geographic Information

An earthquake of Mw 6.0 struck central Italy on 2016-08-24 at 01:36:32 GMT (Bollettino sismico INGV), in the vicinity of Amatrice, causing diffuse building collapse and about 270 casualties. The causative fault is normal, the prevalent style of faulting in the area. The location of the epicentre and the distribution of strong-motion stations are reported in Figure 1. Figure 2 shows the MMI shakemap of the event that includes the records published on 24/08/2016 and in the subsequent days as more data became available. The shakemap has been adjourned accordingly as more data or information (finite fault) have become available and published on the INGV Shakemap web site (Michelini et al., 2008). The shakemaps of Figure 2 provide a description of the recorded strong ground motion according to different measurables of engineering interest.

The Amatrice seismic sequence struck an area where several large earthquakes occurred in the past. According to the recent historical catalog CPTI15 (Rovida et al., 2016 **http://emidius.mi.ingv.it/CPTI15-DBMI15/**, updated to 2015) the strongest earthquake occurred on 1639 (Amatrice, Io 9-10 MCS, Mw 6.2) and destroyed the Amatrice village and its neighbourhood (Figure 3).

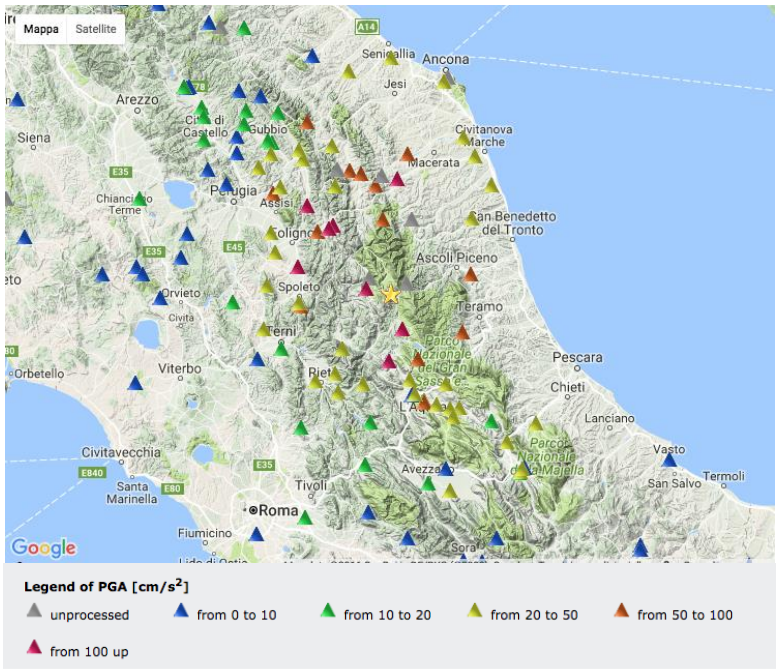

Figure 1: location of the epicentre (yellow star) and strong motion stations within 200 km from the epicentre. The square indicate strong-motion stations and the colors correspond to the PGA values (gal).

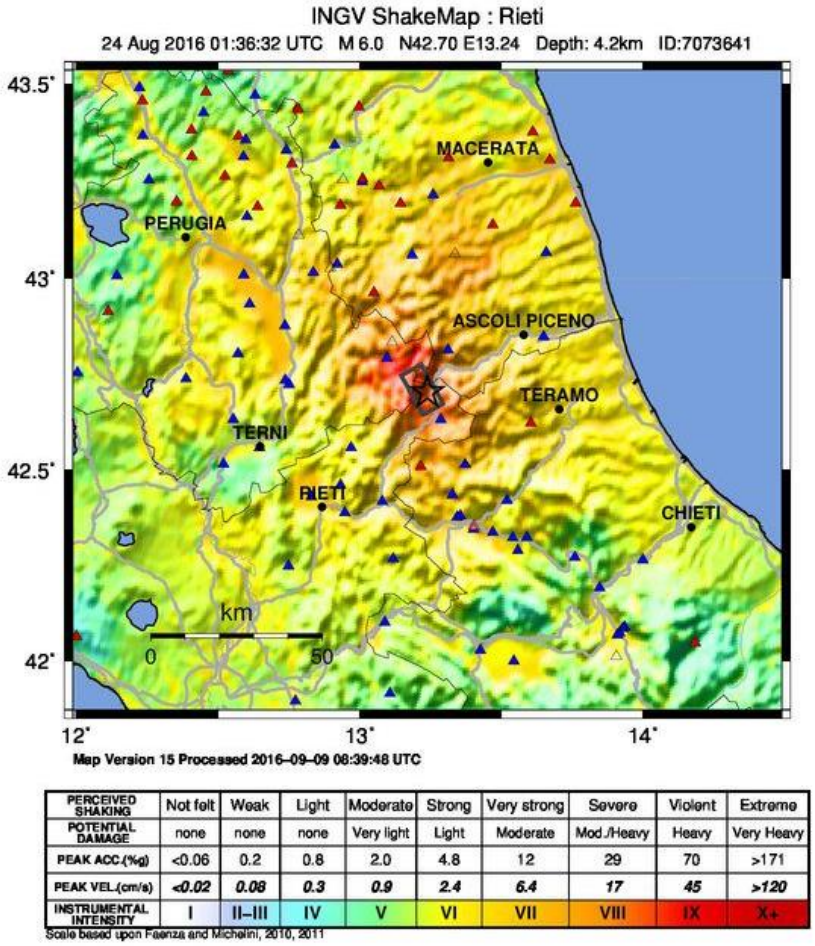
INGV ShakeMap : Rieti
24 Aug 2016 01:36:32 UTC M 6.0 N42.70 E13.24 Depth: 4.2km ID:7073641
MACERATA
PERUGIA
ASCOLI PICENO
TERAMO
TERNI
RIETI
CHIETI
km
0
50
43.5°
43°
42.5°
42°
12°
13°
14°
Map Version 15 Processed 2016-09-09 08:39:48 UTC
PERCEIVED SHAKING | Not felt | Weak | Light | Moderate | Strong | Very strong | Severe | Violent | Extreme
POTENTIAL DAMAGE | none | none | none | Very light | Light | Moderate | Mod./Heavy | Heavy | Very Heavy
PEAK ACC.(%g) | <0.06 | 0.2 | 0.8 | 2.0 | 4.8 | 12 | 29 | 70 | >171
PEAK VEL.(cm/s) | <0.02 | 0.08 | 0.3 | 0.9 | 2.4 | 6.4 | 17 | 45 | >120
INSTRUMENTAL INTENSITY | I | II–III | IV | V | VI | VII | VIII | IX | X+
Scale based upon Faenza and Michelini, 2010, 2011

a.

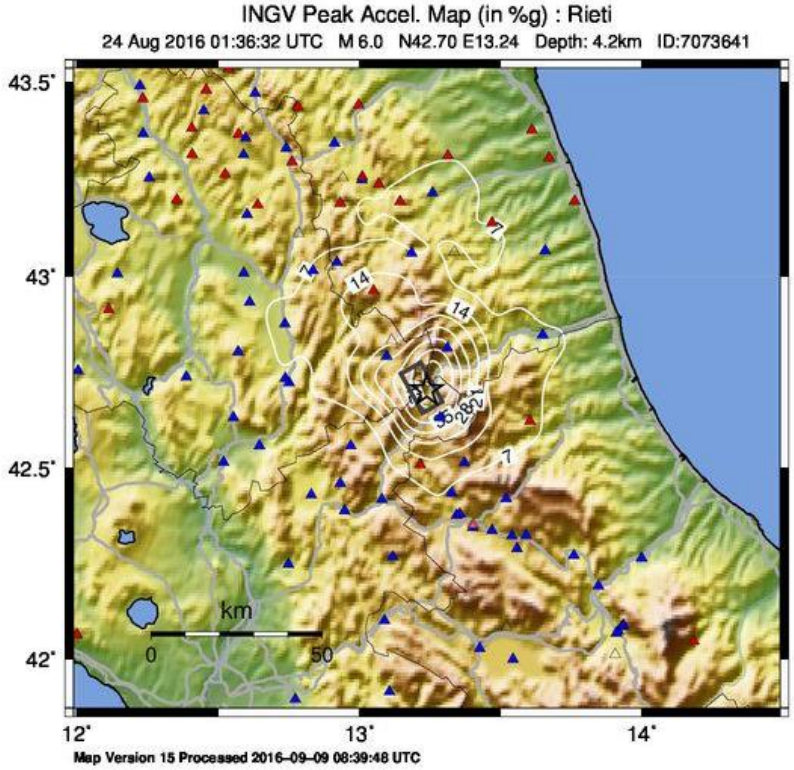
INGV Peak Accel. Map (in %g) : Rieti
24 Aug 2016 01:36:32 UTC M 6.0 N42.70 E13.24 Depth: 4.2km ID:7073641
7
14
14
28
7
km
0
50
43.5°
43°
42.5°
42°
12°
13°
14°
Map Version 15 Processed 2016-09-09 08:39:48 UTC

b.

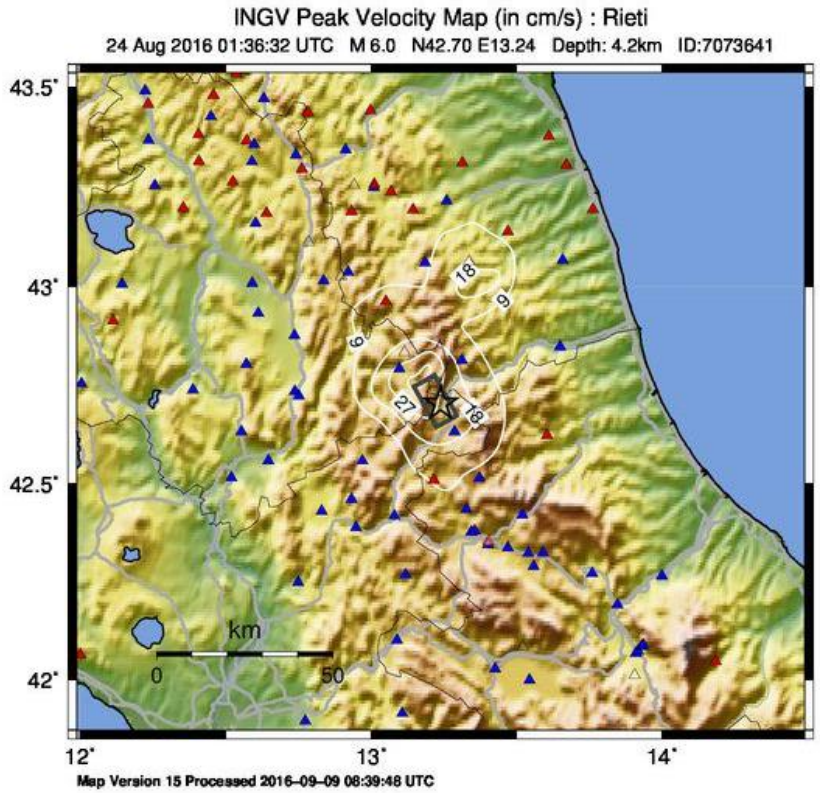
INGV Peak Velocity Map (in cm/s) : Rieti
24 Aug 2016 01:36:32 UTC M 6.0 N42.70 E13.24 Depth: 4.2km ID:7073641
43.5°
43°
42.5°
42°
12°
13°
14°
18
6
6
27
18
km
0
50
Map Version 15 Processed 2016-09-09 08:39:48 UTC

c.

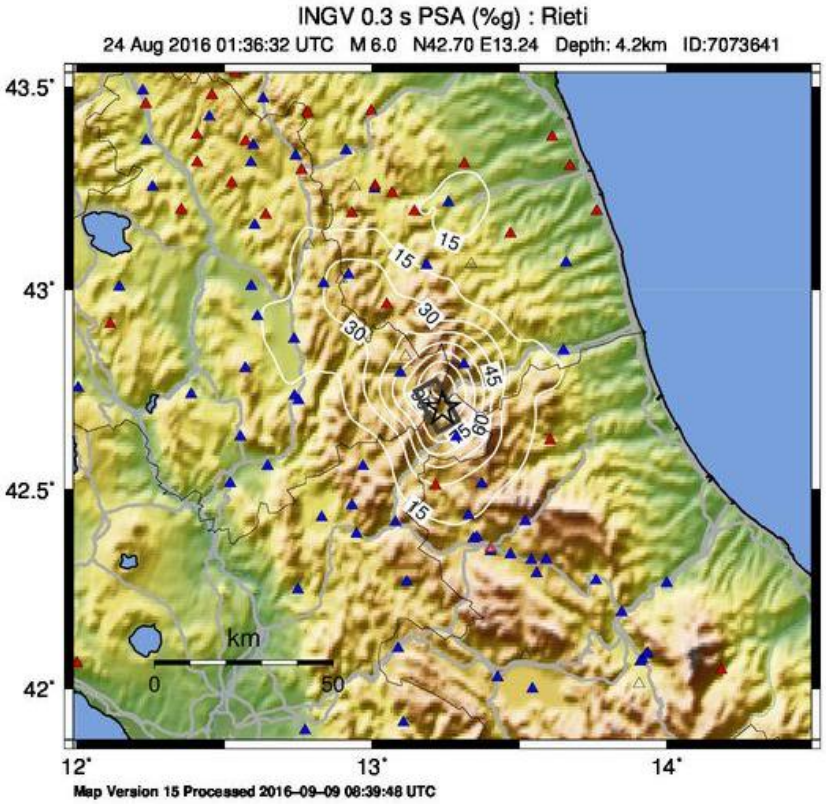
INGV 0.3 s PSA (%g) : Rieti
24 Aug 2016 01:36:32 UTC M 6.0 N42.70 E13.24 Depth: 4.2km ID:7073641
43.5°
43°
42.5°
42°
12°
13°
14°
15
15
30
30
45
60
15
km
0
50
Map Version 15 Processed 2016-09-09 08:39:48 UTC

d.

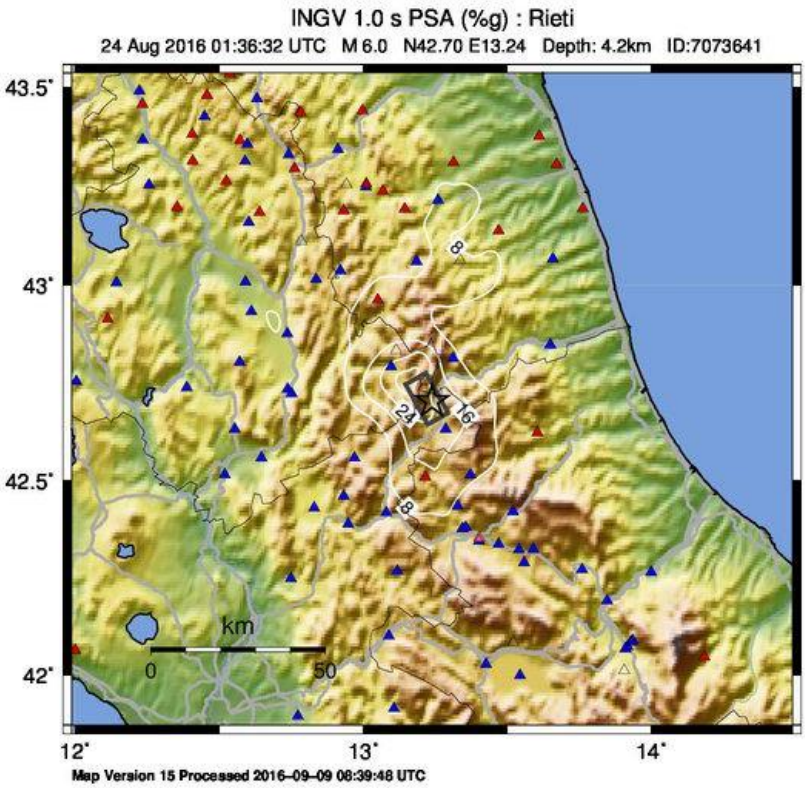

e.

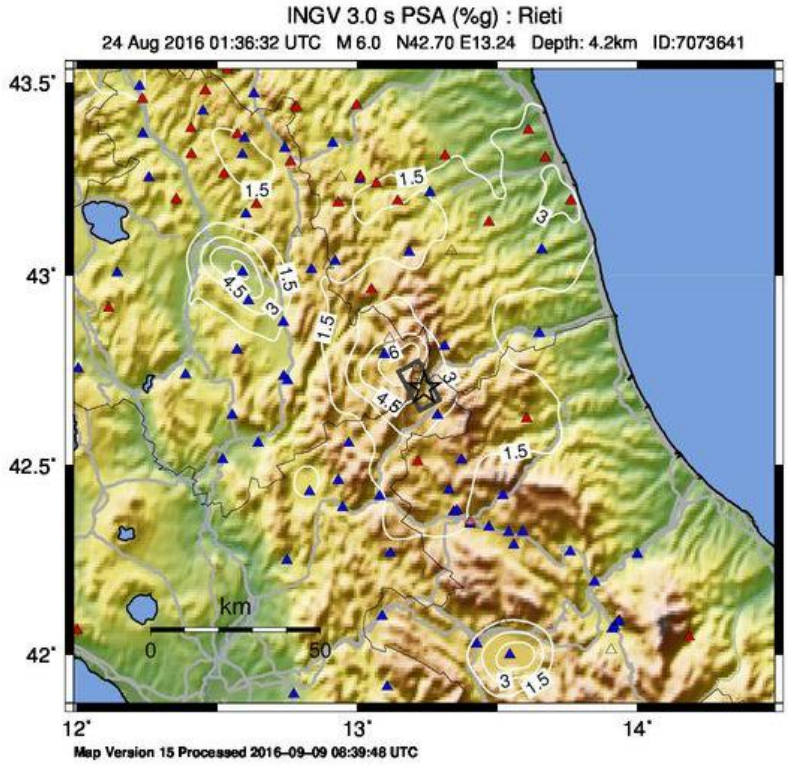

f.

Figure 2: Revised shakemap of the mainshock. a.) MCS intensity; b.) PGA; c.) PGV; d.) PSA 0.3 s period; e.) PSA 1.0 s period; f.) PSA 3.0 s period.
(Downloaded on 9/09/2016 from http://shakemap.rm.ingv.it/shake/7073641/intensity.html)

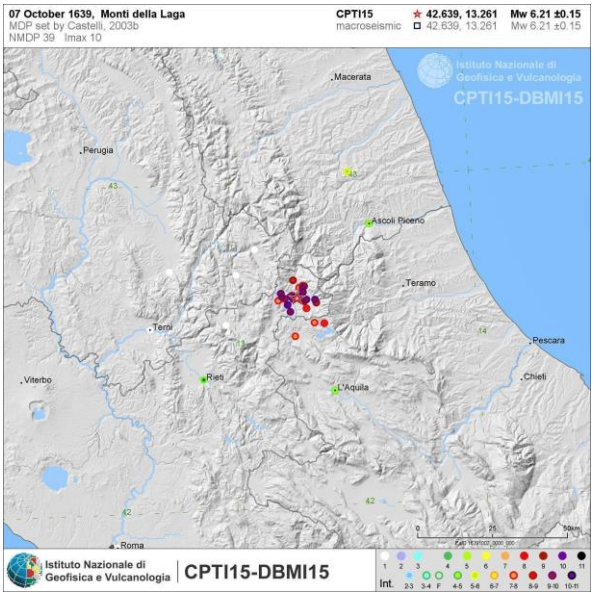

Figure 3: macroseismic field of the 1639 Mw 6.2 Amatrice earthquake (from http://emidius.mi.ingv.it/CPTI15-DBMI15/)

4. Strong Motion Data

The Italian Accelerometric Network (RAN), managed by the Department of Civil Protection (DPC), and the Italian seismic network, managed by the Istituto Nazionale di Geofisica e Vulcanologia (INGV) have made available the records of about 200 accelerometric stations. Appendix 1 lists networks id, station id, geographic coordinates of the station and soil type, where available. These data are also available at the Engineering Strong-motion database (esm.mi.ingv.it).

The largest Peak Ground Acceleration (PGA) have been recorded at short epicentral distances (< 15 km) at the stations Amatrice (AMT, 452.60 gal, uncorrected value, E-W component), Norcia (NRC, 376.96, N-S component) and Arquata del Tronto (RQT, 447.87 gal, E-W component, N-S component not available). The peak parameters of the available records are reported in the following table:

Table 1. Peak parameters recorded during the earthquake. For each recording station, the following is provided: station code, direction of record, distance from the epicentre (R_{epi}), peak ground acceleration (PGA), peak ground velocity (PGV), peak ground displacement (PGD).

Station Code	Component	R_{epi} (km)	PGA (cm/s/s)	PGV (cm/s)	PGD (cm)
AMT	E-W	8.90	424.98	21.52	1.54
AMT	N-S	8.90	183.48	20.48	4.26
AMT	Vertical	8.90	194.04	16.72	4.46
NRC	E-W	13.70	352.65	29.67	5.71
NRC	N-S	13.70	366.32	23.77	6.96
NRC	Vertical	13.70	211.48	11.68	3.26
RM33	E-W	22.30	100.36	9.30	2.39
RM33	N-S	22.30	99.03	6.24	2.01
RM33	Vertical	22.30	35.18	4.99	1.76

SPD	E-W	23.70	51.91	4.98	0.95
SPD	N-S	23.70	99.85	7.63	1.78
SPD	Vertical	23.70	53.69	6.29	1.90
LSS	E-W	27.40	21.78	1.78	0.51
LSS	N-S	27.40	18.15	1.99	0.64
LSS	Vertical	27.40	14.49	1.61	0.66
PZI1	E-W	30.70	44.34	4.34	1.29
PZI1	N-S	30.70	45.15	4.71	1.25
PZI1	Vertical	30.70	25.44	3.13	1.12
TERO	E-W	32.90	55.54	3.16	1.27
TERO	N-S	32.90	83.55	4.31	1.52
TERO	Vertical	32.90	35.03	2.84	0.98
ANT	E-W	34.30	14.09	2.42	1.33
ANT	N-S	34.30	23.08	3.82	1.46
ANT	Vertical	34.30	8.96	2.05	0.88
TRL	E-W	36.30	34.88	3.96	1.02
TRL	N-S	36.30	38.43	3.74	1.24
TRL	Vertical	36.30	17.83	2.05	0.91
AQF	E-W	37.20	43.38	2.62	0.85
AQF	N-S	37.20	37.25	2.40	0.92
AQF	Vertical	37.20	32.66	2.51	0.79
ASP	E-W	37.20	84.91	3.19	0.54
ASP	N-S	37.20	81.77	2.75	0.54
ASP	Vertical	37.20	37.82	1.95	0.57
AQV	E-W	37.30	59.60	3.93	0.83
AQV	N-S	37.30	45.27	4.40	0.90
AQV	Vertical	37.30	22.75	2.69	0.84
AQA	E-W	37.40	2.32	0.18	0.07
AQA	N-S	37.40	2.39	0.19	0.06
AQA	Vertical	37.40	0.84	0.16	0.05
SPM	E-W	38.40	65.95	2.39	0.73
SPM	N-S	38.40	63.55	3.04	1.46
SPM	Vertical	38.40	20.57	1.39	0.61
MNF	E-W	38.90	71.66	4.77	1.31
MNF	N-S	38.90	43.46	2.90	1.43
MNF	Vertical	38.90	59.66	4.65	1.97
GSA	E-W	39.00	35.40	1.90	0.57
GSA	N-S	39.00	36.42	2.56	0.94
GSA	Vertical	39.00	18.16	1.93	0.77
SPO1	E-W	41.20	47.84	3.60	0.88
SPO1	N-S	41.20	44.81	4.43	1.54
SPO1	Vertical	41.20	31.95	2.21	0.57
AQK	E-W	42.10	49.52	9.03	2.66
AQK	N-S	42.10	57.03	9.80	2.76
AQK	Vertical	42.10	33.00	4.17	0.85
CTD	E-W	42.10	31.39	2.07	0.78

CTD	N-S	42.10	23.22	1.99	0.63
CTD	Vertical	42.10	13.88	1.40	0.84
AQU	E-W	42.40	23.08	3.25	1.35
AQU	N-S	42.40	25.34	4.29	1.37
AQU	Vertical	42.40	12.83	2.20	0.65
TRE	E-W	43.70	62.96	6.11	1.10
TRE	N-S	43.70	108.50	7.81	2.09
TRE	Vertical	43.70	44.71	3.40	0.79
CLF	E-W	43.80	122.98	8.70	1.56
CLF	N-S	43.80	128.78	11.64	2.02
CLF	Vertical	43.80	103.06	9.38	2.10
FOC	E-W	44.00	256.20	8.10	0.83
FOC	N-S	44.00	322.54	10.18	1.34
FOC	Vertical	44.00	125.61	5.75	1.56
RTI	E-W	44.70	29.25	4.12	1.03
RTI	N-S	44.70	27.63	4.34	1.52
RTI	Vertical	44.70	12.66	1.49	0.78
BZZ	E-W	46.20	24.73	2.84	0.53
BZZ	N-S	46.20	28.88	3.49	0.82
BZZ	Vertical	46.20	31.79	3.04	0.71
FOS	E-W	47.70	58.70	5.26	1.16
FOS	N-S	47.70	74.99	4.83	1.54
FOS	Vertical	47.70	40.15	2.84	1.11
FMG	E-W	49.40	16.91	1.92	1.12
FMG	N-S	49.40	15.88	1.99	0.90
FMG	Vertical	49.40	10.87	1.49	0.71
TRN1	E-W	50.00	9.17	1.00	0.72
TRN1	N-S	50.00	13.64	1.08	0.64
TRN1	Vertical	50.00	6.62	0.91	0.53

Table 2 reports some integral measures reported for the same records.

Table 2. Integral measures recorded during the earthquake. For each recording station, the following are provided: station code, direction of component, Arias Intensity (I_A), Significant duration estimated between 5% and 95% of the I_A (D_{5-95}), Significant duration estimated between 5% and 75% of the I_A (D_{5-75}), spectral intensity (Housner intensity) between 0.10 and 2.5 s (SI).

Station Code	Component	I_A (cm/s)	D_{5-95} (s)	D_{5-75} (s)	SI (cm)
AMT	E-W	46.22	3.75	0.97	37.06
AMT	N-S	17.78	3.18	0.83	55.95
AMT	Vertical	13.95	4.86	1.71	42.94
NRC	E-W	104.55	6.03	1.74	107.11
NRC	N-S	82.67	6.33	1.60	80.20
NRC	Vertical	37.89	5.56	2.38	34.96
RM33	E-W	8.72	9.47	2.96	35.93
RM33	N-S	6.13	10.07	3.83	23.99

RM33	Vertical	1.80	14.34	8.16	16.88
SPD	E-W	3.95	10.39	4.62	22.06
SPD	N-S	7.16	8.62	2.44	28.43
SPD	Vertical	3.57	10.09	3.77	25.74
LSS	E-W	0.74	16.72	7.05	6.01
LSS	N-S	0.67	18.90	7.16	6.23
LSS	Vertical	0.40	18.87	9.48	5.40
PZI1	E-W	2.38	11.63	5.60	20.60
PZI1	N-S	2.87	14.89	5.25	21.45
PZI1	Vertical	0.73	14.77	7.13	9.69
TERO	E-W	4.78	12.79	5.92	11.48
TERO	N-S	7.65	11.33	4.61	16.84
TERO	Vertical	1.74	14.68	7.48	8.83
ANT	E-W	0.68	25.19	9.81	9.33
ANT	N-S	1.13	20.96	8.30	13.67
ANT	Vertical	0.26	23.91	10.55	6.15
TRL	E-W	2.58	20.84	9.69	12.36
TRL	N-S	3.79	20.28	11.17	11.95
TRL	Vertical	0.55	19.71	10.96	4.33
AQF	E-W	1.96	12.03	4.37	10.15
AQF	N-S	1.71	14.96	4.64	9.26
AQF	Vertical	1.22	13.13	5.58	10.41
ASP	E-W	10.35	11.35	5.24	9.75
ASP	N-S	7.41	12.05	4.65	9.92
ASP	Vertical	2.24	16.27	8.60	7.24
AQV	E-W	3.00	14.23	5.42	13.81
AQV	N-S	2.82	15.89	6.19	13.56
AQV	Vertical	0.70	18.28	8.26	10.64
AQA	E-W	0.00	14.86	6.20	0.72
AQA	N-S	0.01	14.94	4.43	0.87
AQA	Vertical	0.00	17.43	8.01	0.63
SPM	E-W	4.93	14.43	7.03	8.98
SPM	N-S	4.99	12.48	8.34	8.01
SPM	Vertical	0.90	16.21	9.15	4.95
MNF	E-W	3.03	6.86	1.67	18.18
MNF	N-S	1.48	10.91	5.18	8.26
MNF	Vertical	2.17	6.59	2.28	15.03
GSA	E-W	1.37	17.12	9.02	10.43
GSA	N-S	1.75	15.33	7.07	8.49
GSA	Vertical	0.68	17.00	9.15	6.92
SPO1	E-W	3.93	22.53	8.59	12.62
SPO1	N-S	4.75	20.63	7.09	14.89
SPO1	Vertical	2.06	22.55	12.35	7.12
AQK	E-W	6.12	21.33	10.27	47.55
AQK	N-S	10.76	14.71	7.68	59.95
AQK	Vertical	2.77	22.26	11.87	18.58

CTD	E-W	1.65	17.56	9.50	7.99
CTD	N-S	1.00	22.18	10.82	5.73
CTD	Vertical	0.31	18.95	11.10	4.93
AQU	E-W	1.15	28.51	9.58	18.23
AQU	N-S	1.27	24.79	8.77	16.72
AQU	Vertical	0.51	17.98	10.09	9.59
TRE	E-W	5.10	14.62	6.19	15.19
TRE	N-S	10.62	14.52	3.36	26.17
TRE	Vertical	2.13	15.16	8.15	10.08
CLF	E-W	18.13	9.03	2.96	35.24
CLF	N-S	14.11	10.80	2.65	36.16
CLF	Vertical	13.98	5.31	2.89	24.35
FOC	E-W	36.24	5.60	1.83	17.56
FOC	N-S	38.48	4.22	1.85	19.62
FOC	Vertical	10.41	8.57	5.78	15.55
RTI	E-W	4.23	43.19	26.03	19.60
RTI	N-S	3.75	49.41	24.11	20.11
RTI	Vertical	0.59	33.12	15.34	4.99
BZZ	E-W	1.02	15.98	7.08	10.31
BZZ	N-S	1.22	14.32	5.78	14.24
BZZ	Vertical	0.94	15.84	6.99	12.84
FOS	E-W	4.64	9.02	2.80	16.58
FOS	N-S	5.94	8.81	3.11	13.80
FOS	Vertical	1.52	13.19	7.58	10.17
FMG	E-W	0.41	19.65	8.36	6.92
FMG	N-S	0.49	20.66	8.42	9.41
FMG	Vertical	0.22	19.20	9.41	4.26
TRN1	E-W	0.21	31.49	11.52	2.69
TRN1	N-S	0.19	29.03	11.68	4.02
TRN1	Vertical	0.11	33.49	13.72	2.48

Figures 4 to 8 are the maps showing the spatial distribution of the peak ground values

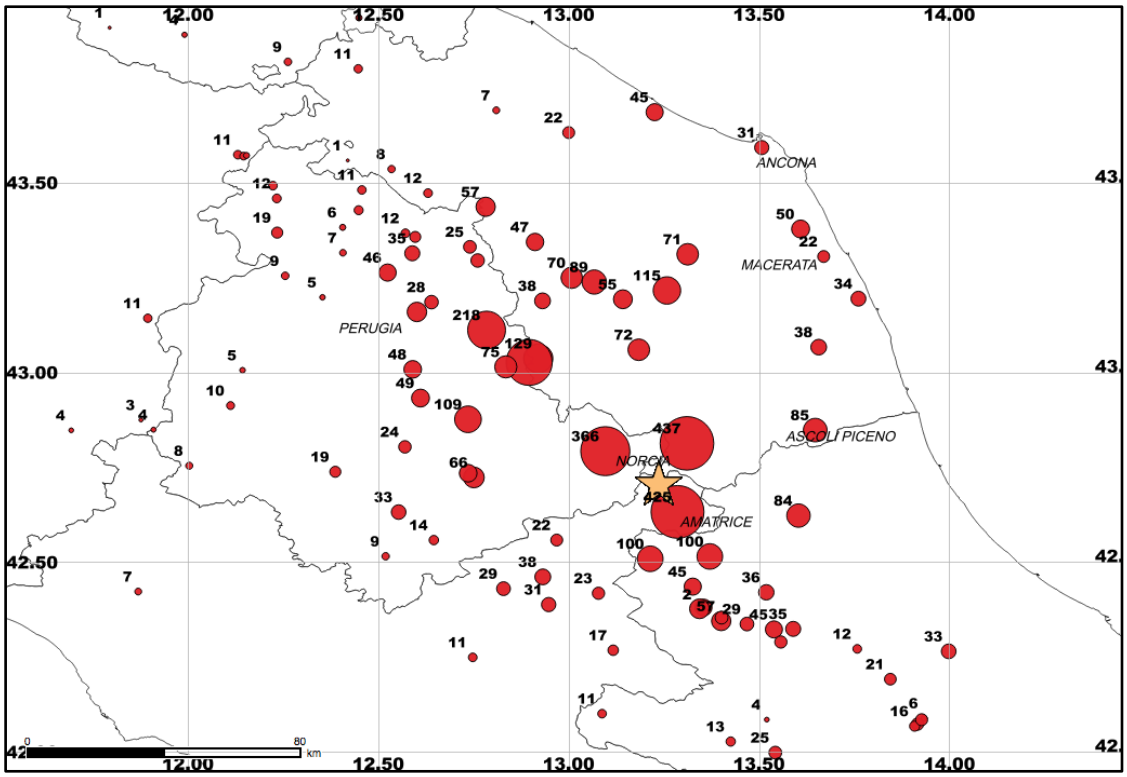

Figure 4. Map of the Peak Ground Acceleration (maximum between horizontal components, in cm/s^2). The star indicates the epicenter of the mainshock

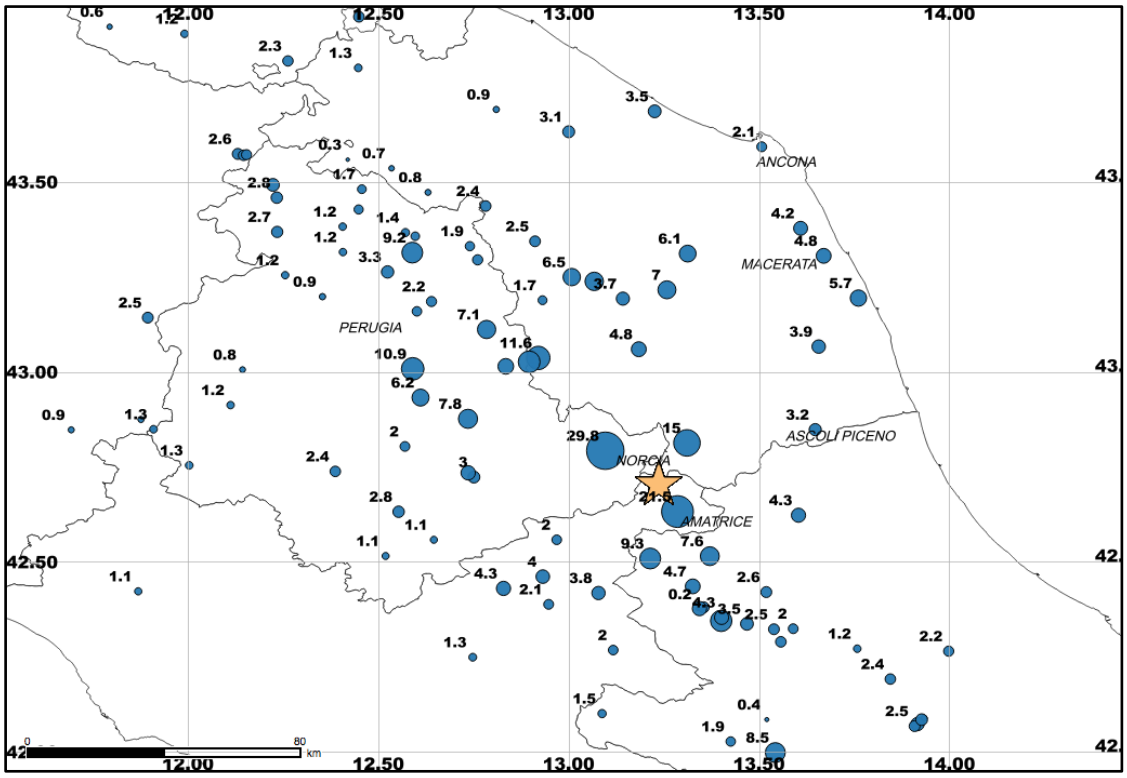

Figure 5. Map of the Peak Ground Velocity (maximum between horizontal components, cm/s). The star indicates the epicenter of the mainshock

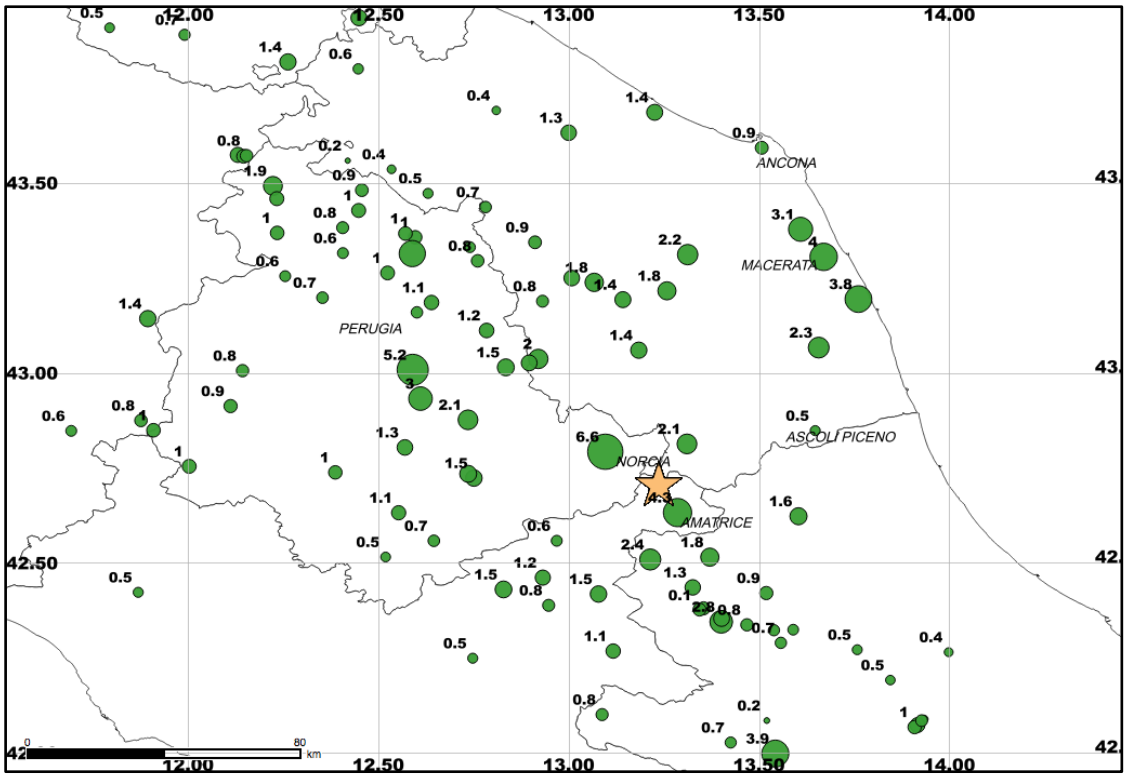

Figure 6. Map of the Peak Ground Displacement (maximum between horizontal components, cm). The star indicates the epicenter of the mainshock

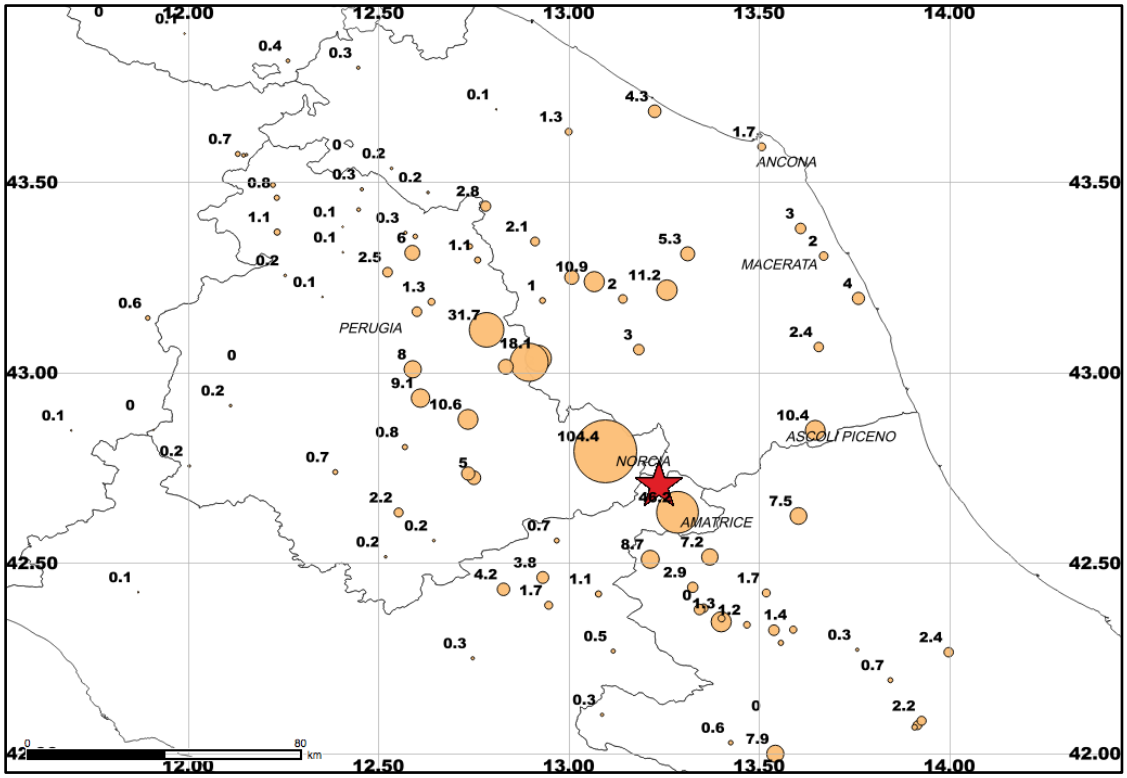

Figure 7. Map of the Arias Intensity (maximum between horizontal components, cm/s). The star indicates the epicenter of the mainshock

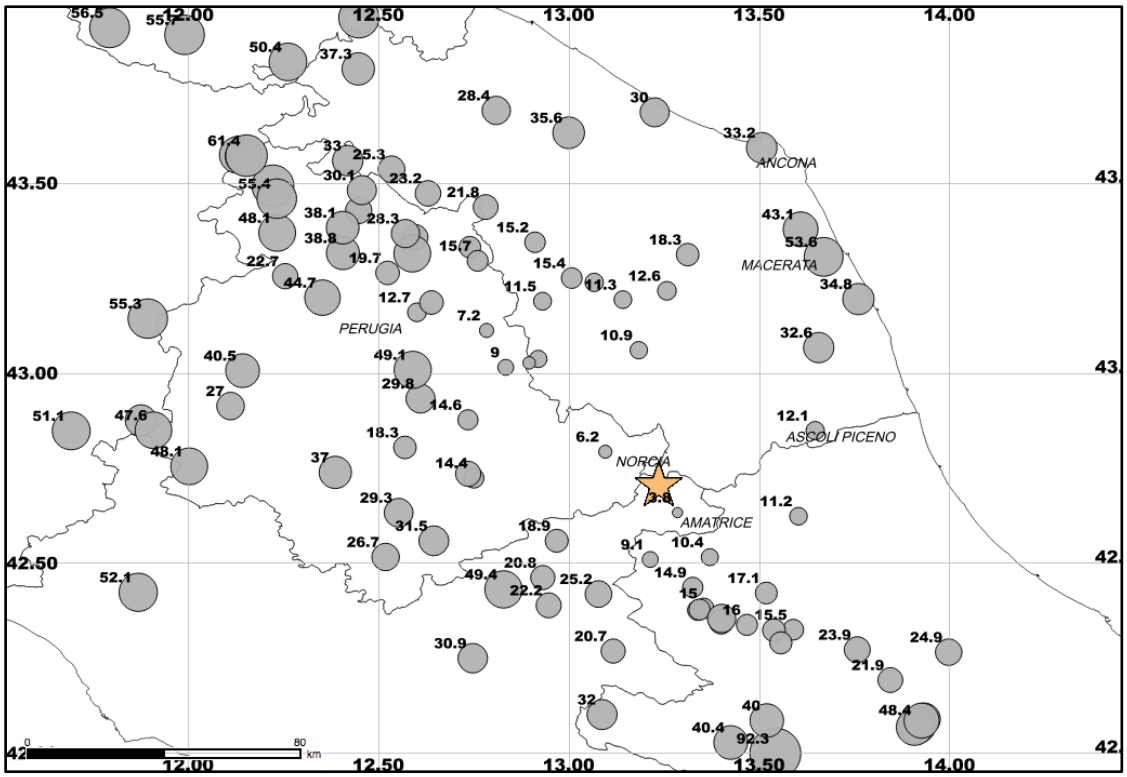

Figure 8. Map of the significant duration (maximum between horizontal components, s). The star indicates the epicenter of the mainshock

5. Data comparison with GMPE

Some GM parameters (PGA, PGV and acceleration spectral ordinates at 0.3, 1 and 3 seconds, period used to calculate shakemaps) are compared to the predictions by Bindi et al (2011). These results can be considered as preliminary since:

- the distance is the Joyner-Boore distance, which has been estimated using the preliminary fault plane geometry by Tinti et al. (2016), with the following characteristics: strike 156°; dip 50°; rake -85°; lenght 28km; width 10.3km;
- the comparison at 3s is outside the range of validity of this GMPE, as authors recommend to use it until 2s.

We calculated the prediction for: PGA, PGV, SA at 0.3s, 1s and 3s (the intensity measures used to calculate shakemaps) for the geometric mean of the horizontal components and the vertical component at two different moment magnitudes, 6.0 and a 6.2. For the vertical component, the SA at 3s was not implemented by Bindi et al (2011), therefore we evaluated the goodness of fit with the prediction at 2s.

Figures 9-18 show the results for Mw 6.0, while Figure 19-28 show the results for Mw 6.2.

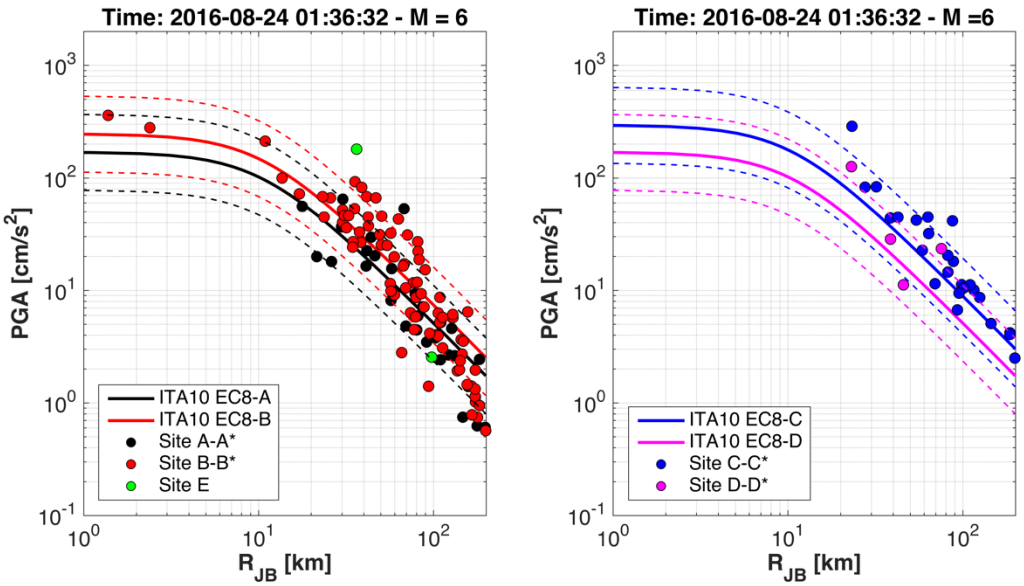

Figure 9: Observed horizontal PGA against Bindi et al (2011): left EC8 A and B sites; right EC8 C and D sites

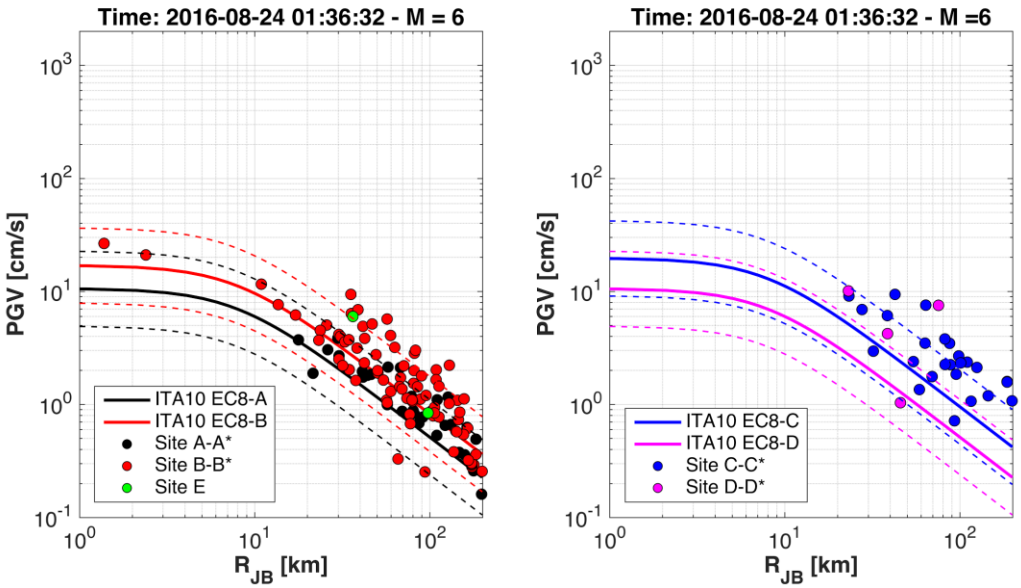

Figure 10: Observed horizontal PGV against Bindi et al (2011): left EC8 A and B sites; right EC8 C and D sites

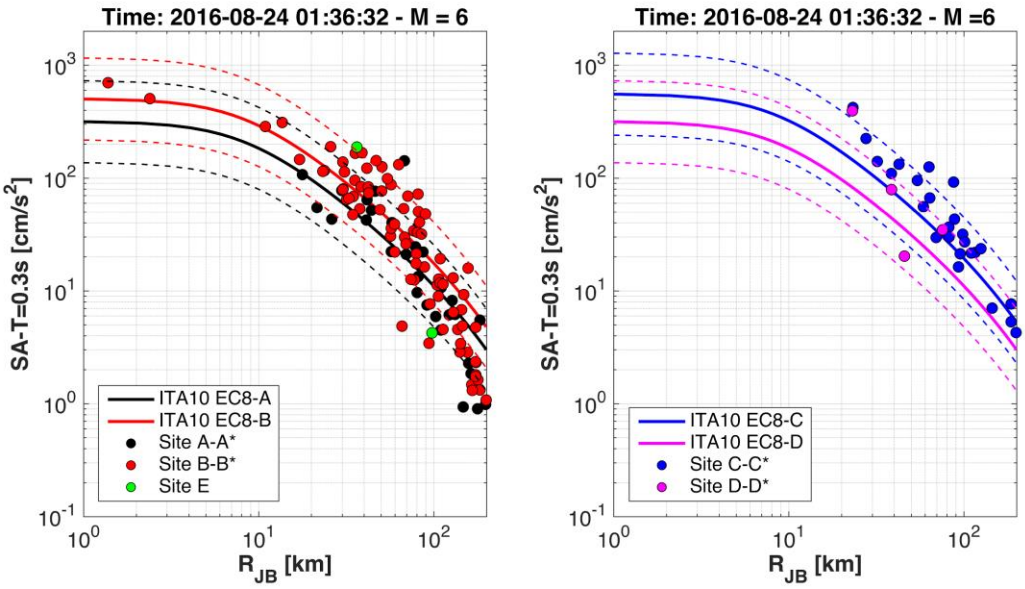

Figure 11: Observed horizontal SA (0.3s) against Bindi et al (2011): left EC8 A and B sites; right EC8 C and D sites

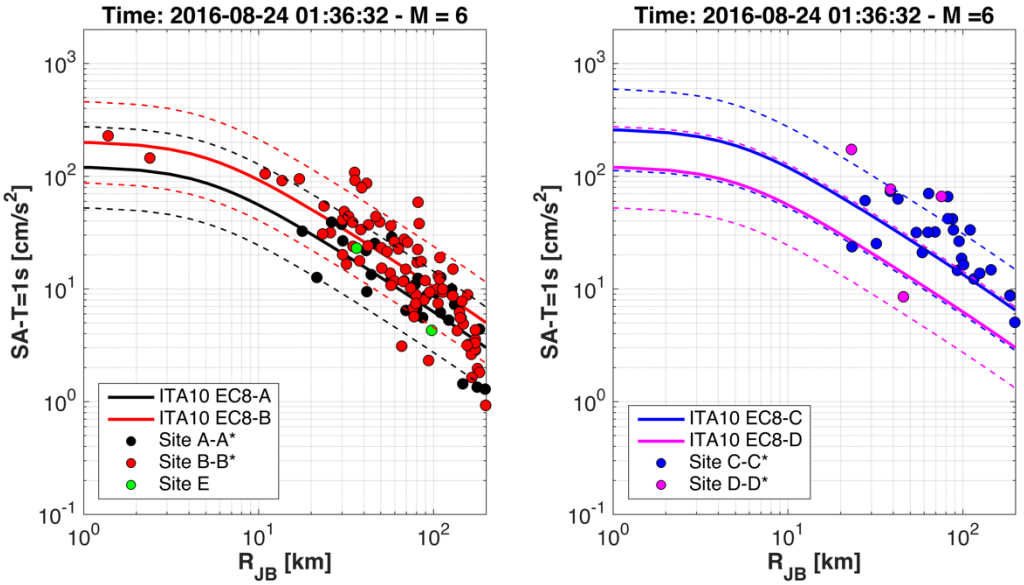

Figure 12: Observed horizontal SA (1s) against Bindi et al (2011): left EC8 A and B sites; right EC8 C and D sites

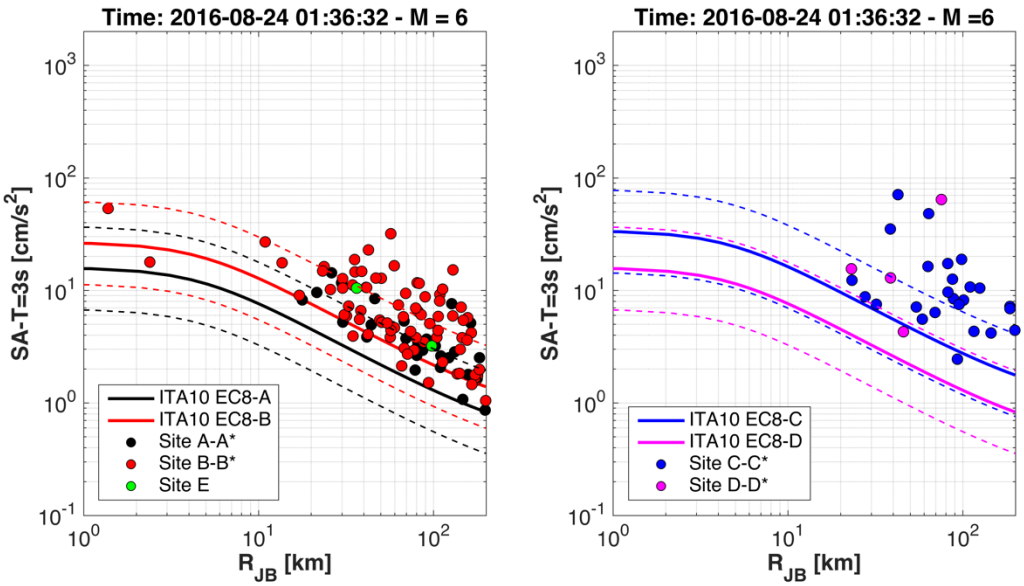

Figure 13: Observed horizontal SA (3s) against Bindi et al (2011): left EC8 A and B sites; right EC8 C and D sites

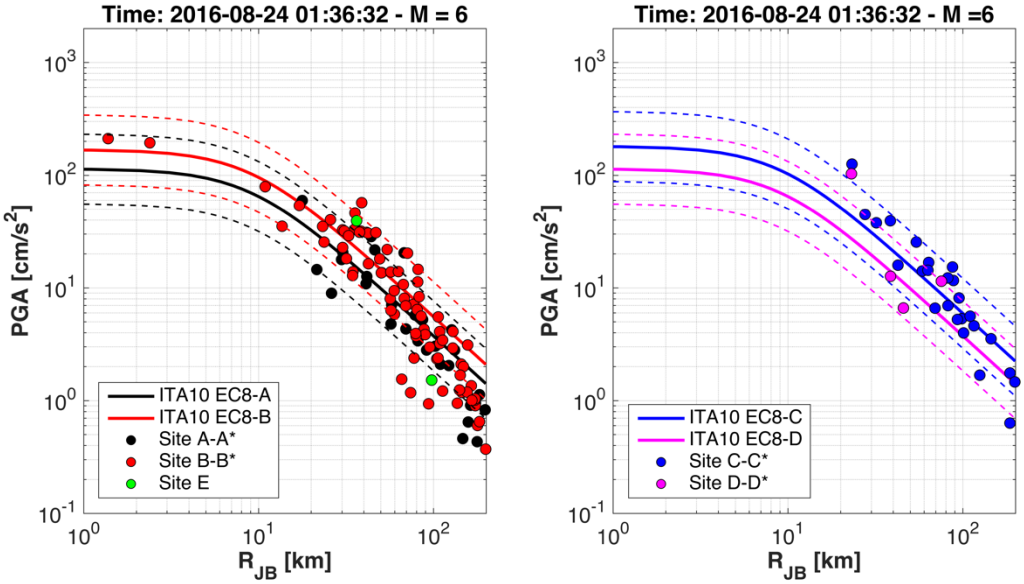

Figure 14: Observed vertical PGA against Bindi et al (2011): left EC8 A and B sites; right EC8 C and D sites

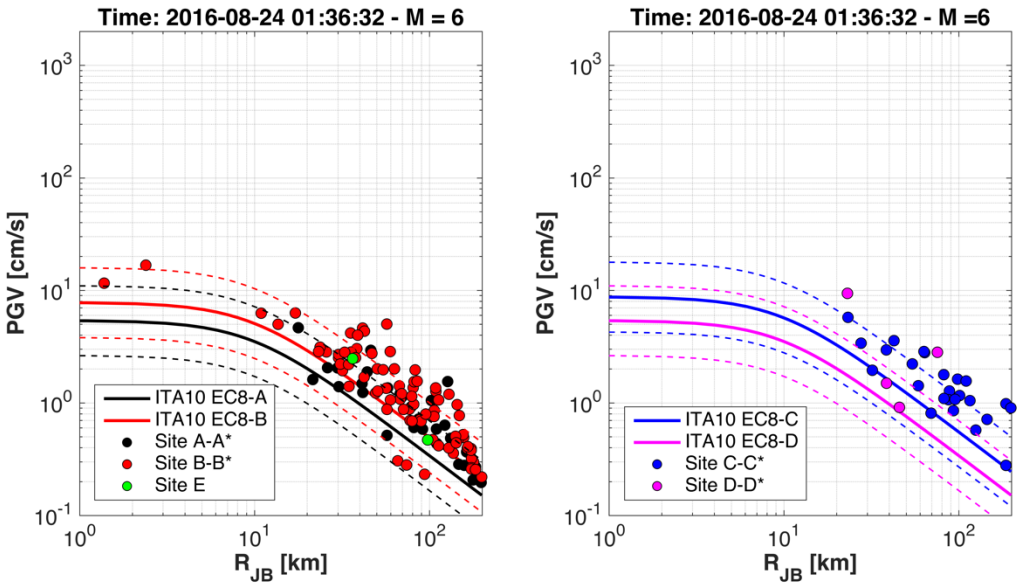

Figure 15: Observed vertical PGV against Bindi et al (2011): left EC8 A and B sites; right EC8 C and D sites

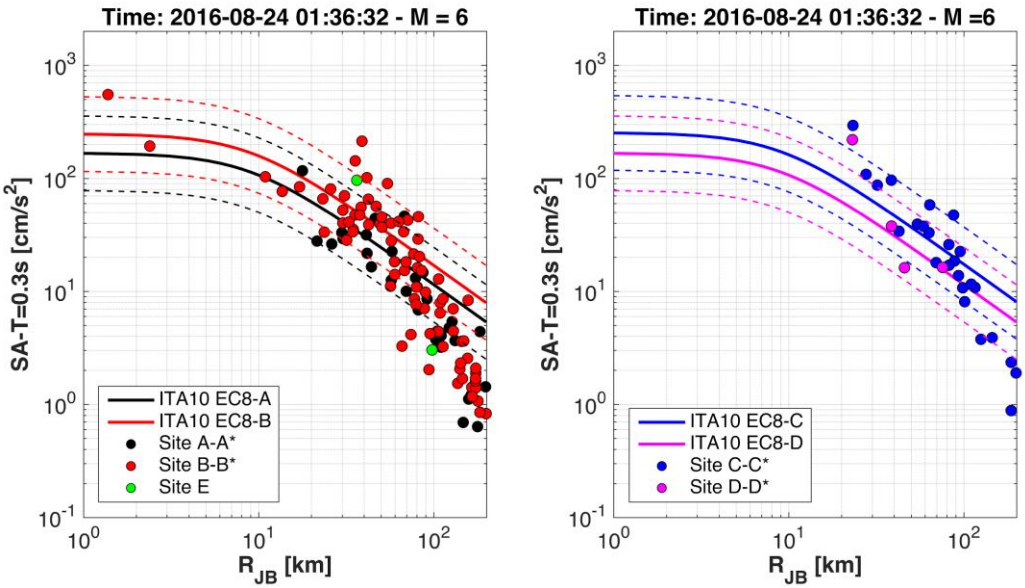

Figure 16: Observed vertical spectral acceleration at 0.3s against Bindi et al (2011): left EC8 A and B sites; right EC8 C and D sites

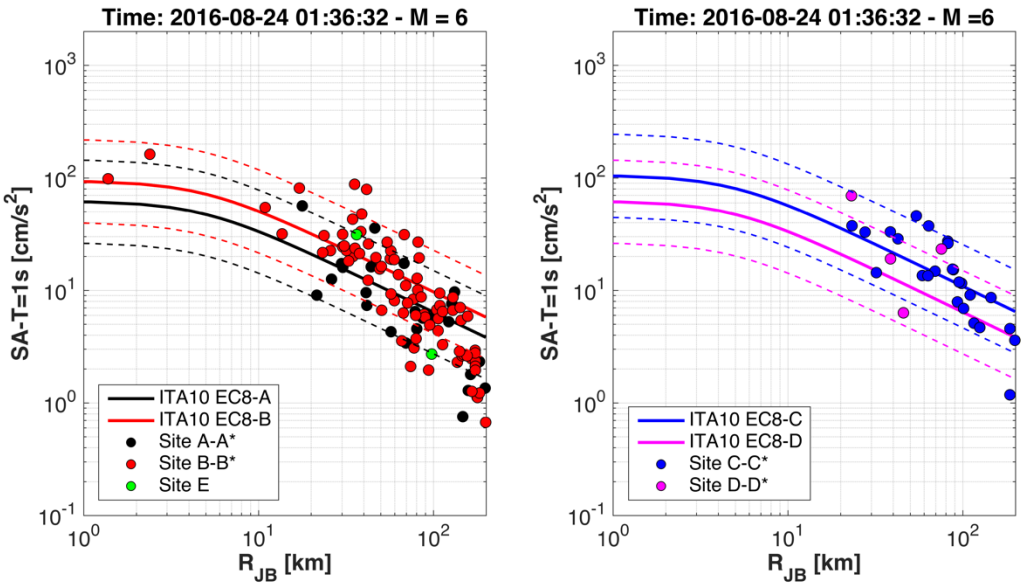

Figure 17: Observed vertical spectral acceleration at 1s against Bindi et al (2011): left EC8 A and B sites; right EC8 C and D sites

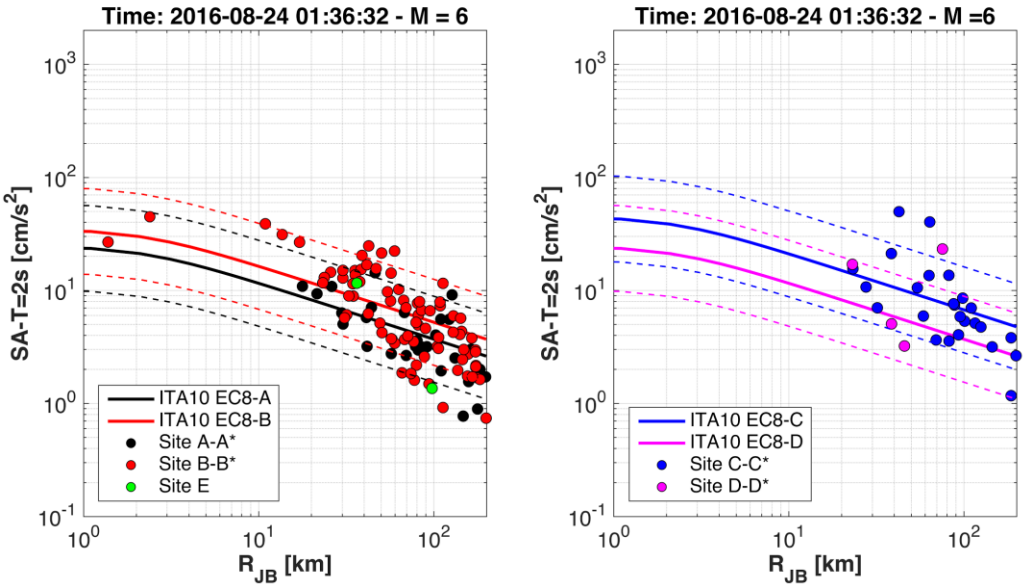

Figure 18: Observed vertical spectral acceleration at 2s against Bindi et al (2011): left EC8 A and B sites; right EC8 C and D sites

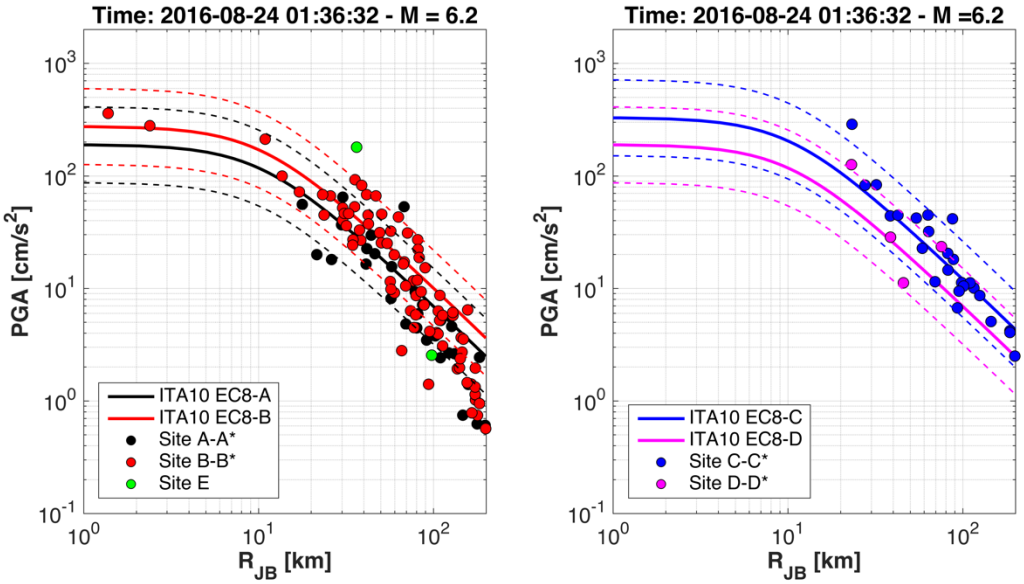

Figure 19: Observed horizontal PGA against Bindi et al (2011): left EC8 A and B sites; right EC8 C and D sites

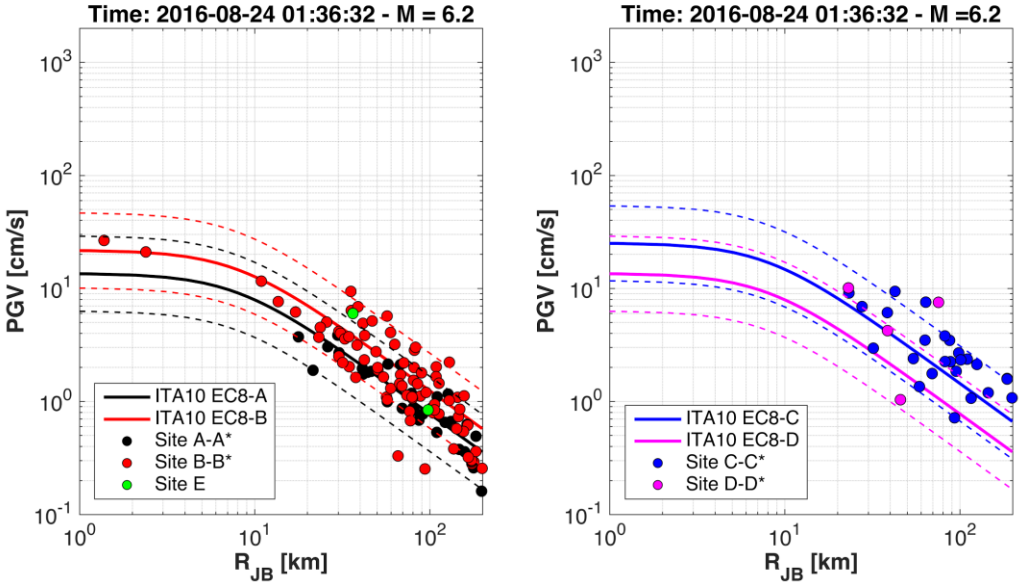

Figure 20: Observed horizontal PGV against Bindi et al (2011): left EC8 A and B sites; right EC8 C and D sites

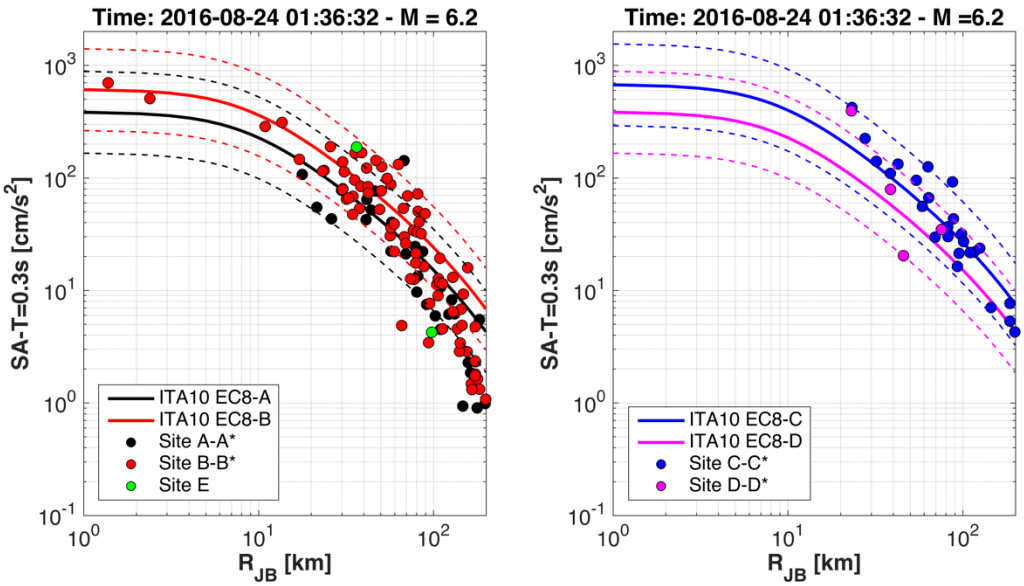

Figure 21: Observed horizontal spectral acceleration (0.3s) against Bindi et al (2011): left EC8 A and B sites; right EC8 C and D sites

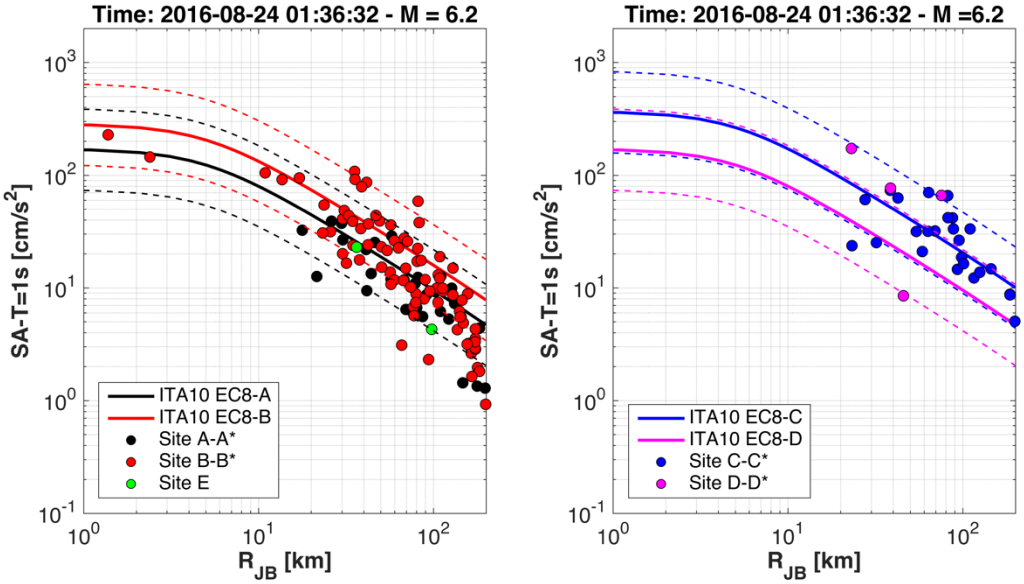

Figure 22: Observed horizontal spectral acceleration (1s) against Bindi et al (2011): left EC8 A and B sites; right EC8 C and D sites

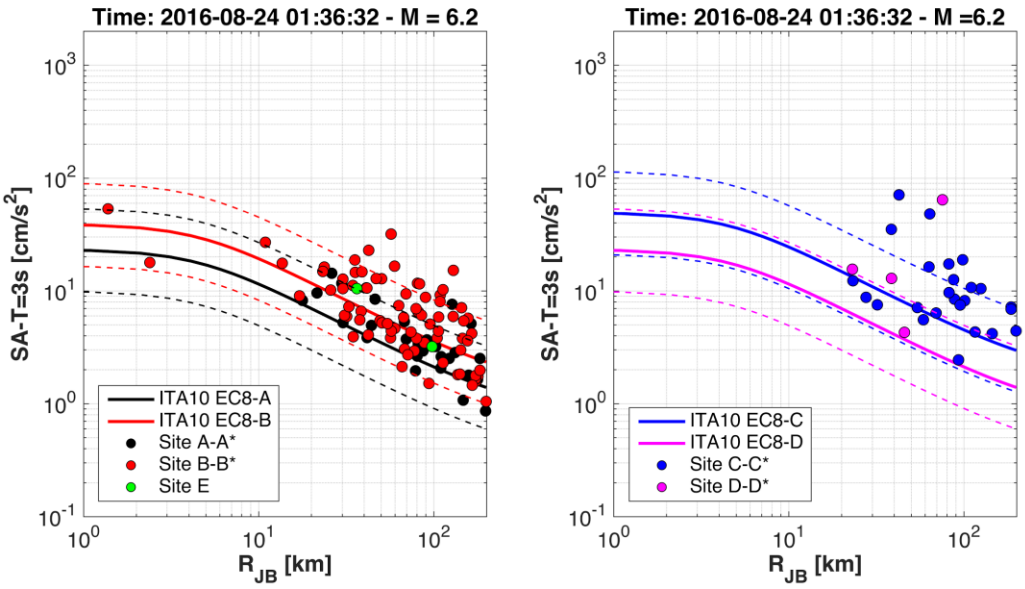

Figure 23: Observed horizontal spectral acceleration (3s) against Bindi et al (2011): left EC8 A and B sites; right EC8 C and D sites

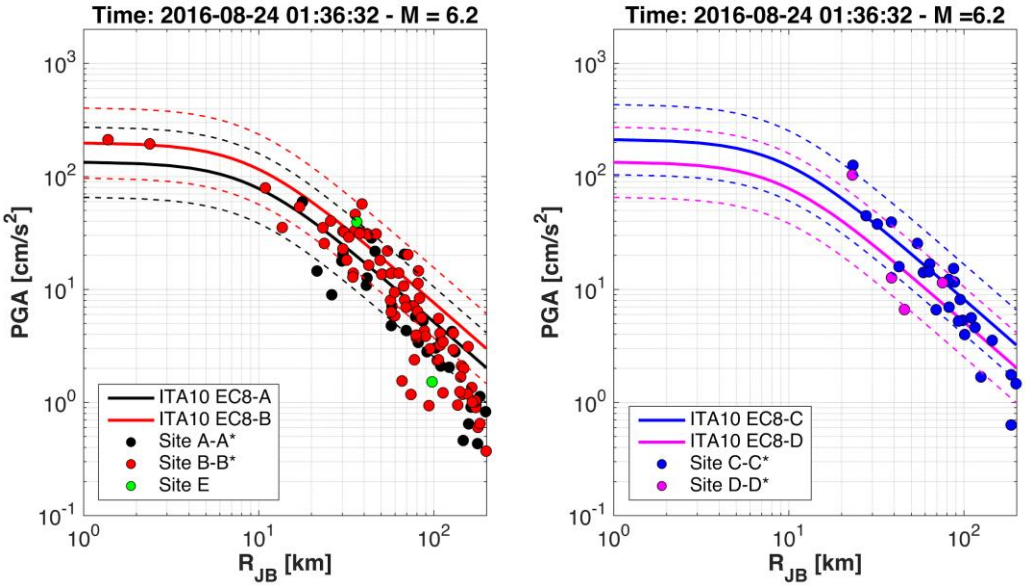

Figure 24: Observed vertical PGA against Bindi et al (2011): left EC8 A and B sites; right EC8 C and D sites

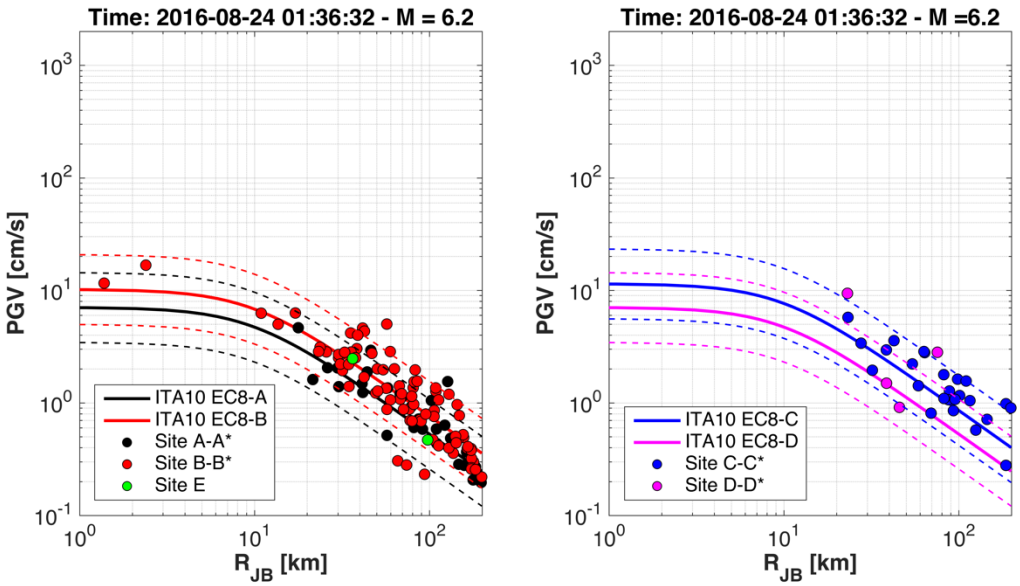

Figure 25: Observed vertical PGV against Bindi et al (2011): left EC8 A and B sites; right EC8 C and D sites

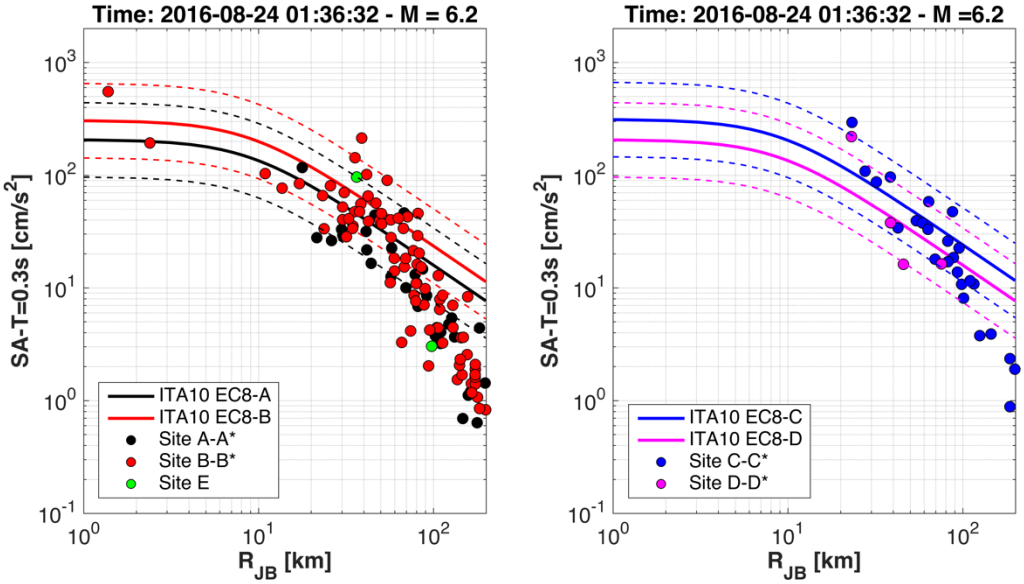

Figure 26: Observed vertical spectral acceleration (0.3s) against Bindi et al (2011): left EC8 A and B sites; right EC8 C and D sites

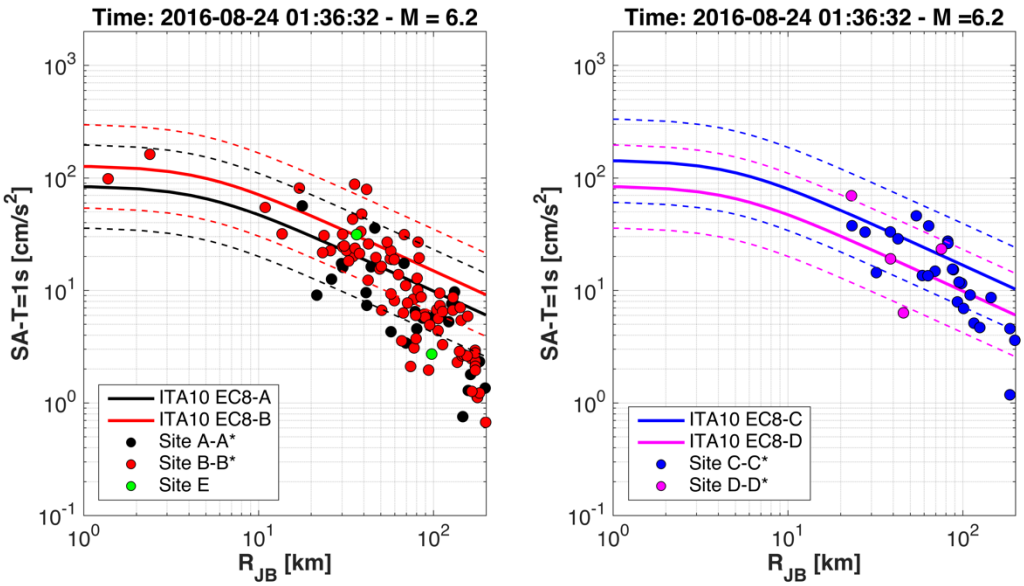

Figure 27: Observed vertical spectral acceleration (1s) against Bindi et al (2011): left EC8 A and B sites; right EC8 C and D sites

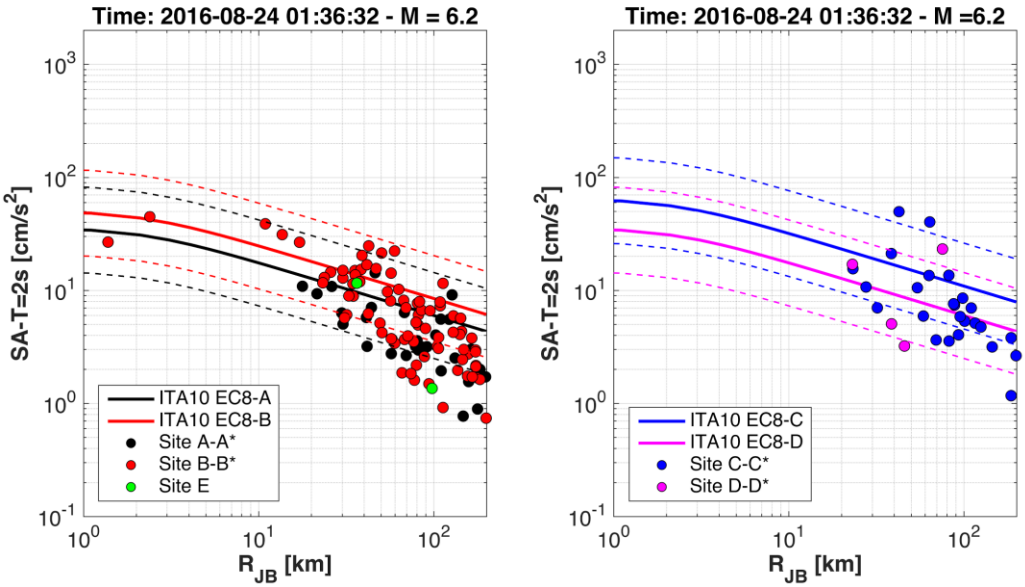

Figure 28: Observed vertical spectral acceleration (2s) against Bindi et al (2011): left EC8 A and B sites; right EC8 C and D sites

In order to estimate the overall performance of the GMPEs against the recording data, the residuals (calculated as the natural logarithm of the difference between observations and predictions) has been plotted against distance and azimuth in Figures 29-38, for the geometric mean of the horizontal components and for the vertical component and a magnitude 6.0 scenario. The azimuth is computed clockwise from the north.

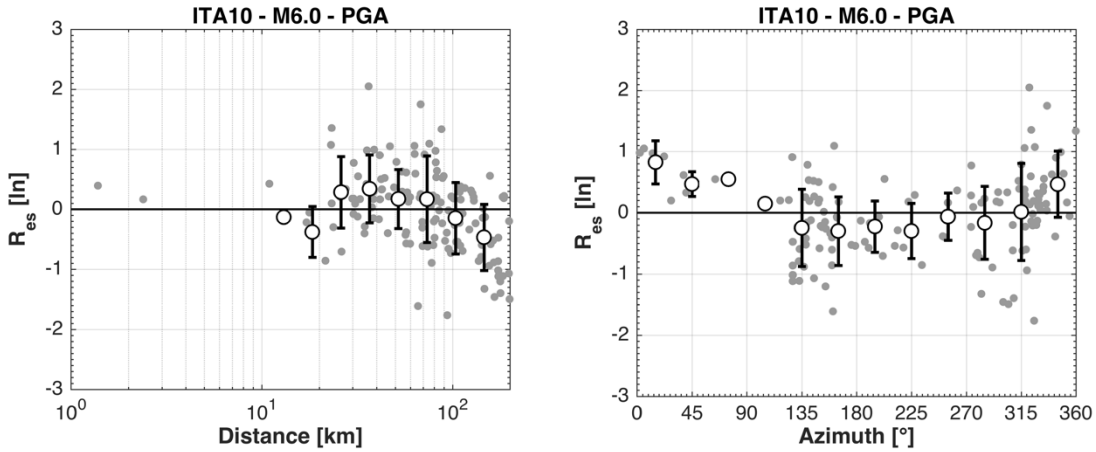

Figure 29. Residuals of the geometric mean of PGA horizontal components, plotted against Joyner-Boore distance (left) and azimuth (right).

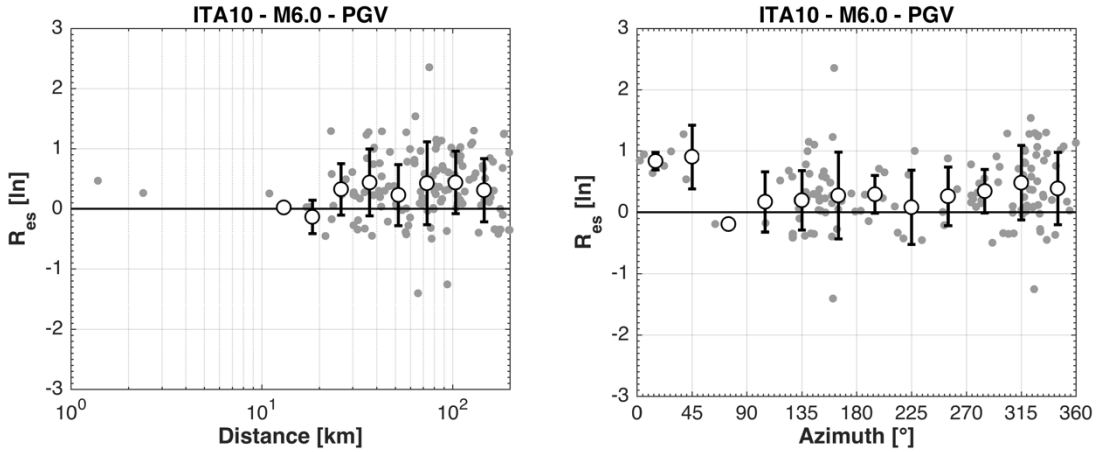

Figure 30. Residuals of the geometric mean of PGV horizontal components, plotted against Joyner-Boore distance (left) and azimuth (right).

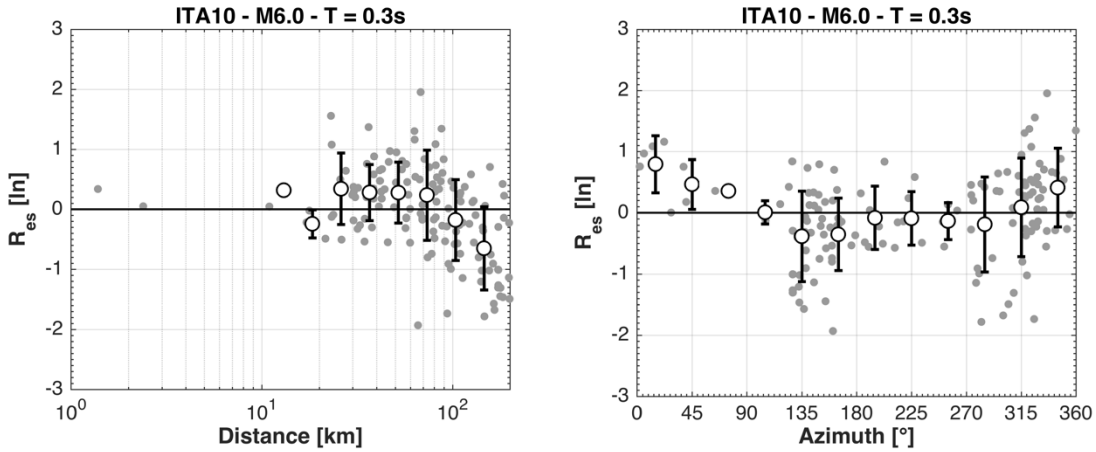

Figure 31. Residuals of the geometric mean of SA (0.3s) horizontal components, plotted against Joyner-Boore distance (left) and azimuth (right).

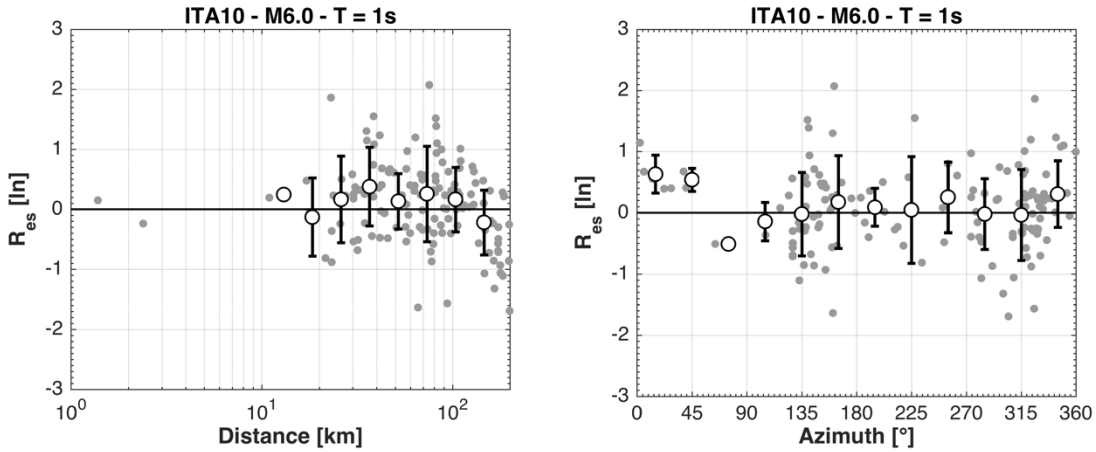

Figure 32. Residuals of the geometric mean of SA (1s) horizontal components, plotted against Joyner-Boore distance (left) and azimuth (right).

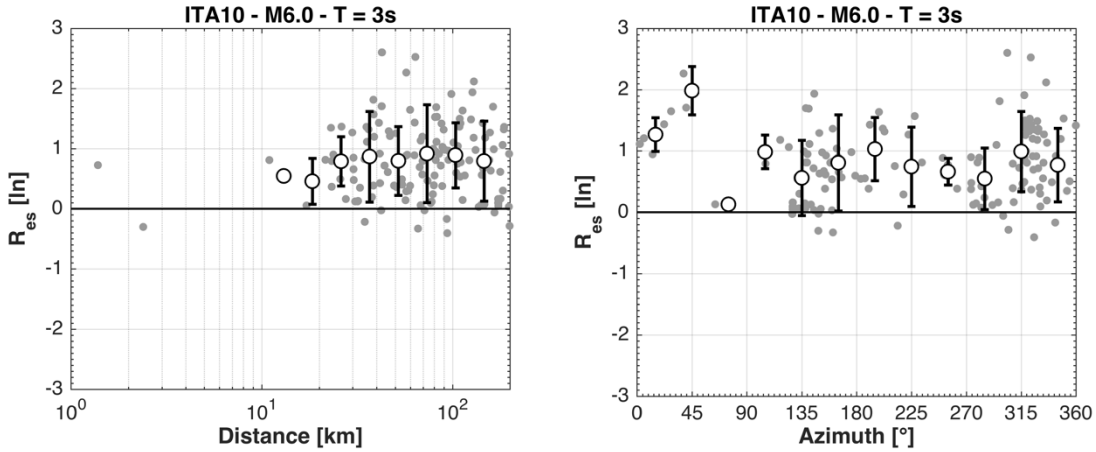

Figure 33. Residuals of the geometric mean of SA (3s) horizontal components, plotted against Joyner-Boore distance (left) and azimuth (right).

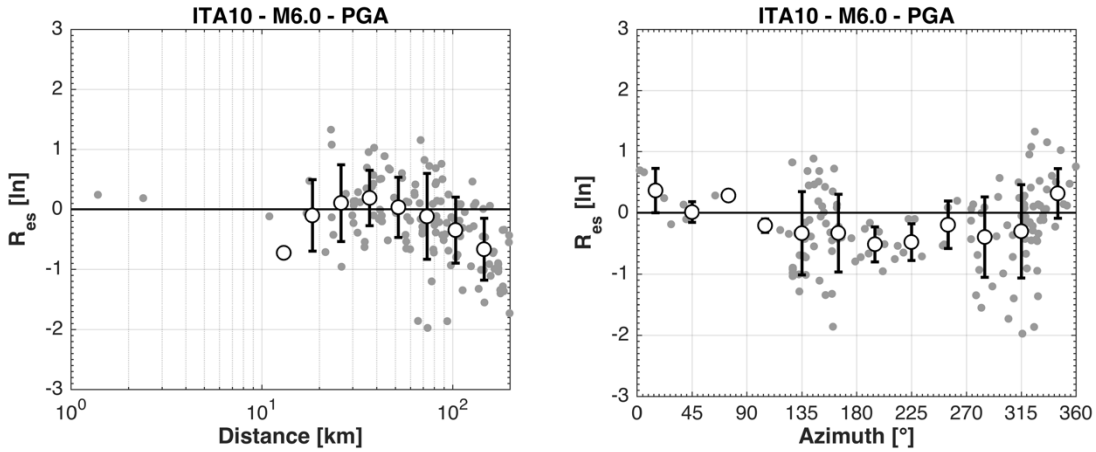

Figure 34. Residuals of PGA vertical components plotted against Joyner-Boore distance (left) and azimuth (right).

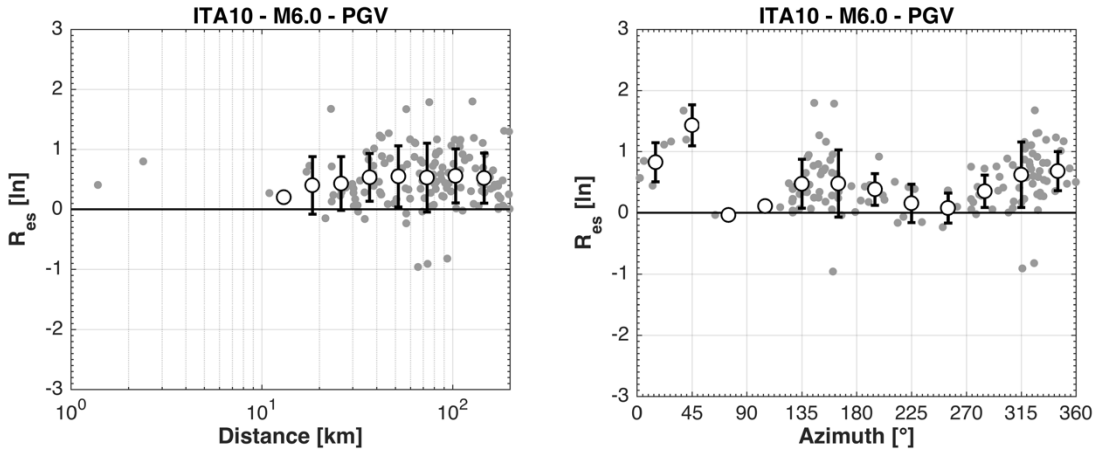

Figure 35. Residuals of PGV vertical components plotted against Joyner-Boore distance (left) and azimuth (right).

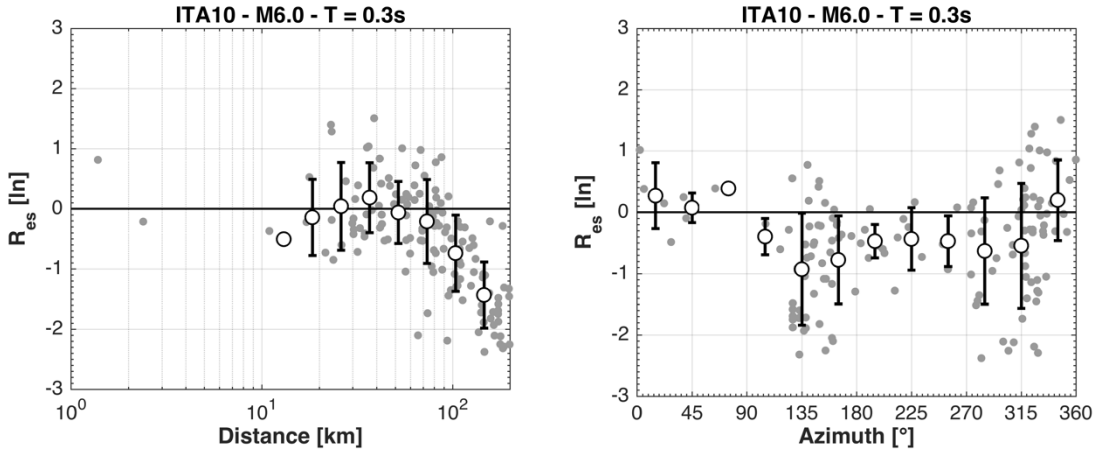

Figure 36. Residuals of SA (0.3s) vertical components plotted against Joyner-Boore distance (left) and azimuth (right).

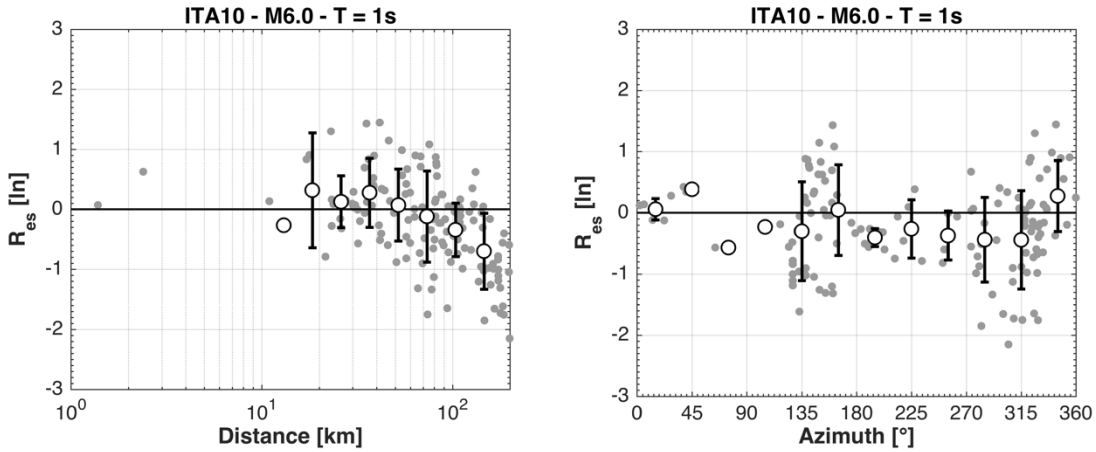

Figure 37. Residuals of SA (1s) vertical components plotted against Joyner-Boore distance (left) and azimuth (right).

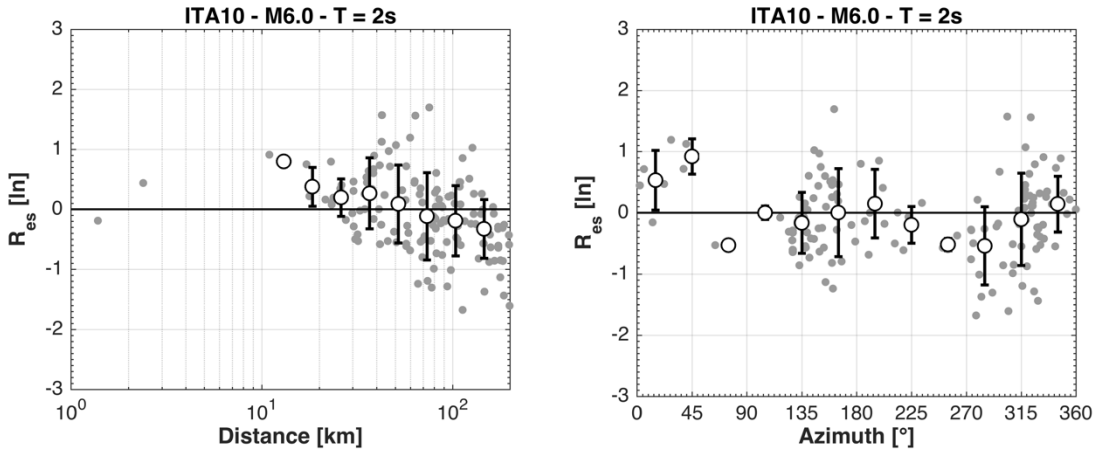

Figure 38. Residuals of SA (2s) vertical components plotted against Joyner-Boore distance (left) and azimuth (right).

6. Elastic and Inelastic Response Spectra

In this section, elastic and inelastic response spectra of the recorded ground motions are provided. With regard to elastic response the pseudo-spectral acceleration (PSA), pseudo-spectral velocity (PSV) and spectral displacement (SD) are reported for all the available records for three different values of damping ratio, (z), that is 2%, 5% and 10%. Additionally, constant-strength inelastic displacement ratios C_R are provided for the horizontal components of ground motion. C_R is defined as the ratio of maximum inelastic displacement response to maximum elastic displacement of the corresponding linear infinitely elastic system, Eq. (1) .

$$C_R = \frac{\delta_{inelastic}^{\max}}{SD(T)} \tag{1}$$

These spectra were calculated for 5% damped, elastic-perfectly plastic oscillators and are reported at three values of reduction factor R=2,4,6, where R is defined as the ratio of elastic response spectral acceleration to yield spectral acceleration, Eq. (2).

$$R = \frac{PSA(T)}{PSA_{yield}(T)} \tag{2}$$

The relevant plots are provided below in sequence of increasing epicentral distance (first horizontal then vertical components) and do not follow the rest of the report's figure enumeration.

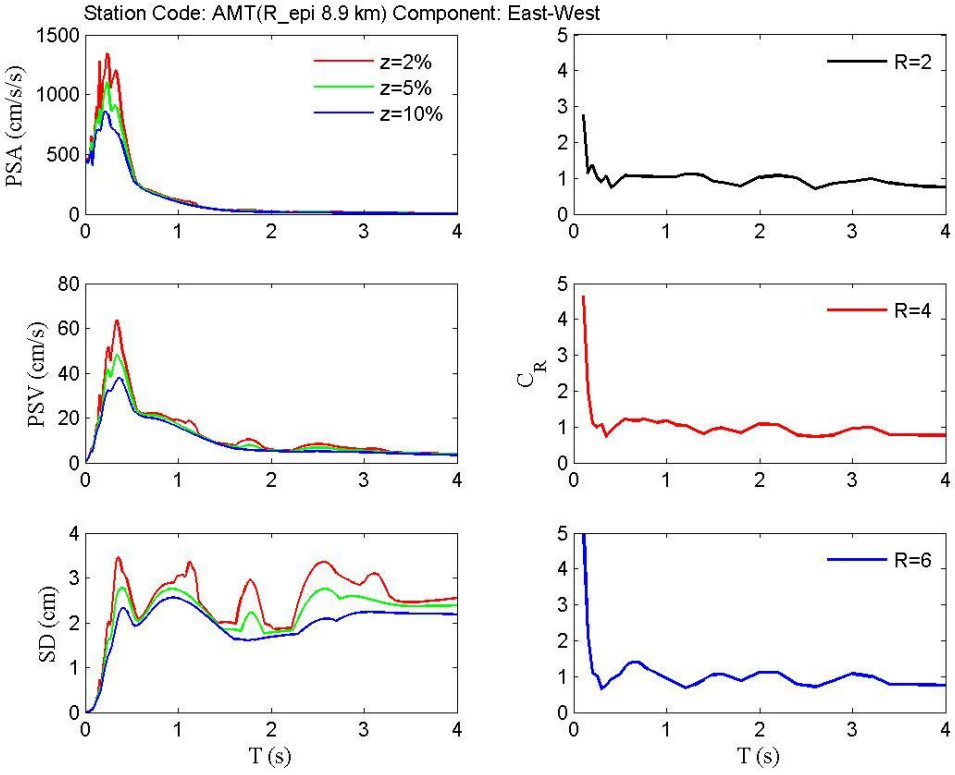
Station Code: AMT(R_epi 8.9 km) Component: East-West
PSA (cm/s/s)
PSV (cm/s)
SD (cm)
T (s)
z=2%
z=5%
z=10%
R=2
R=4
R=6
C_R

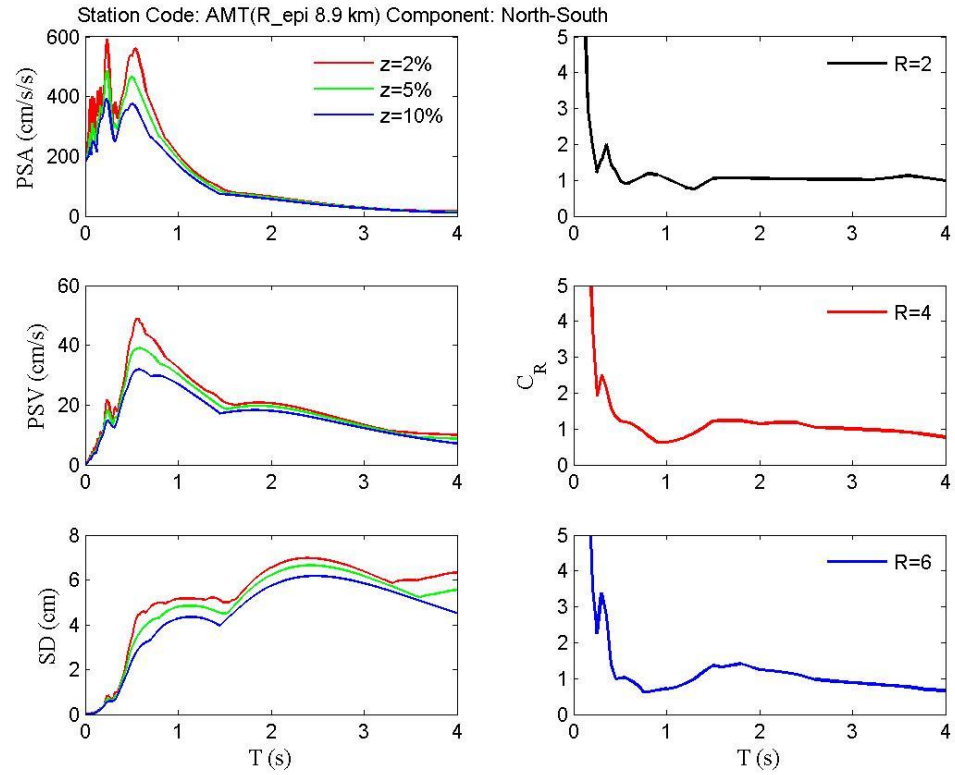
Station Code: AMT(R_epi 8.9 km) Component: North-South
PSA (cm/s/s)
PSV (cm/s)
SD (cm)
T (s)
z=2%
z=5%
z=10%
R=2
R=4
R=6
C_R

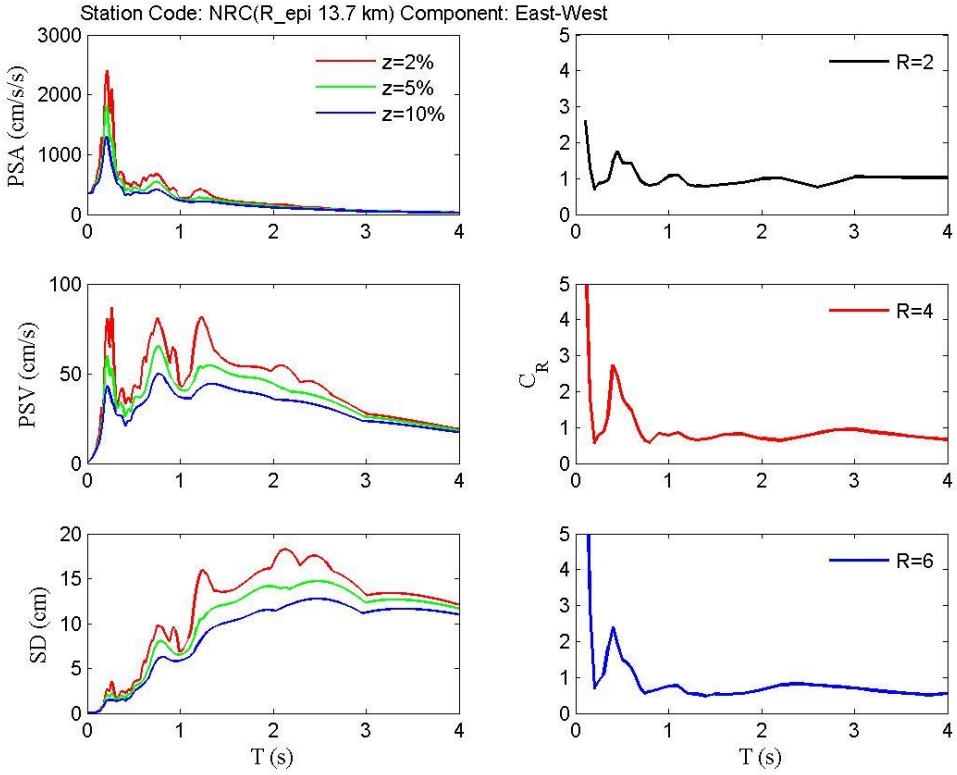
Station Code: NRC(R_epi 13.7 km) Component: East-West
PSA (cm/s/s)
PSV (cm/s)
SD (cm)
T (s)
z=2%
z=5%
z=10%
R=2
R=4
R=6
C_R

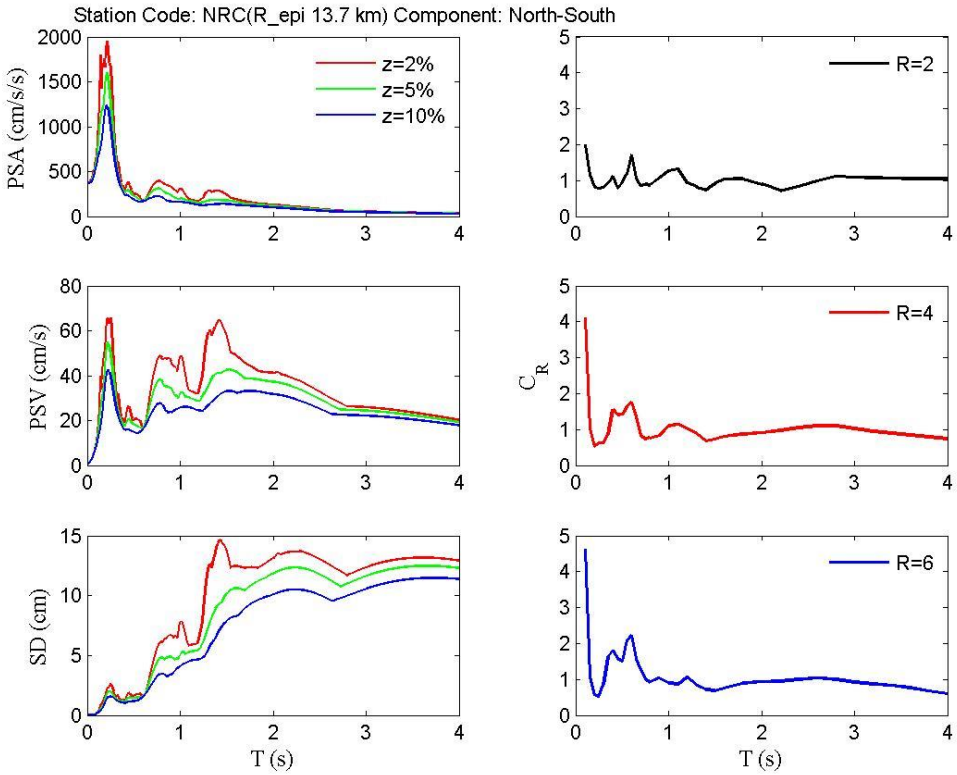
Station Code: NRC(R_epi 13.7 km) Component: North-South
PSA (cm/s/s)
PSV (cm/s)
SD (cm)
T (s)
z=2%
z=5%
z=10%
R=2
R=4
R=6
C_R

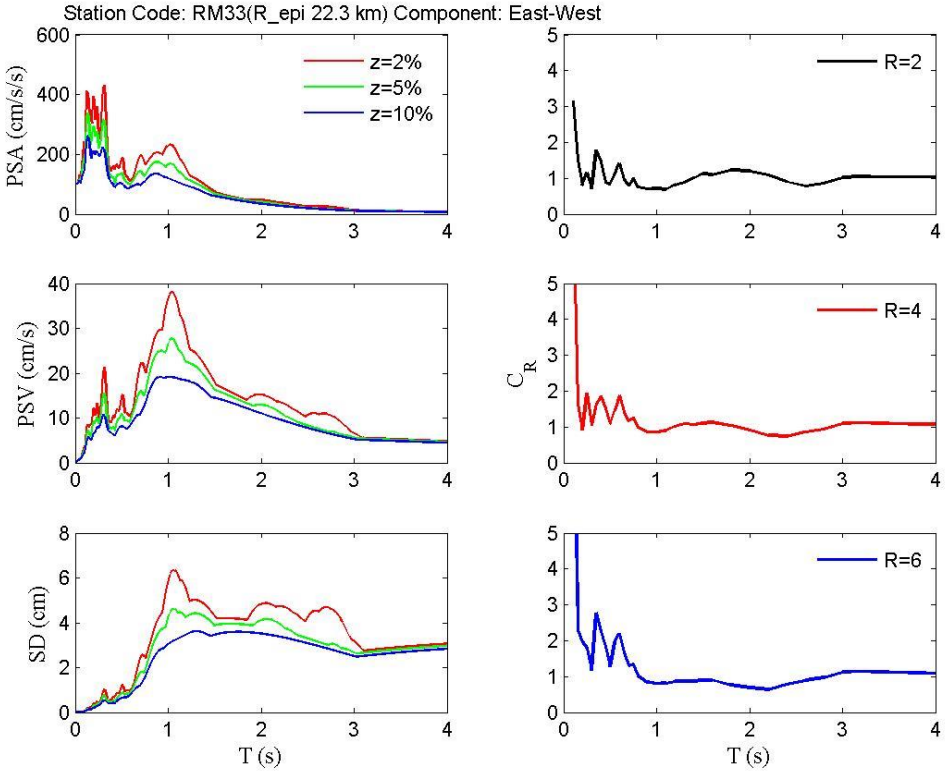
Station Code: RM33(R_epi 22.3 km) Component: East-West
PSA (cm/s/s)
PSV (cm/s)
SD (cm)
T (s)
z=2%
z=5%
z=10%
R=2
R=4
R=6
C_R

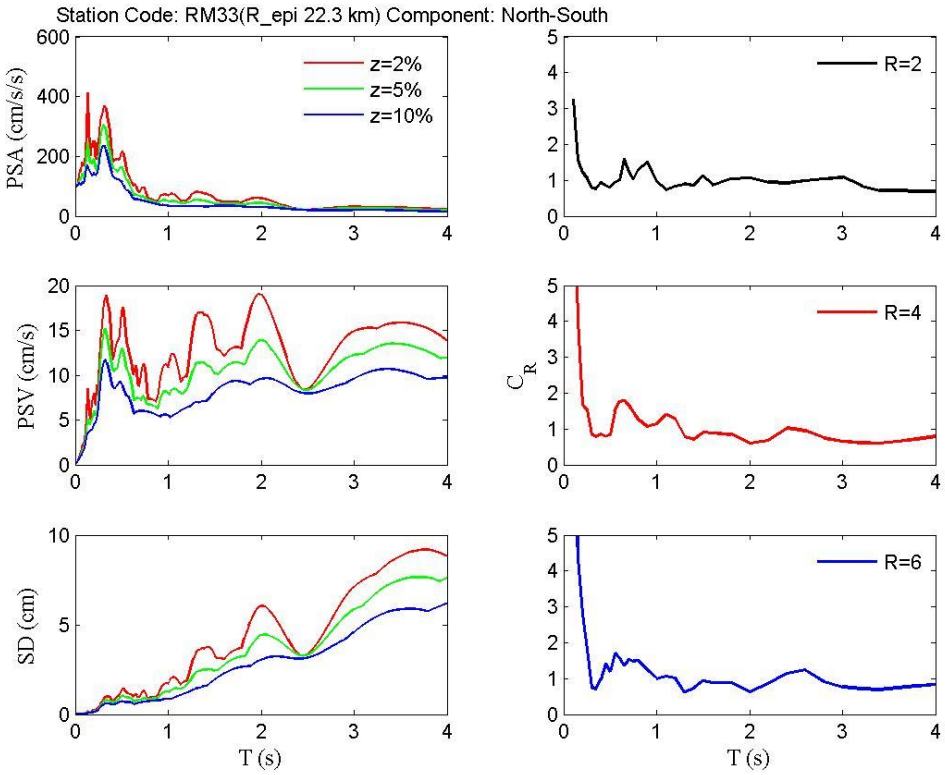
Station Code: RM33(R_epi 22.3 km) Component: North-South
PSA (cm/s/s)
PSV (cm/s)
SD (cm)
T (s)
z=2%
z=5%
z=10%
R=2
R=4
R=6
C_R

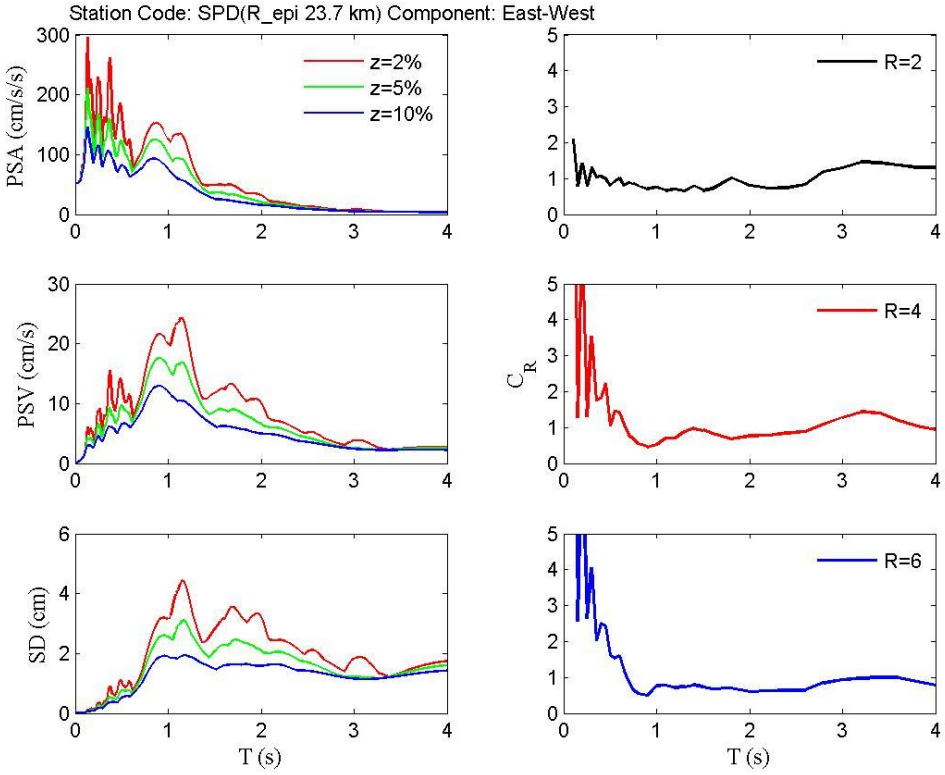
Station Code: SPD(R_epi 23.7 km) Component: East-West
PSA (cm/s/s)
PSV (cm/s)
SD (cm)
T (s)
z=2%
z=5%
z=10%
R=2
R=4
R=6
C_R

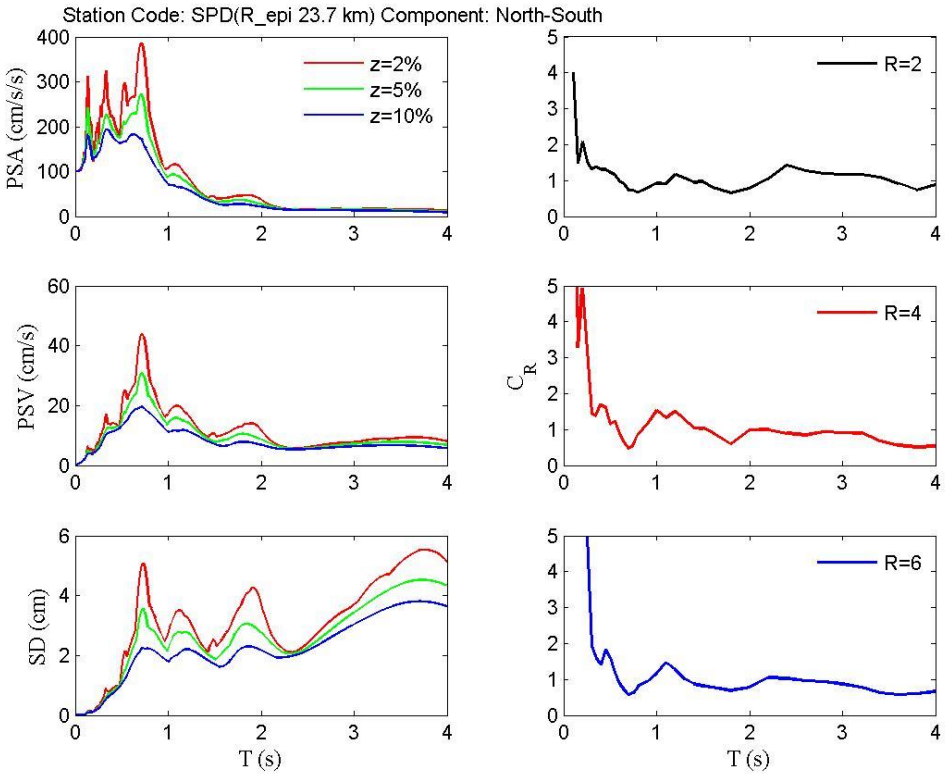
Station Code: SPD(R_epi 23.7 km) Component: North-South
PSA (cm/s/s)
PSV (cm/s)
SD (cm)
T (s)
z=2%
z=5%
z=10%
R=2
R=4
R=6
C_R

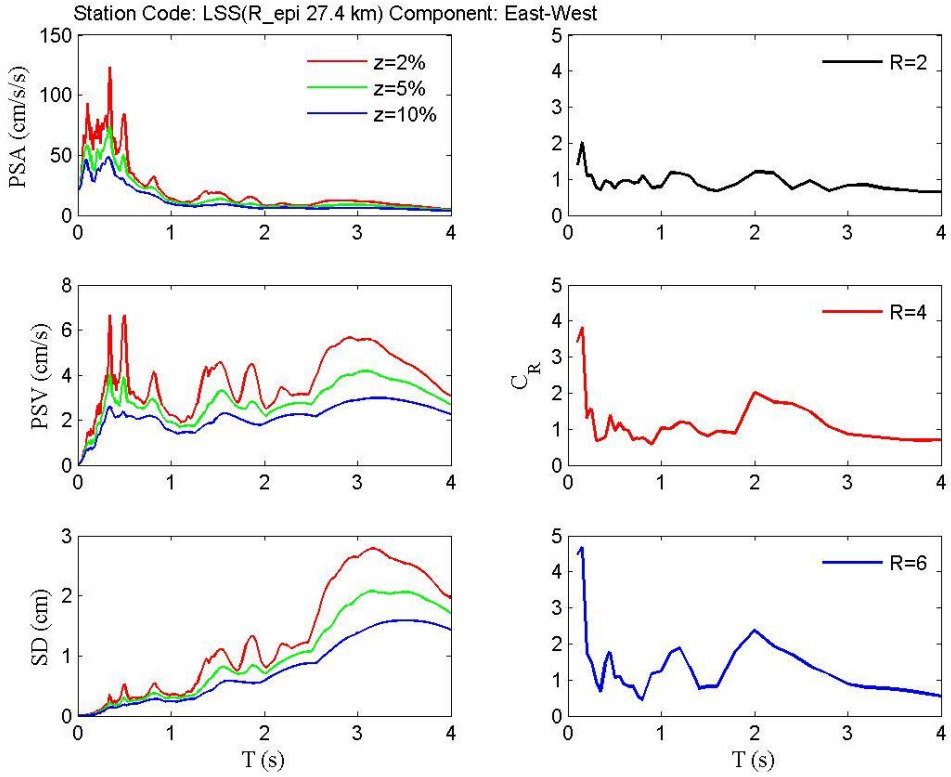
Station Code: LSS(R_epi 27.4 km) Component: East-West
PSA (cm/s/s)
PSV (cm/s)
SD (cm)
T (s)
z=2%
z=5%
z=10%
R=2
R=4
R=6
C_R

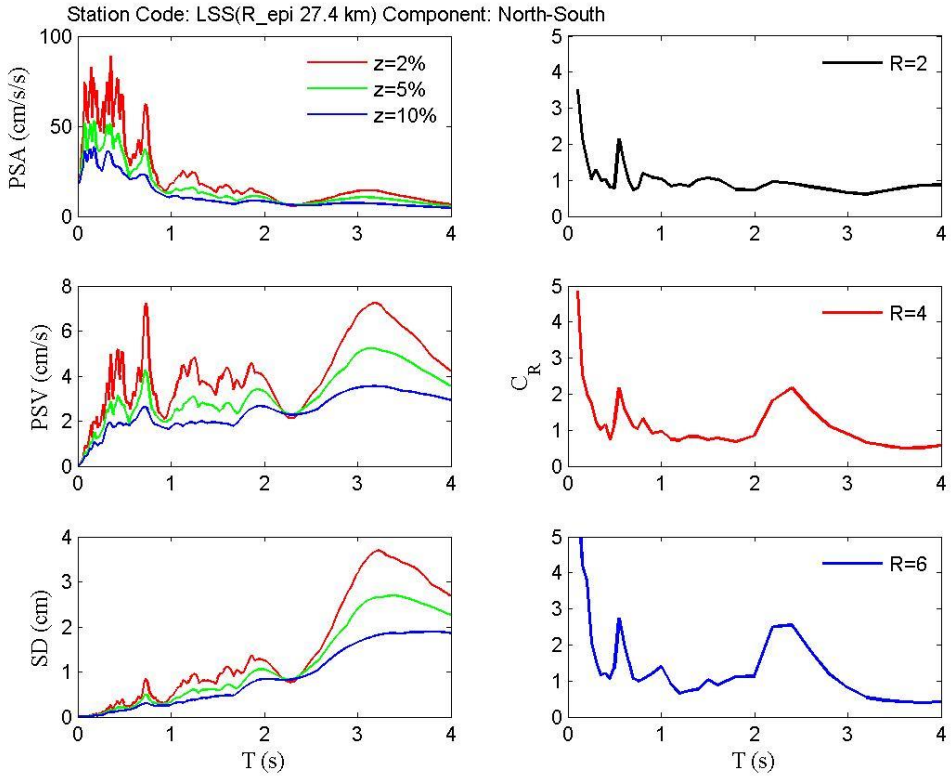
Station Code: LSS(R_epi 27.4 km) Component: North-South
PSA (cm/s/s)
PSV (cm/s)
SD (cm)
T (s)
z=2%
z=5%
z=10%
R=2
R=4
R=6
C_R

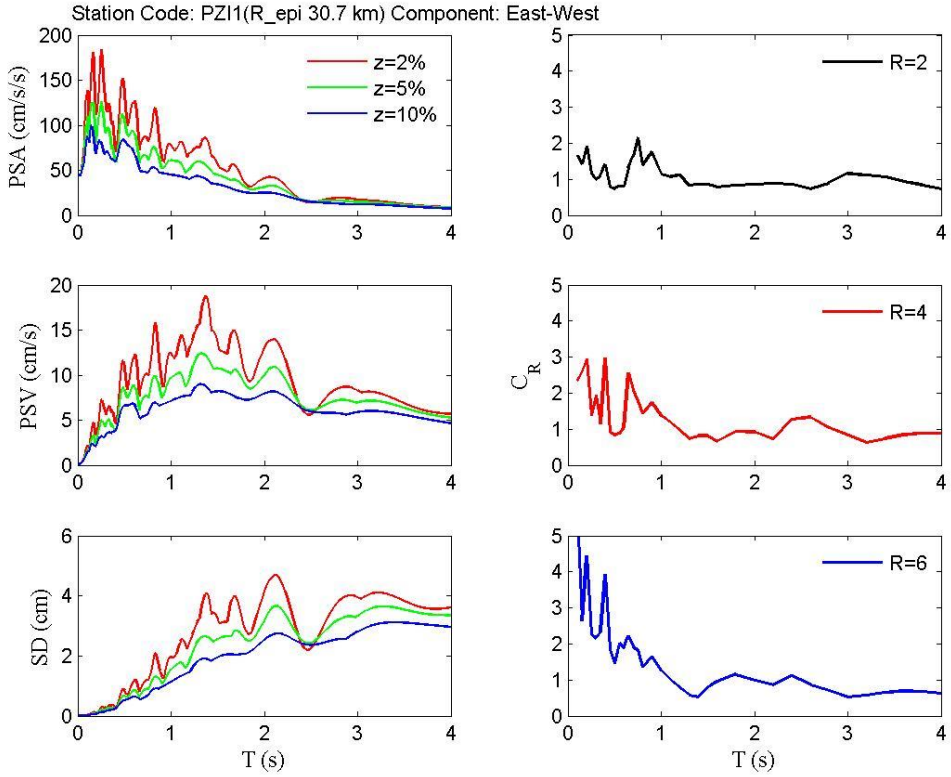
Station Code: PZI1(R_epi 30.7 km) Component: East-West
PSA (cm/s/s)
PSV (cm/s)
SD (cm)
T (s)
z=2%
z=5%
z=10%
R=2
R=4
R=6
C_R

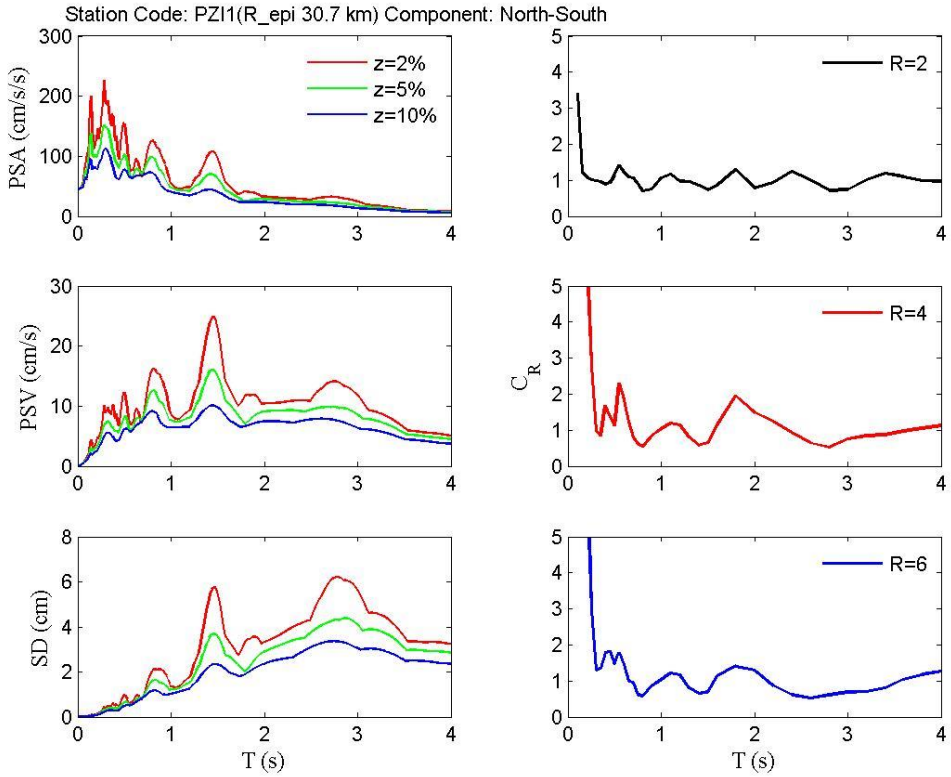
Station Code: PZI1(R_epi 30.7 km) Component: North-South
PSA (cm/s/s)
PSV (cm/s)
SD (cm)
T (s)
z=2%
z=5%
z=10%
R=2
R=4
R=6
C_R

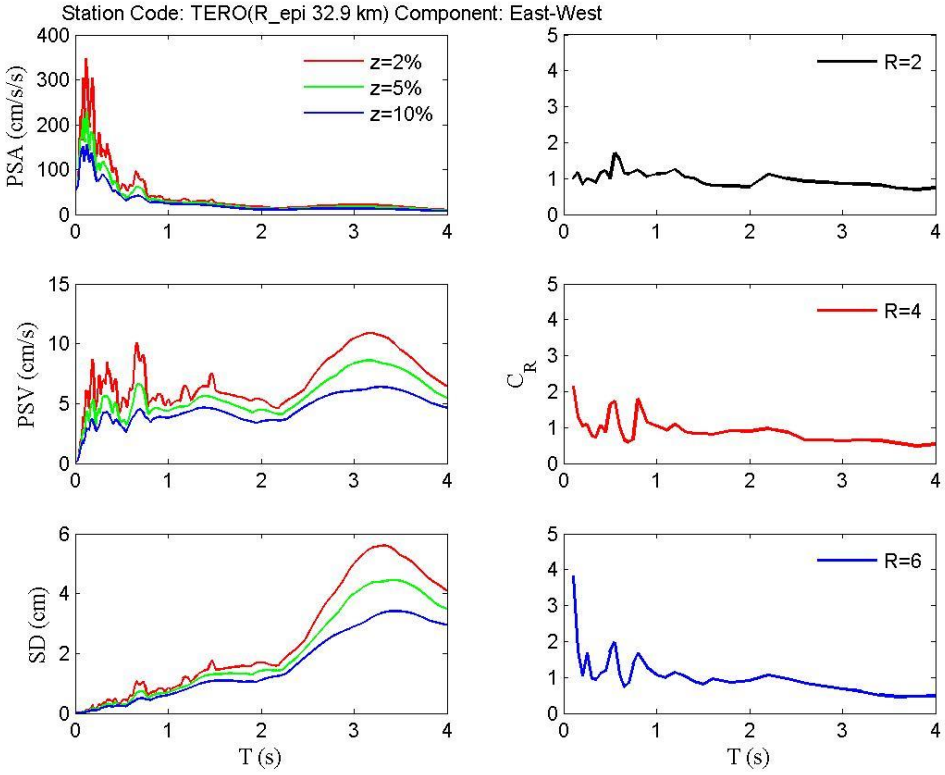
Station Code: TERO(R_epi 32.9 km) Component: East-West
PSA (cm/s/s)
PSV (cm/s)
SD (cm)
T (s)
z=2%
z=5%
z=10%
R=2
R=4
R=6
C_R

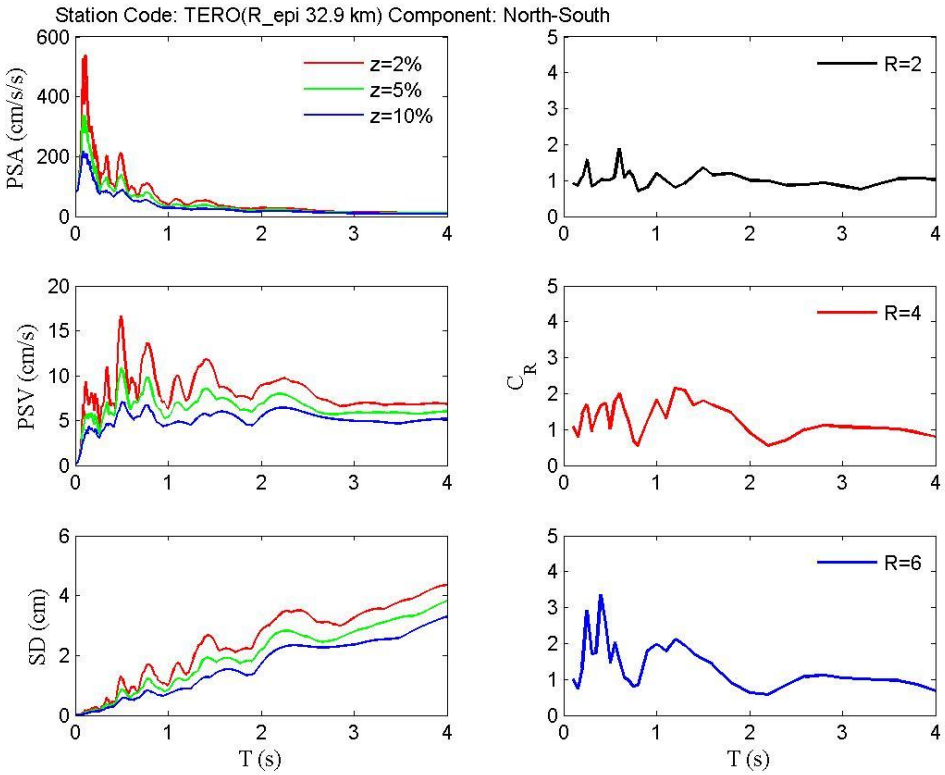
Station Code: TERO(R_epi 32.9 km) Component: North-South
PSA (cm/s/s)
PSV (cm/s)
SD (cm)
T (s)
z=2%
z=5%
z=10%
R=2
R=4
R=6
C_R

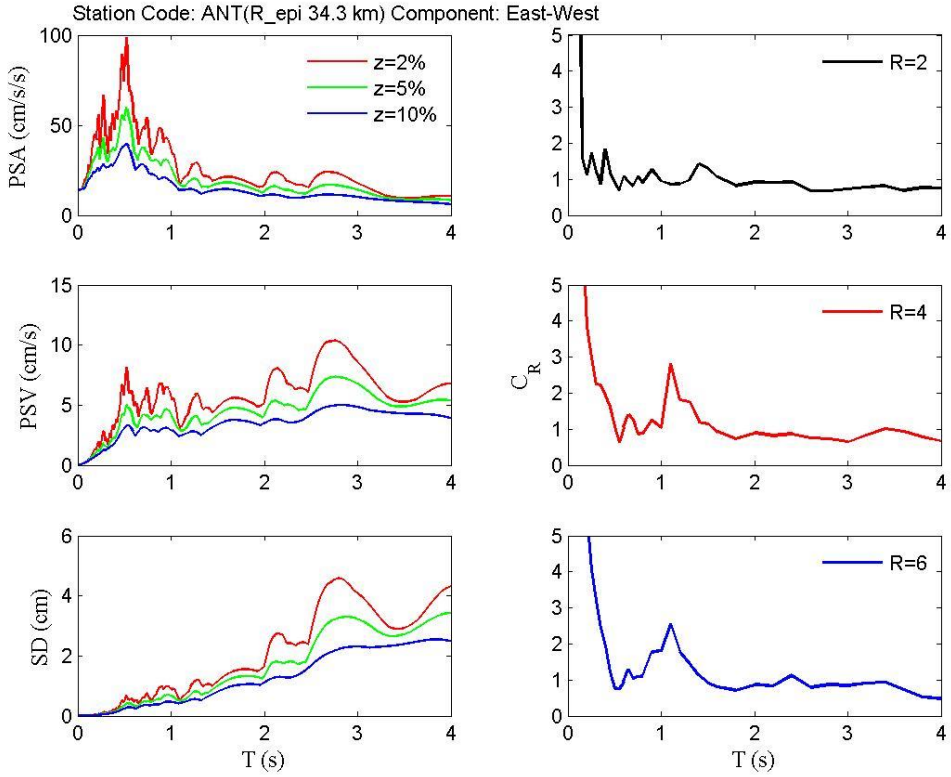
Station Code: ANT(R_epi 34.3 km) Component: East-West
PSA (cm/s/s)
PSV (cm/s)
SD (cm)
T (s)
z=2%
z=5%
z=10%
R=2
R=4
R=6
C_R

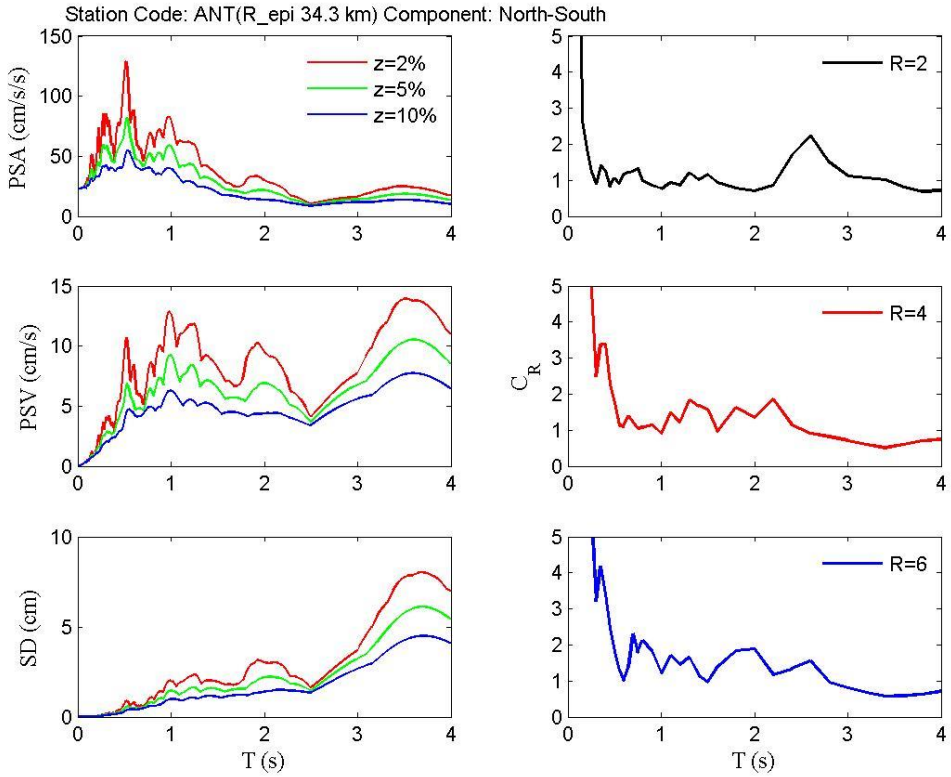
Station Code: ANT(R_epi 34.3 km) Component: North-South
PSA (cm/s/s)
PSV (cm/s)
SD (cm)
T (s)
z=2%
z=5%
z=10%
R=2
R=4
R=6
C_R

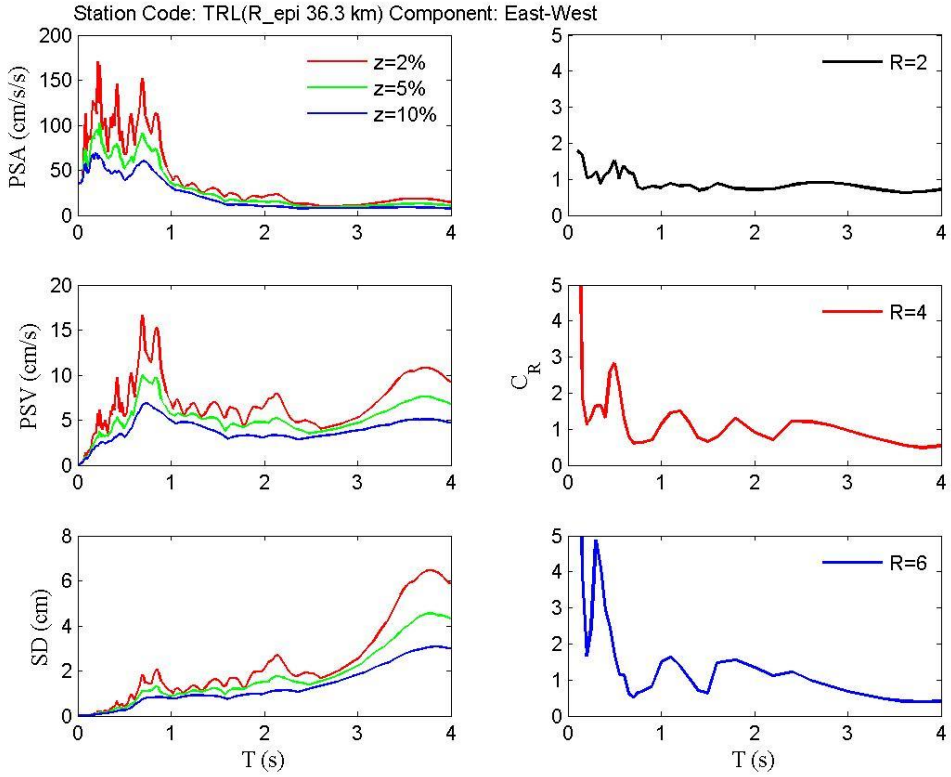
Station Code: TRL(R_epi 36.3 km) Component: East-West
PSA (cm/s/s)
PSV (cm/s)
SD (cm)
T (s)
z=2%
z=5%
z=10%
R=2
R=4
R=6
C_R

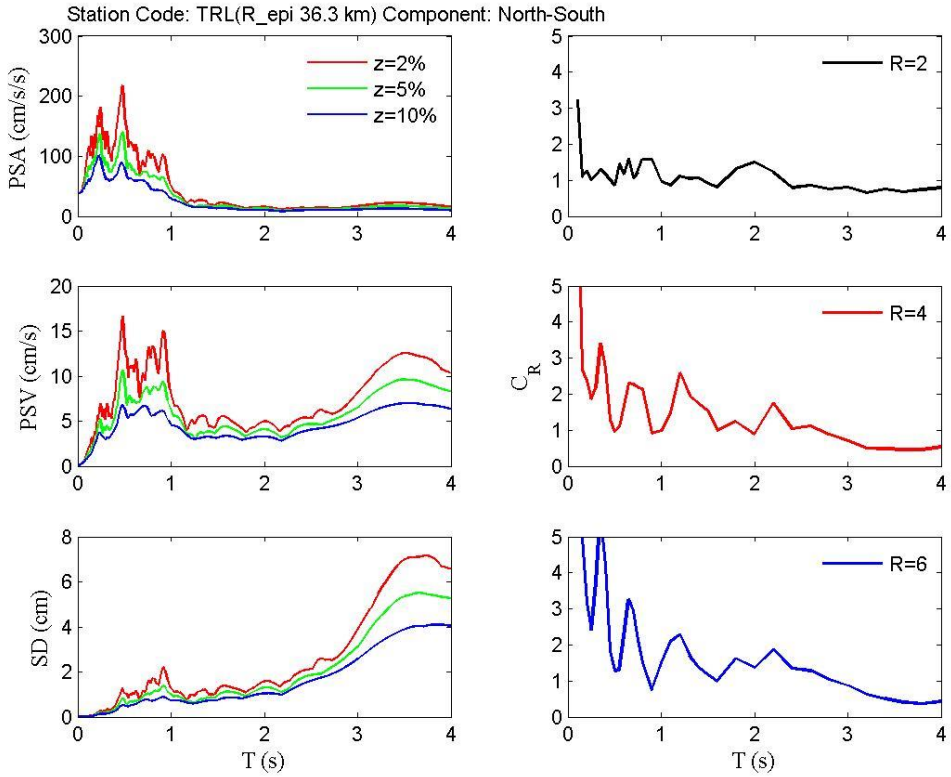
Station Code: TRL(R_epi 36.3 km) Component: North-South
PSA (cm/s/s)
PSV (cm/s)
SD (cm)
T (s)
z=2%
z=5%
z=10%
R=2
R=4
R=6
C_R

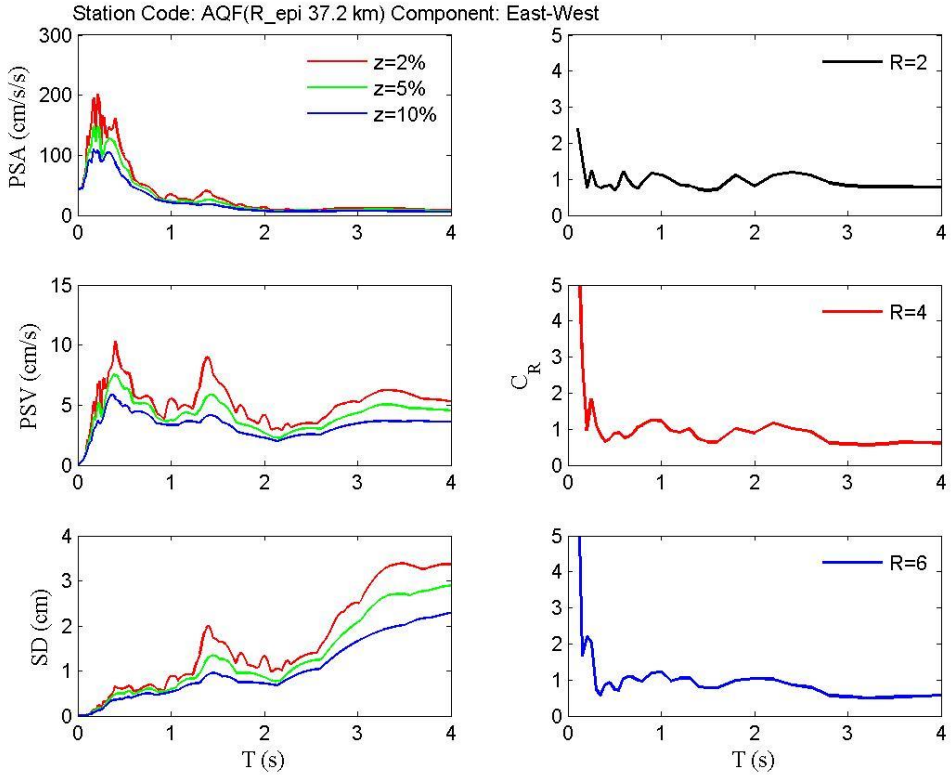
Station Code: AQF(R_epi 37.2 km) Component: East-West
PSA (cm/s/s)
PSV (cm/s)
SD (cm)
T (s)
z=2%
z=5%
z=10%
R=2
R=4
R=6
C_R

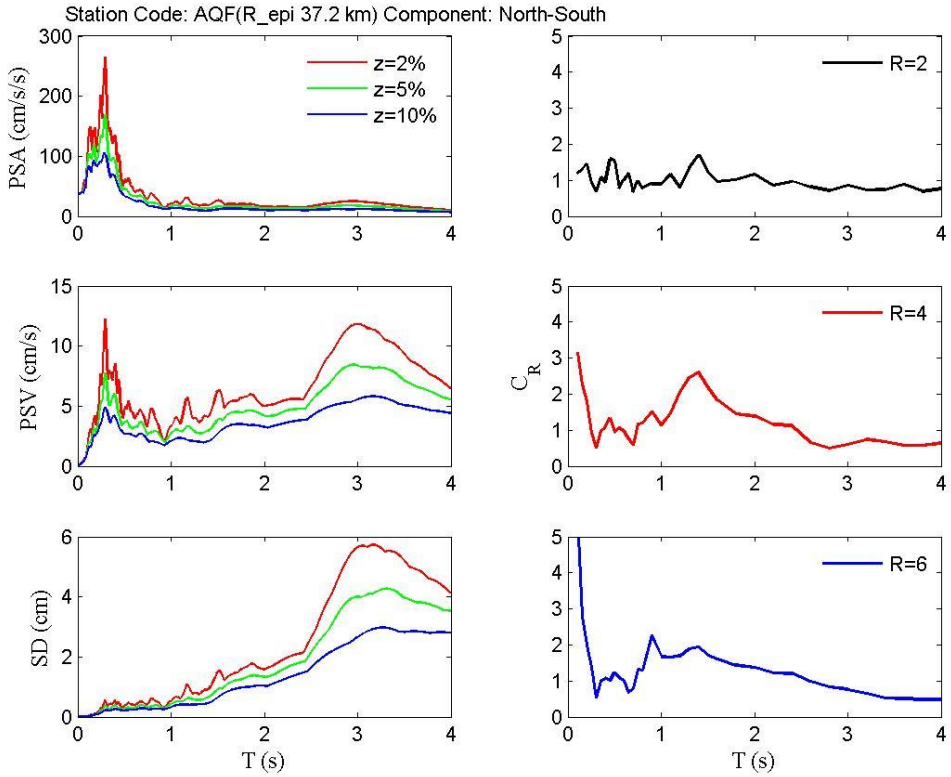
Station Code: AQF(R_epi 37.2 km) Component: North-South
PSA (cm/s/s)
PSV (cm/s)
SD (cm)
T (s)
z=2%
z=5%
z=10%
R=2
R=4
R=6
C_R

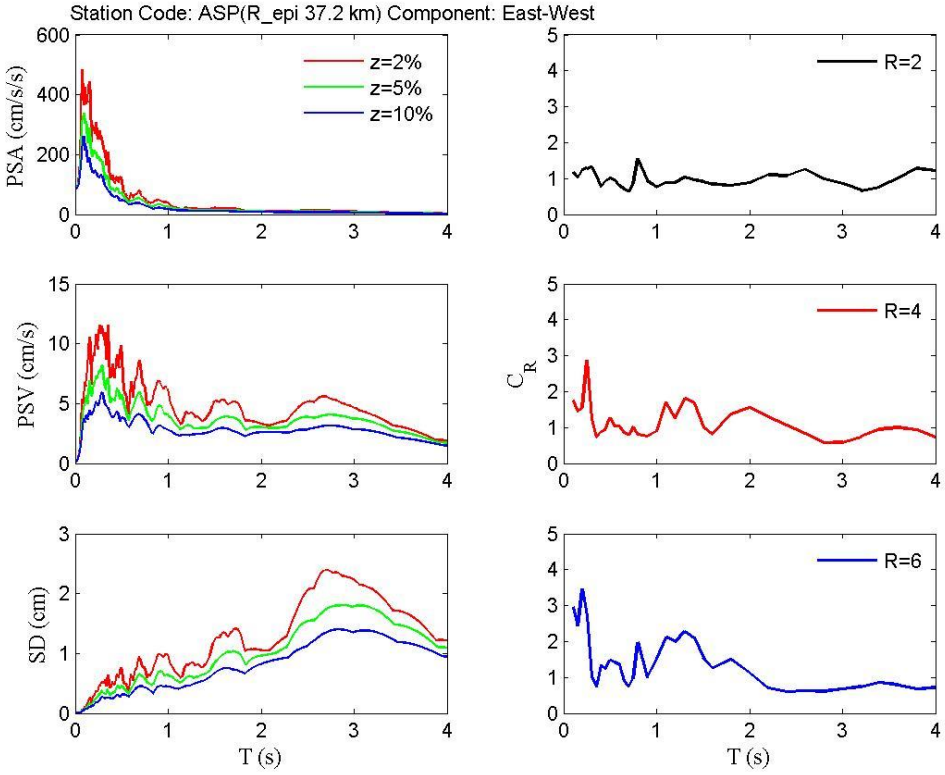
Station Code: ASP(R_epi 37.2 km) Component: East-West
PSA (cm/s/s)
PSV (cm/s)
SD (cm)
T (s)
z=2%
z=5%
z=10%
R=2
R=4
R=6
C_R

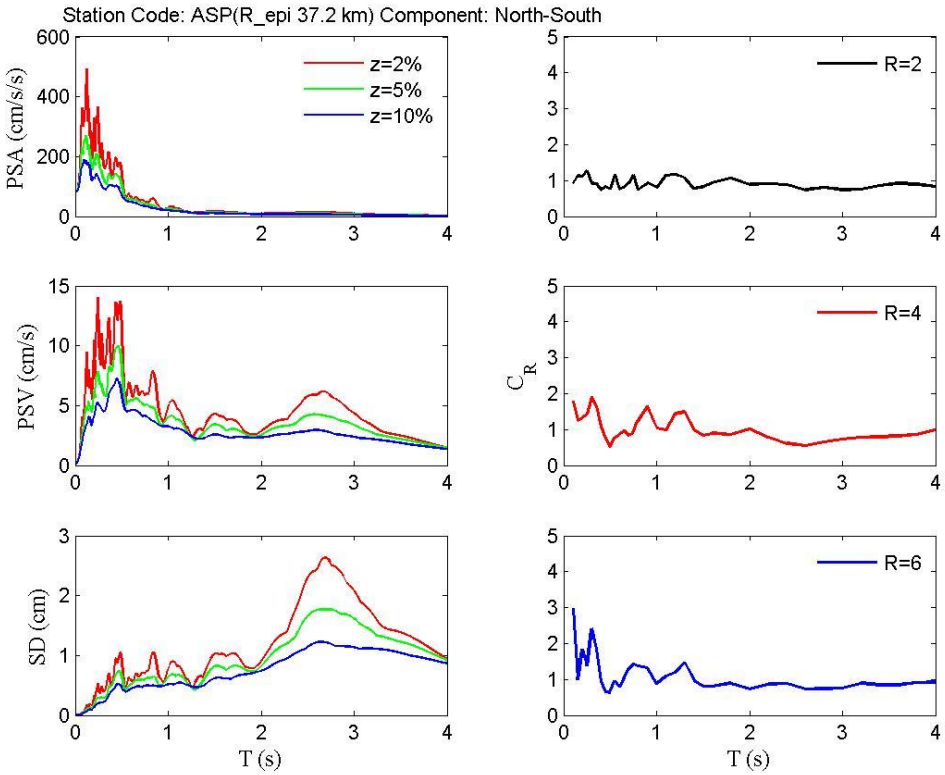
Station Code: ASP(R_epi 37.2 km) Component: North-South
PSA (cm/s/s)
PSV (cm/s)
SD (cm)
T (s)
z=2%
z=5%
z=10%
R=2
R=4
R=6
C_R

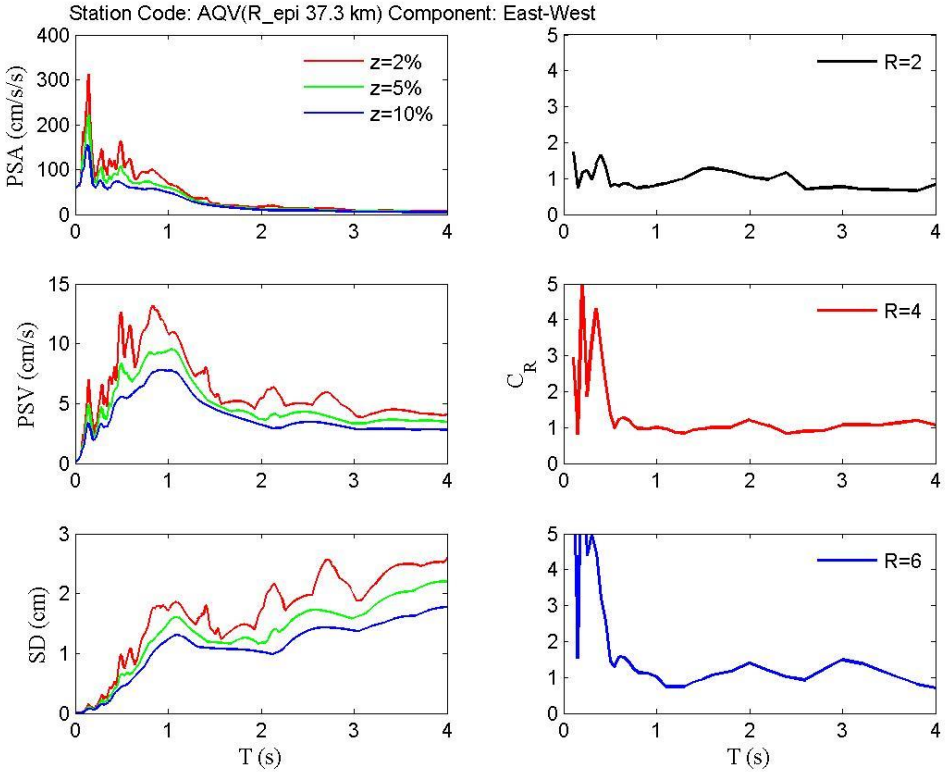
Station Code: AQV(R_epi 37.3 km) Component: East-West
PSA (cm/s/s)
PSV (cm/s)
SD (cm)
T (s)
z=2%
z=5%
z=10%
R=2
R=4
R=6
C_R

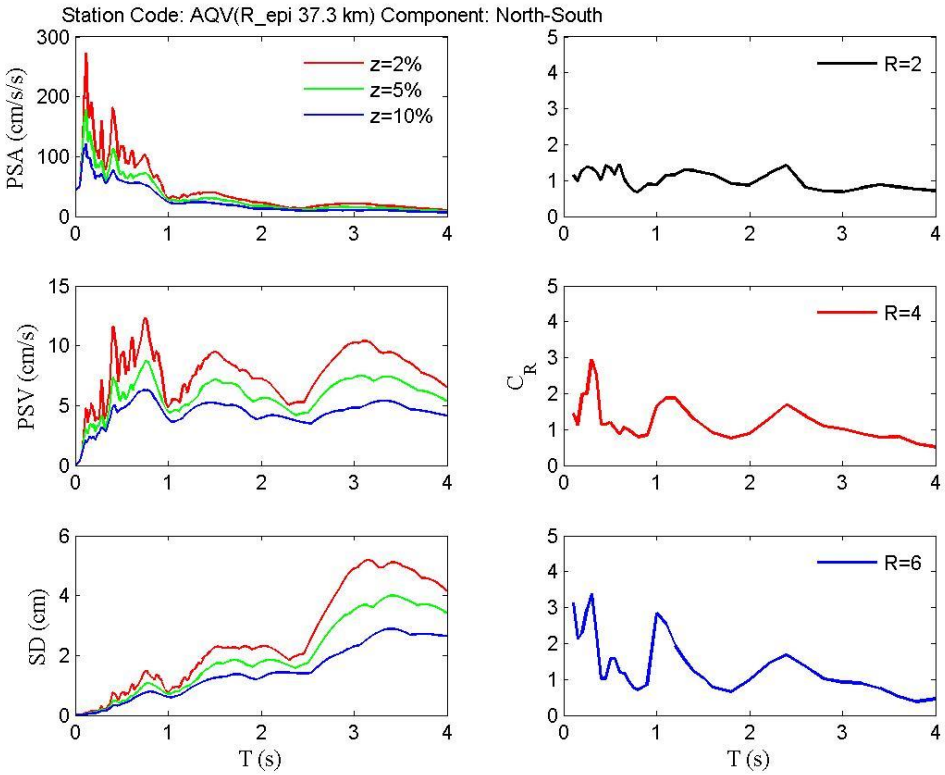
Station Code: AQV(R_epi 37.3 km) Component: North-South
PSA (cm/s/s)
PSV (cm/s)
SD (cm)
T (s)
z=2%
z=5%
z=10%
R=2
R=4
R=6
C_R

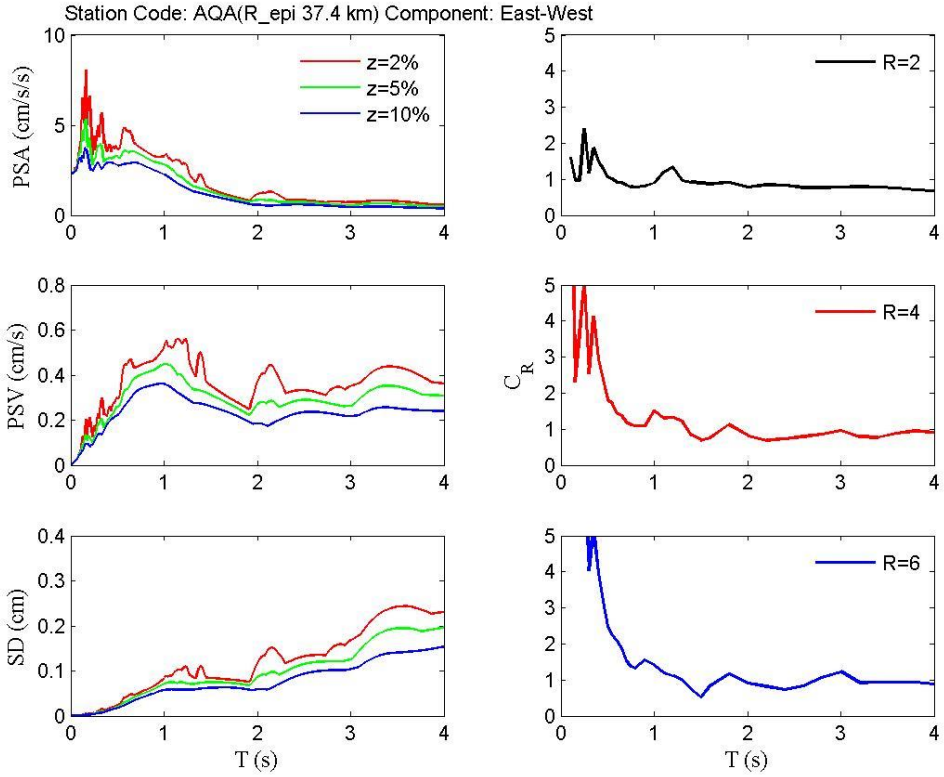
Station Code: AQA(R_epi 37.4 km) Component: East-West
PSA (cm/s/s)
PSV (cm/s)
SD (cm)
T (s)
z=2%
z=5%
z=10%
R=2
R=4
R=6
C_R

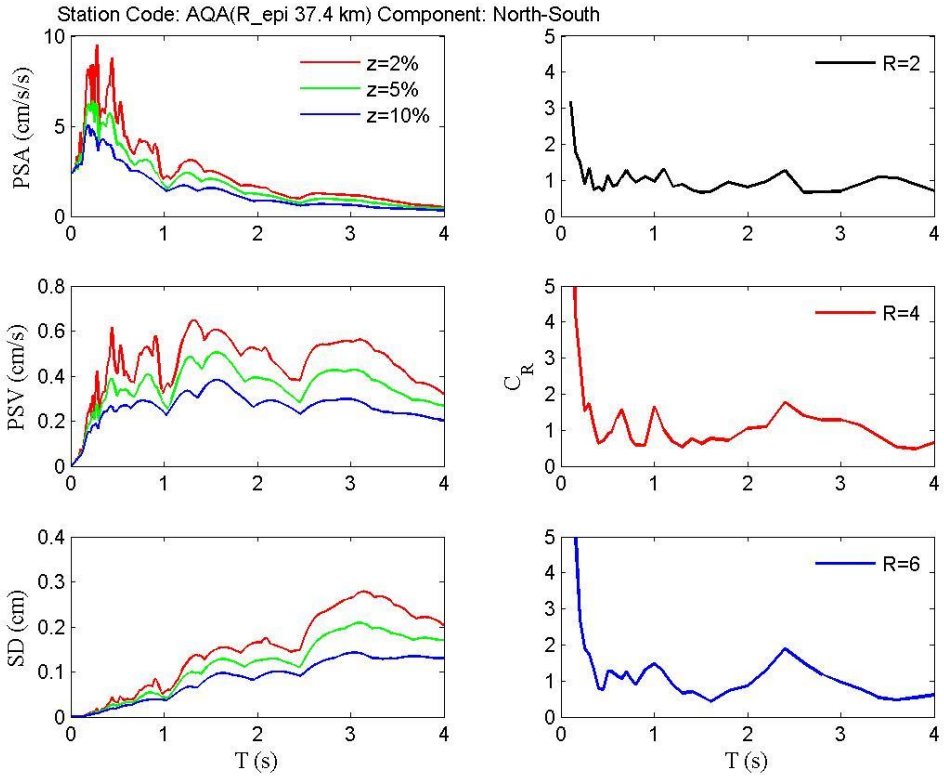
Station Code: AQA(R_epi 37.4 km) Component: North-South
PSA (cm/s/s)
PSV (cm/s)
SD (cm)
T (s)
z=2%
z=5%
z=10%
R=2
R=4
R=6
C_R

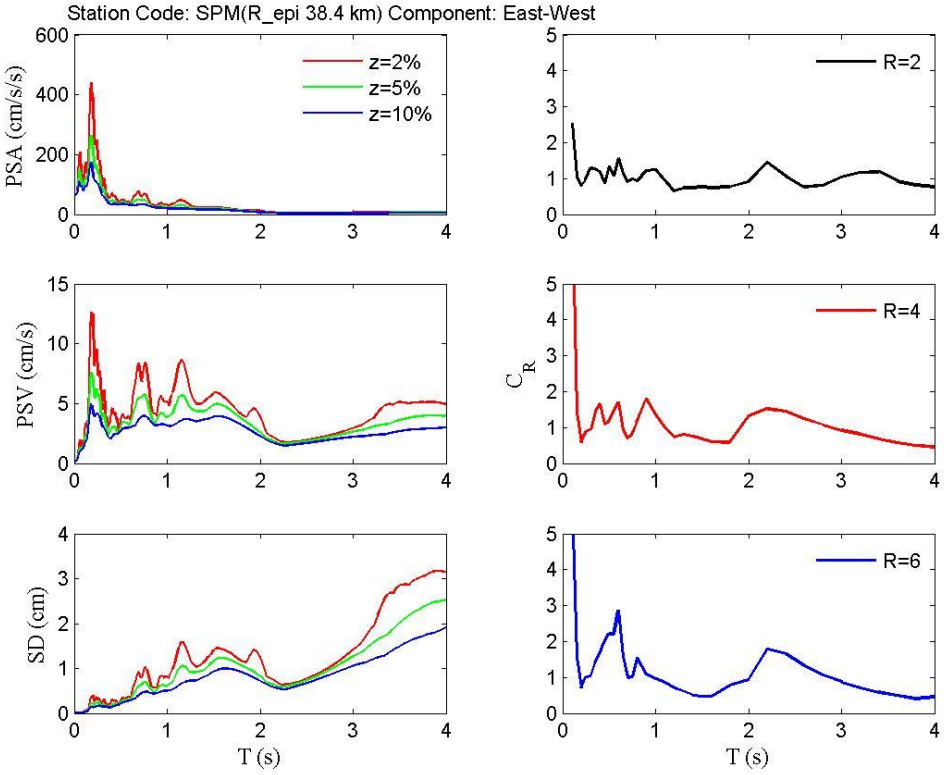
Station Code: SPM(R_epi 38.4 km) Component: East-West
PSA (cm/s/s)
PSV (cm/s)
SD (cm)
T (s)
z=2%
z=5%
z=10%
R=2
R=4
R=6
C_R

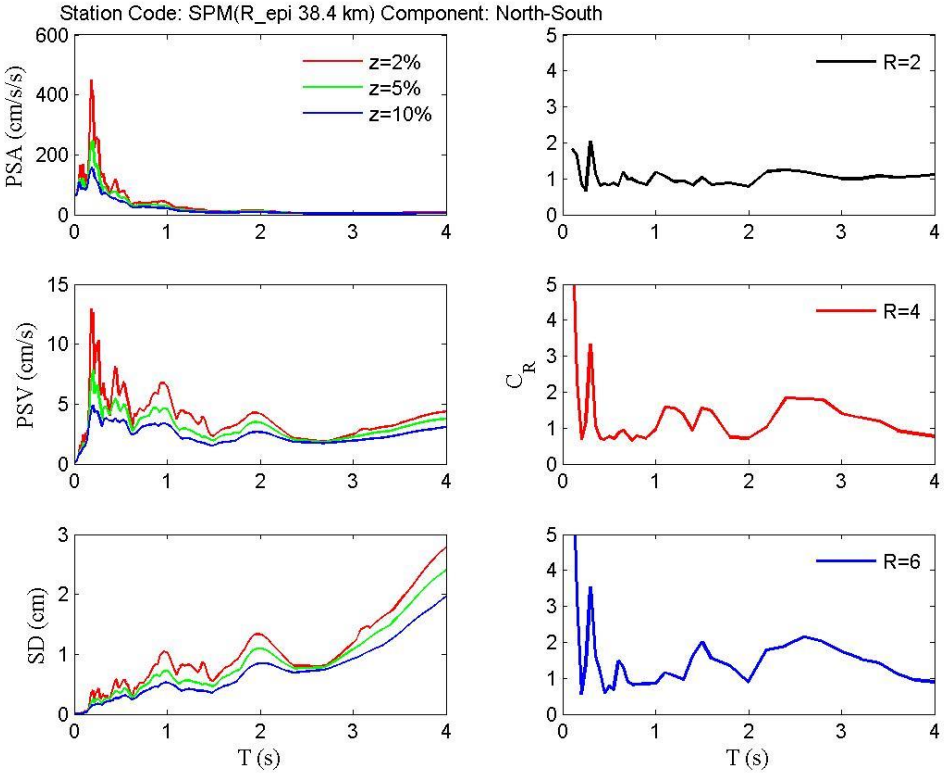
Station Code: SPM(R_epi 38.4 km) Component: North-South
PSA (cm/s/s)
PSV (cm/s)
SD (cm)
T (s)
z=2%
z=5%
z=10%
R=2
R=4
R=6
C_R

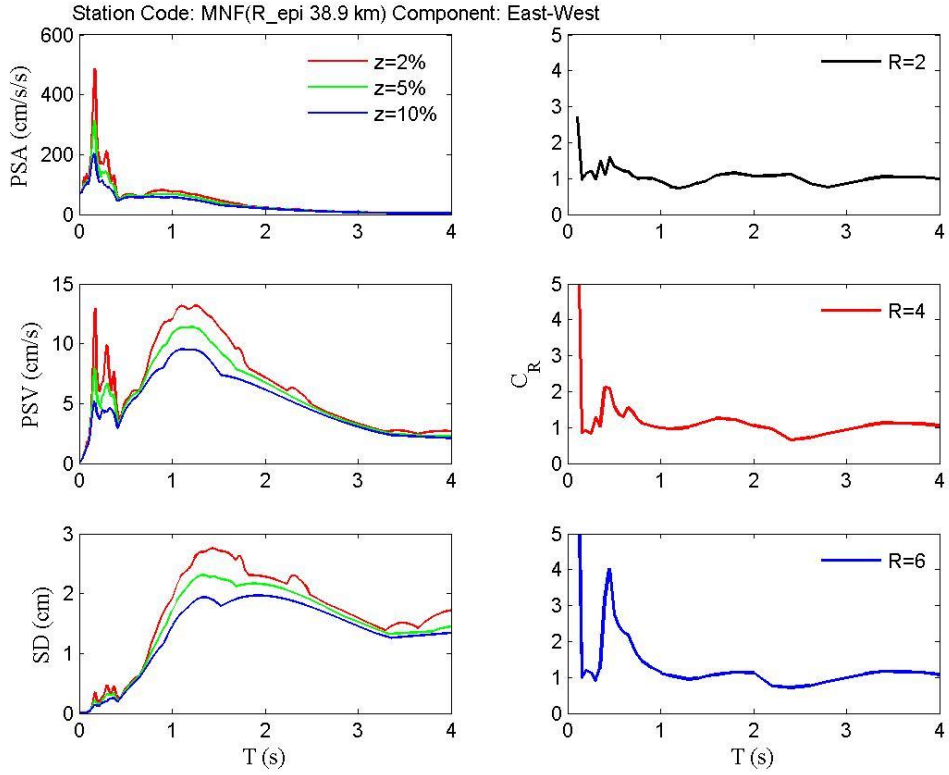
Station Code: MNF(R_epi 38.9 km) Component: East-West
PSA (cm/s/s)
PSV (cm/s)
SD (cm)
T (s)
z=2%
z=5%
z=10%
R=2
R=4
R=6
C_R

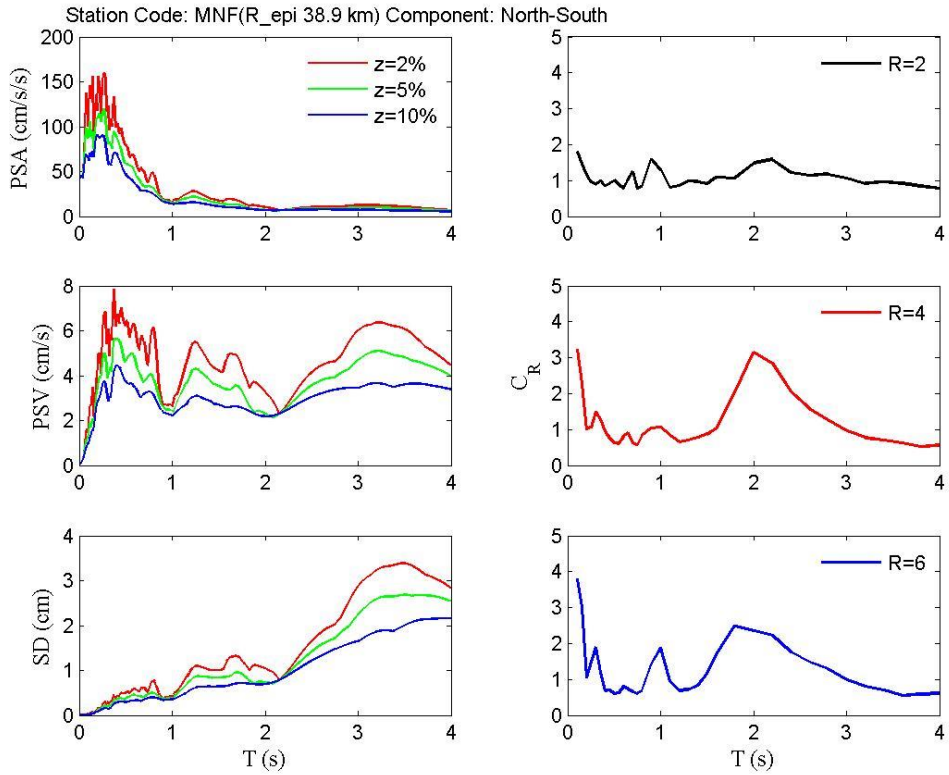
Station Code: MNF(R_epi 38.9 km) Component: North-South
PSA (cm/s/s)
PSV (cm/s)
SD (cm)
T (s)
z=2%
z=5%
z=10%
R=2
R=4
R=6
C_R

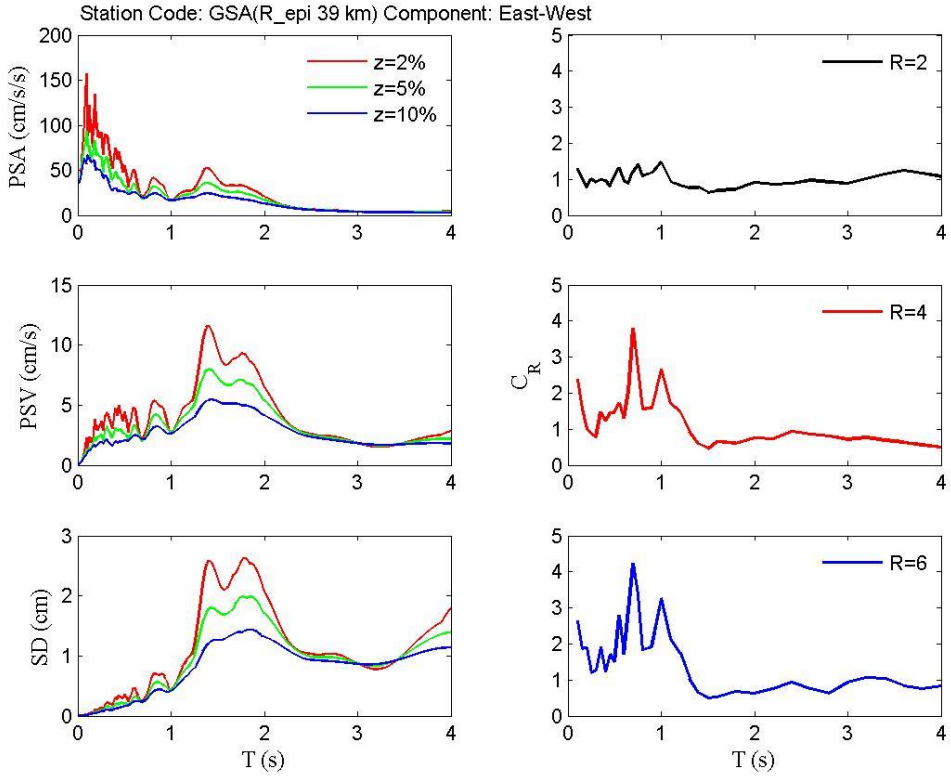
Station Code: GSA(R_epi 39 km) Component: East-West
PSA (cm/s/s)
PSV (cm/s)
SD (cm)
T (s)
z=2%
z=5%
z=10%
R=2
R=4
R=6
C_R

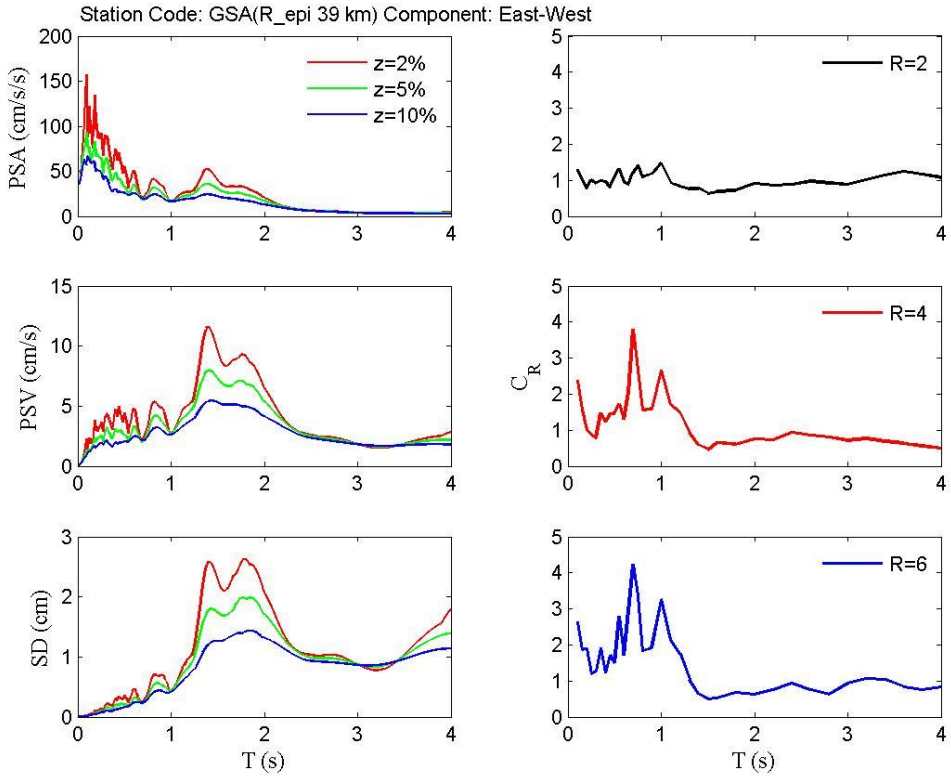
Station Code: GSA(R_epi 39 km) Component: East-West
PSA (cm/s/s)
PSV (cm/s)
SD (cm)
T (s)
z=2%
z=5%
z=10%
R=2
R=4
R=6
C_R

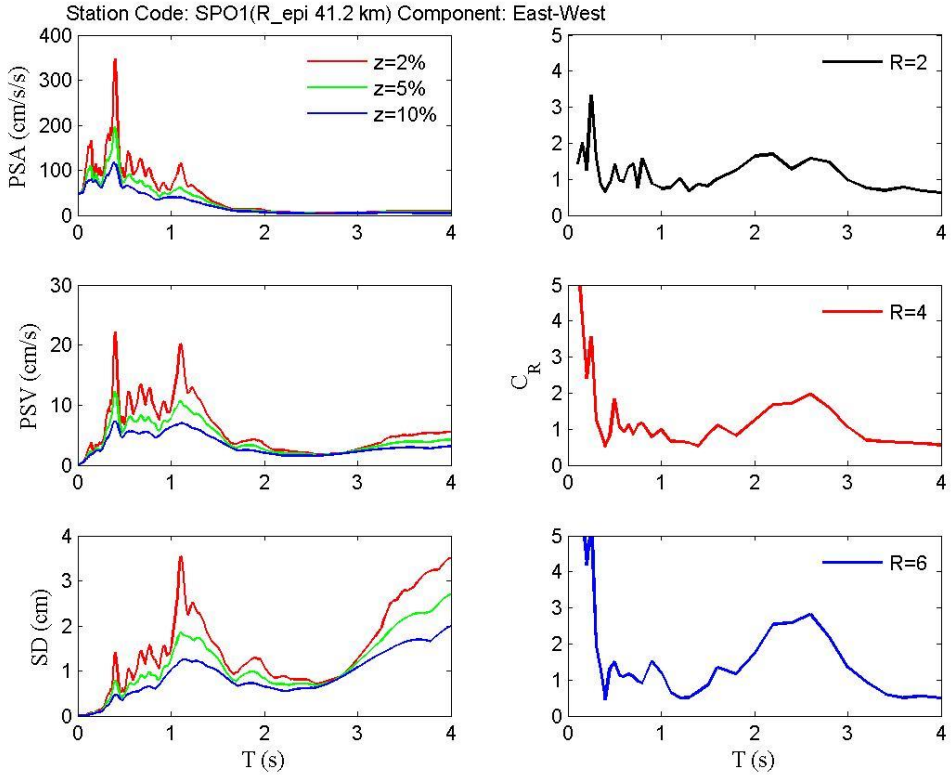
Station Code: SPO1(R_epi 41.2 km) Component: East-West
PSA (cm/s/s)
PSV (cm/s)
SD (cm)
T (s)
z=2%
z=5%
z=10%
R=2
R=4
R=6
C_R
T (s)

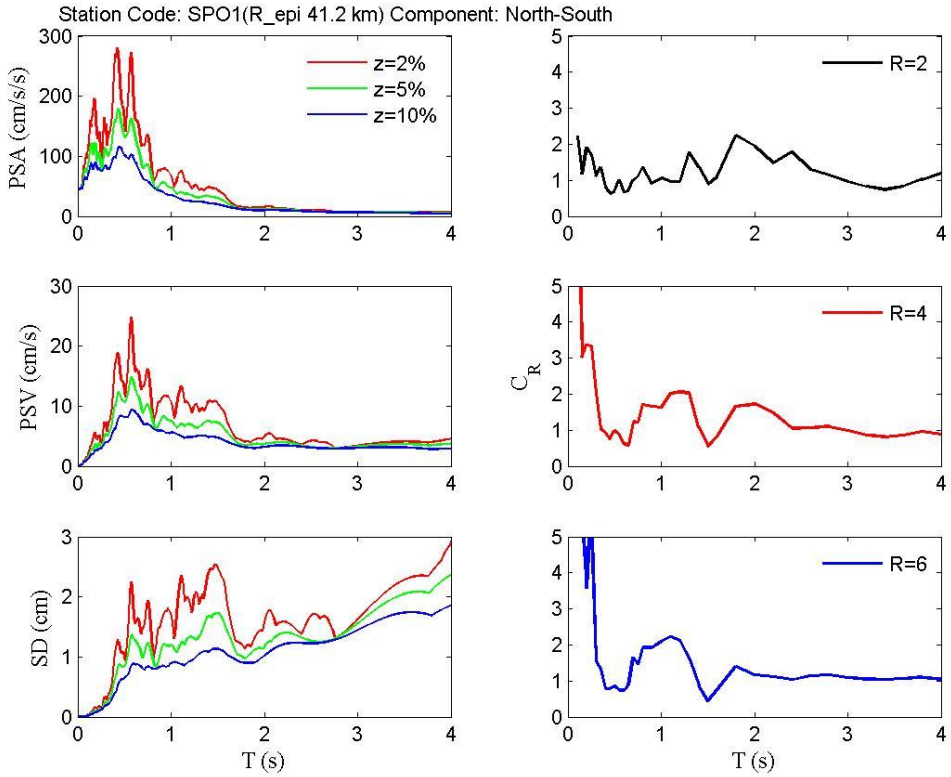
Station Code: SPO1(R_epi 41.2 km) Component: North-South
PSA (cm/s/s)
PSV (cm/s)
SD (cm)
T (s)
z=2%
z=5%
z=10%
R=2
R=4
R=6
C_R
T (s)

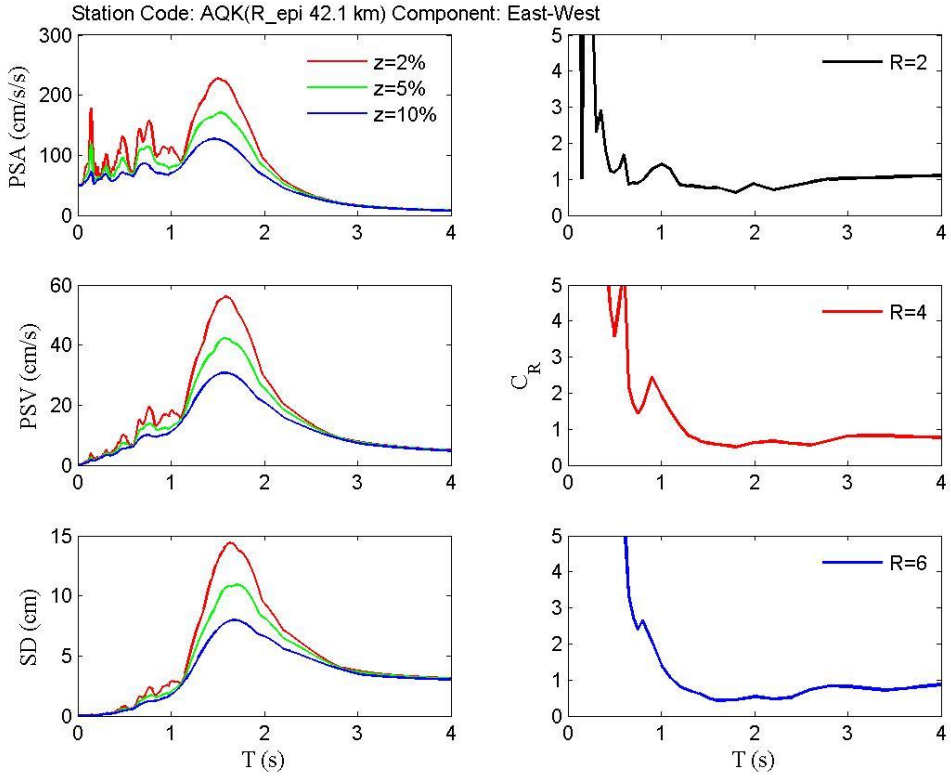
Station Code: AQK(R_epi 42.1 km) Component: East-West
PSA (cm/s/s)
PSV (cm/s)
SD (cm)
T (s)
z=2%
z=5%
z=10%
R=2
R=4
R=6
C_R

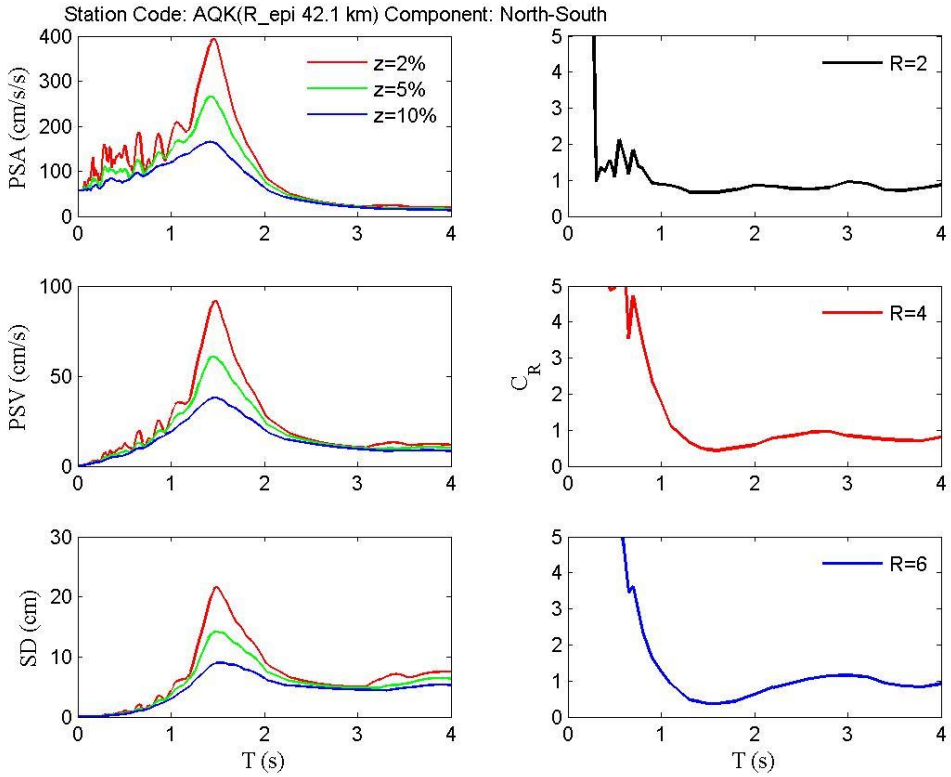
Station Code: AQK(R_epi 42.1 km) Component: North-South
PSA (cm/s/s)
PSV (cm/s)
SD (cm)
T (s)
z=2%
z=5%
z=10%
R=2
R=4
R=6
C_R

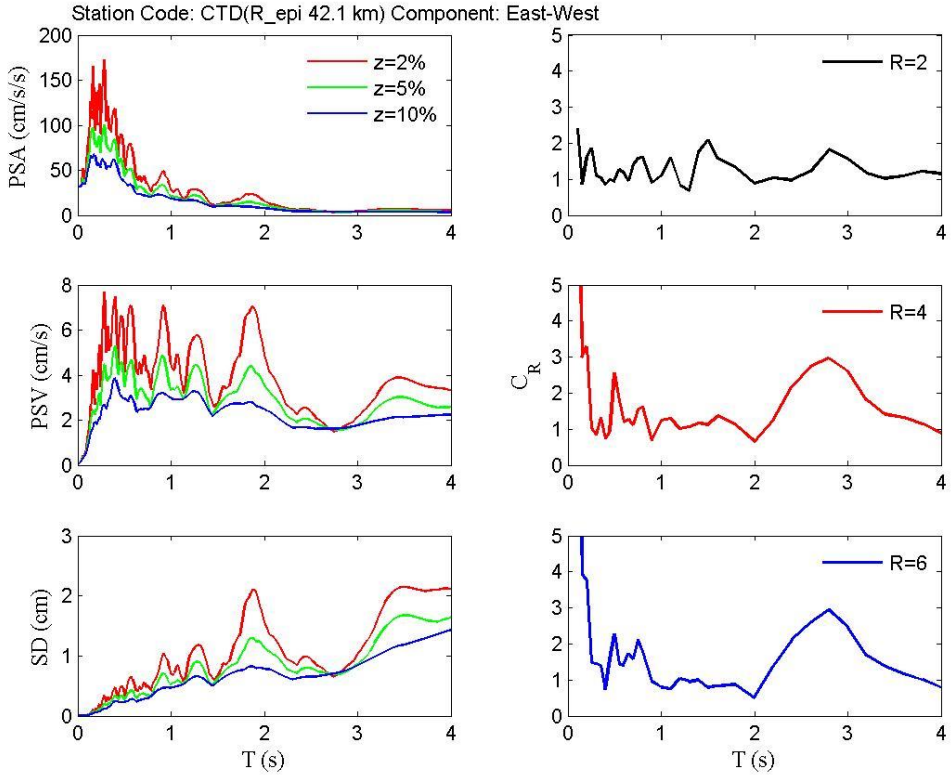
Station Code: CTD(R_epi 42.1 km) Component: East-West
PSA (cm/s/s)
PSV (cm/s)
SD (cm)
T (s)
z=2%
z=5%
z=10%
R=2
R=4
R=6
C_R

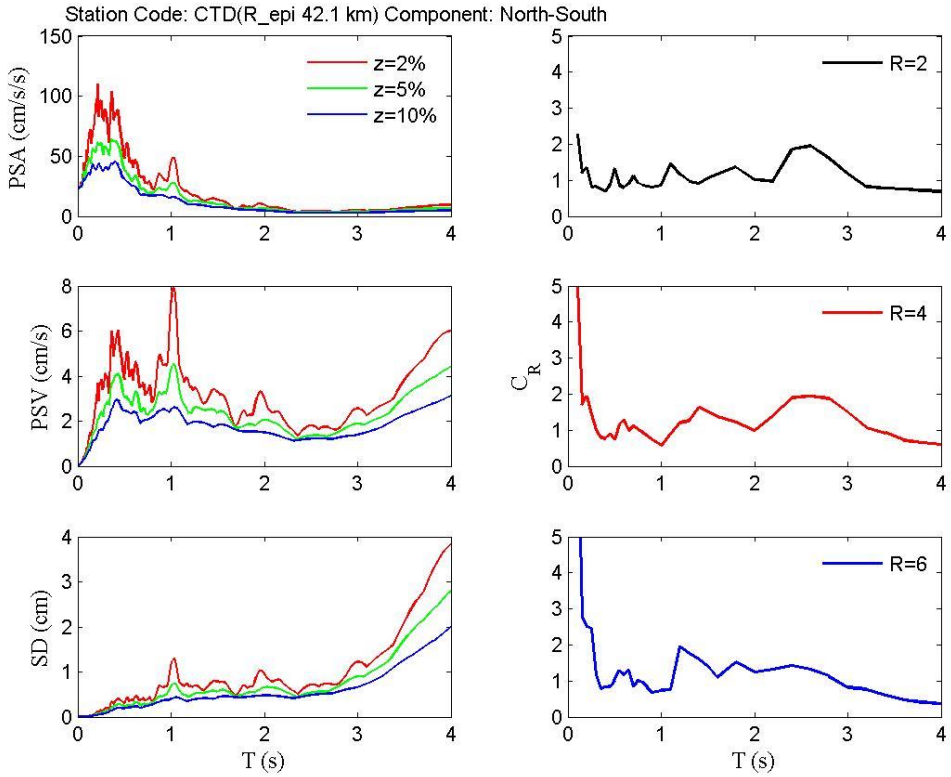
Station Code: CTD(R_epi 42.1 km) Component: North-South
PSA (cm/s/s)
PSV (cm/s)
SD (cm)
T (s)
z=2%
z=5%
z=10%
R=2
R=4
R=6
C_R

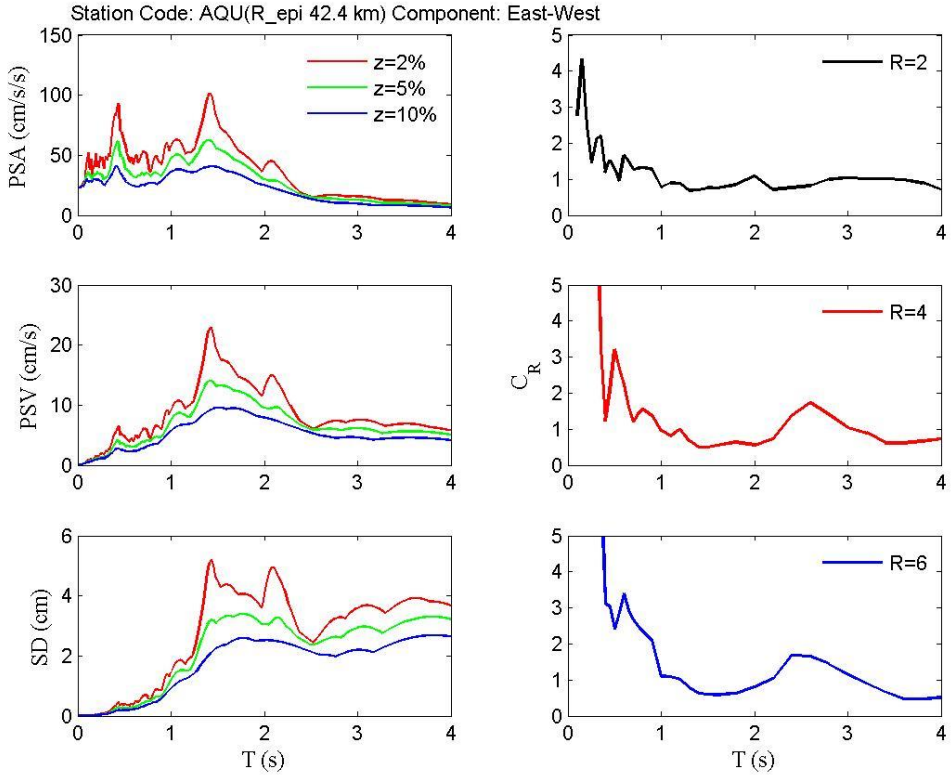
Station Code: AQU(R_epi 42.4 km) Component: East-West
PSA (cm/s/s)
PSV (cm/s)
SD (cm)
T (s)
z=2%
z=5%
z=10%
R=2
R=4
R=6
C_R

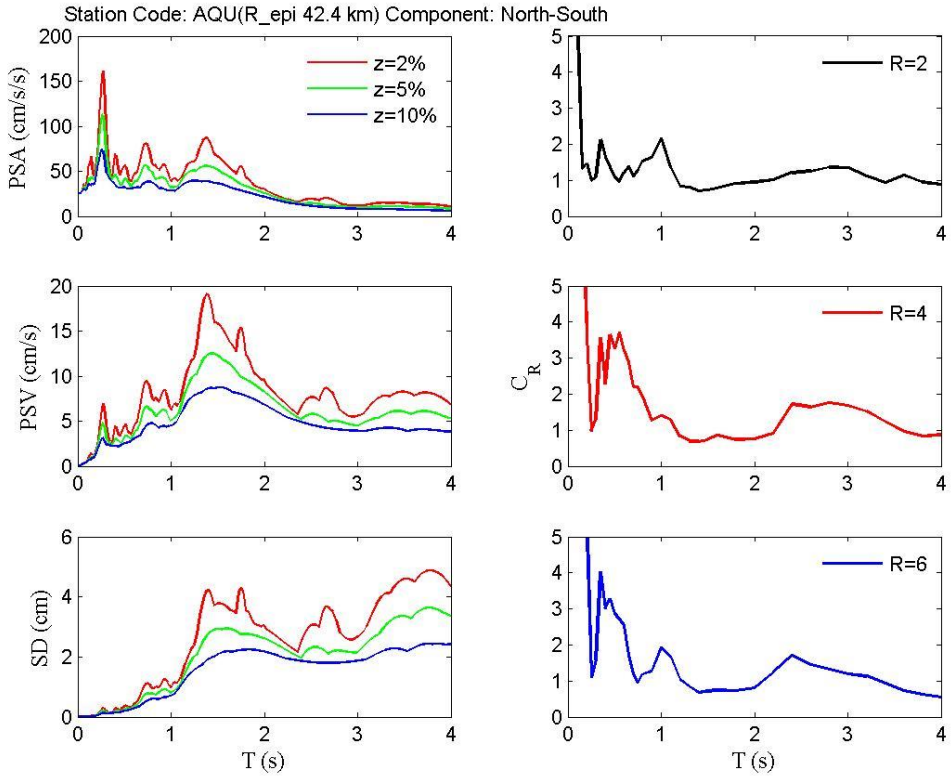
Station Code: AQU(R_epi 42.4 km) Component: North-South
PSA (cm/s/s)
PSV (cm/s)
SD (cm)
T (s)
z=2%
z=5%
z=10%
R=2
R=4
R=6
C_R

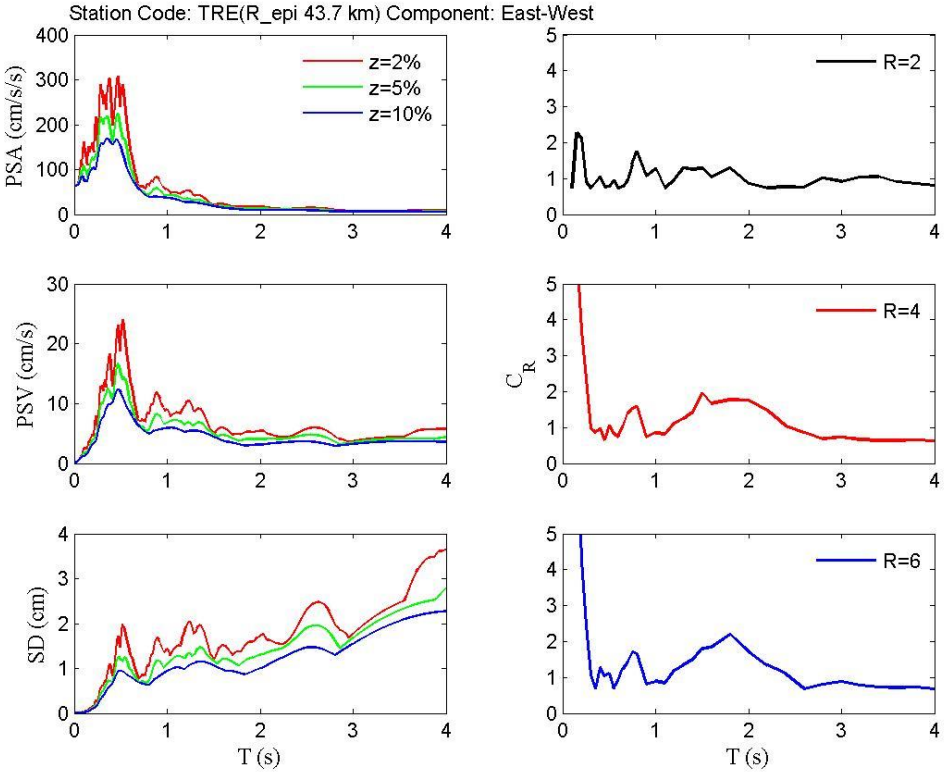
Station Code: TRE(R_epi 43.7 km) Component: East-West
PSA (cm/s/s)
PSV (cm/s)
SD (cm)
T (s)
z=2%
z=5%
z=10%
R=2
R=4
R=6
C_R

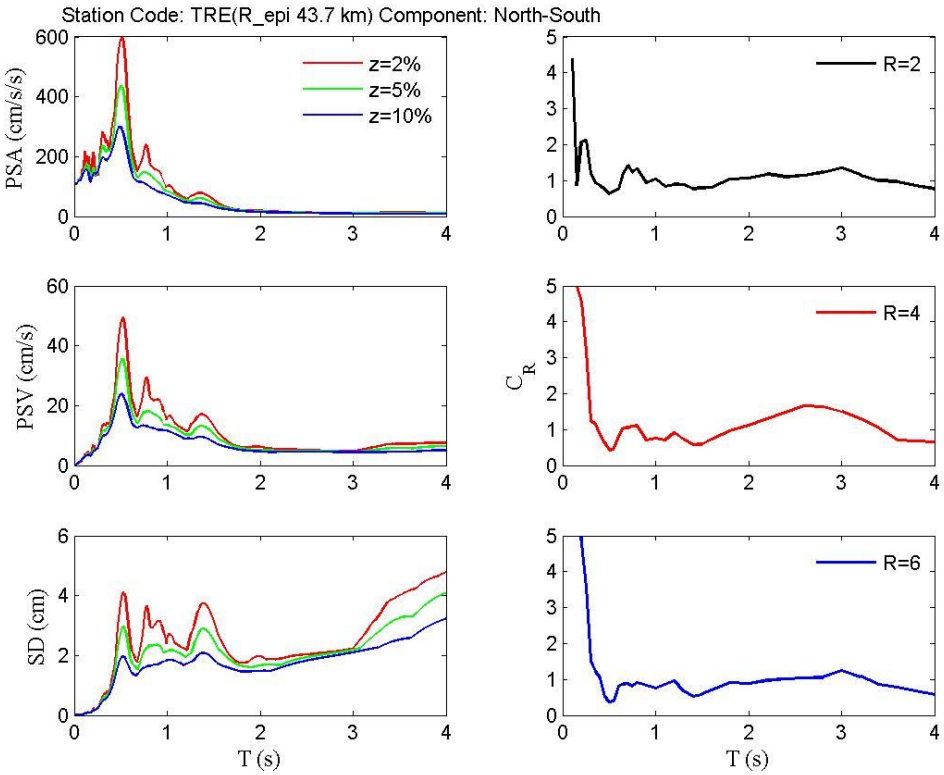
Station Code: TRE(R_epi 43.7 km) Component: North-South
PSA (cm/s/s)
PSV (cm/s)
SD (cm)
T (s)
z=2%
z=5%
z=10%
R=2
R=4
R=6
C_R

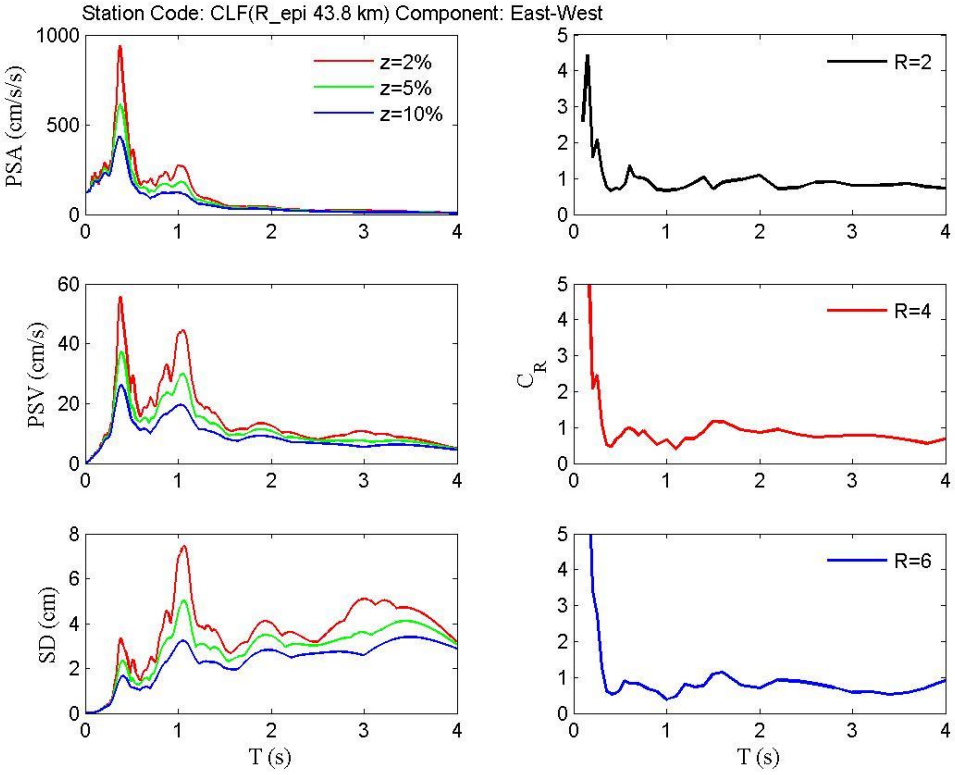
Station Code: CLF(R_epi 43.8 km) Component: East-West
PSA (cm/s/s)
PSV (cm/s)
SD (cm)
T (s)
z=2%
z=5%
z=10%
R=2
R=4
R=6
C_R

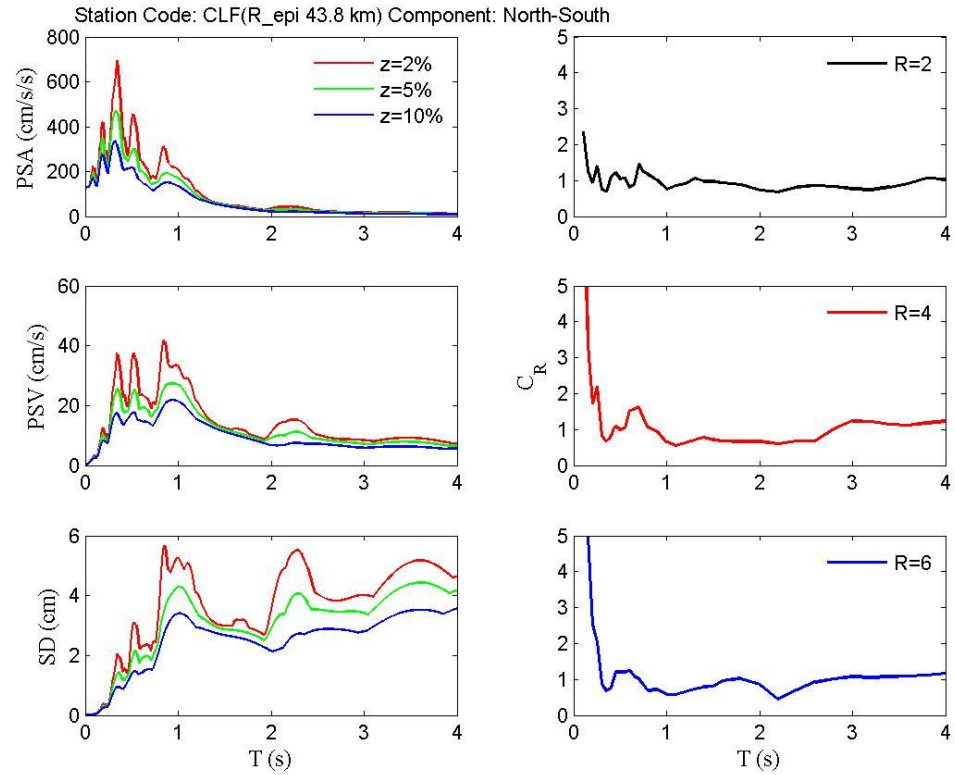
Station Code: CLF(R_epi 43.8 km) Component: North-South
PSA (cm/s/s)
PSV (cm/s)
SD (cm)
T (s)
z=2%
z=5%
z=10%
R=2
R=4
R=6
C_R

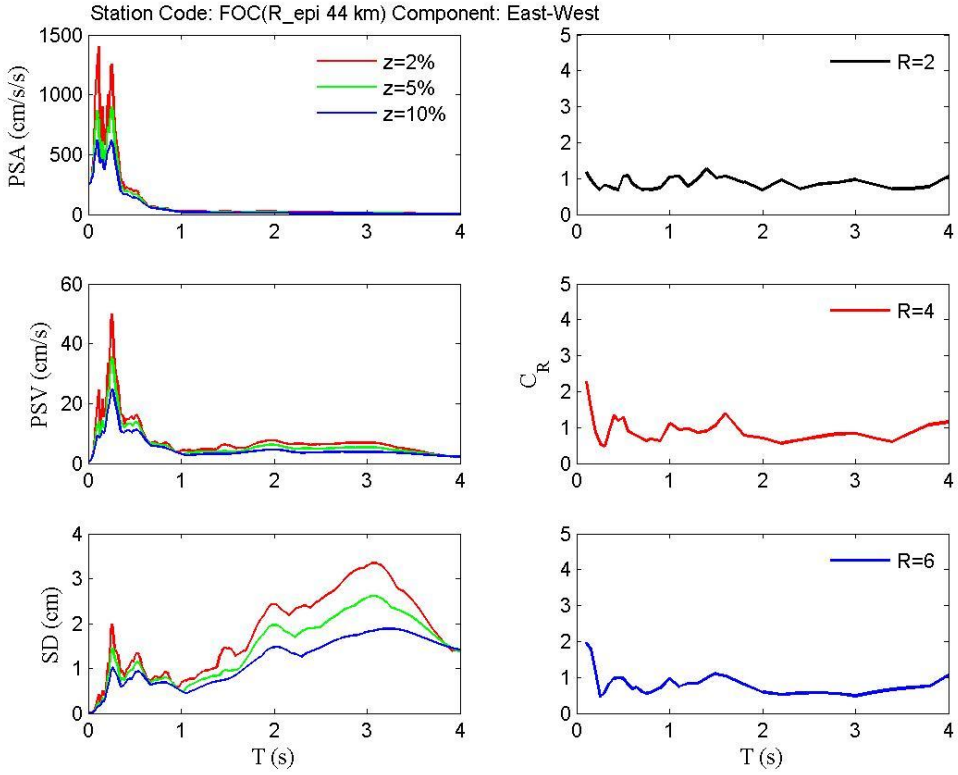
Station Code: FOC(R_epi 44 km) Component: East-West
PSA (cm/s/s)
PSV (cm/s)
SD (cm)
T (s)
z=2%
z=5%
z=10%
R=2
R=4
R=6
C_R

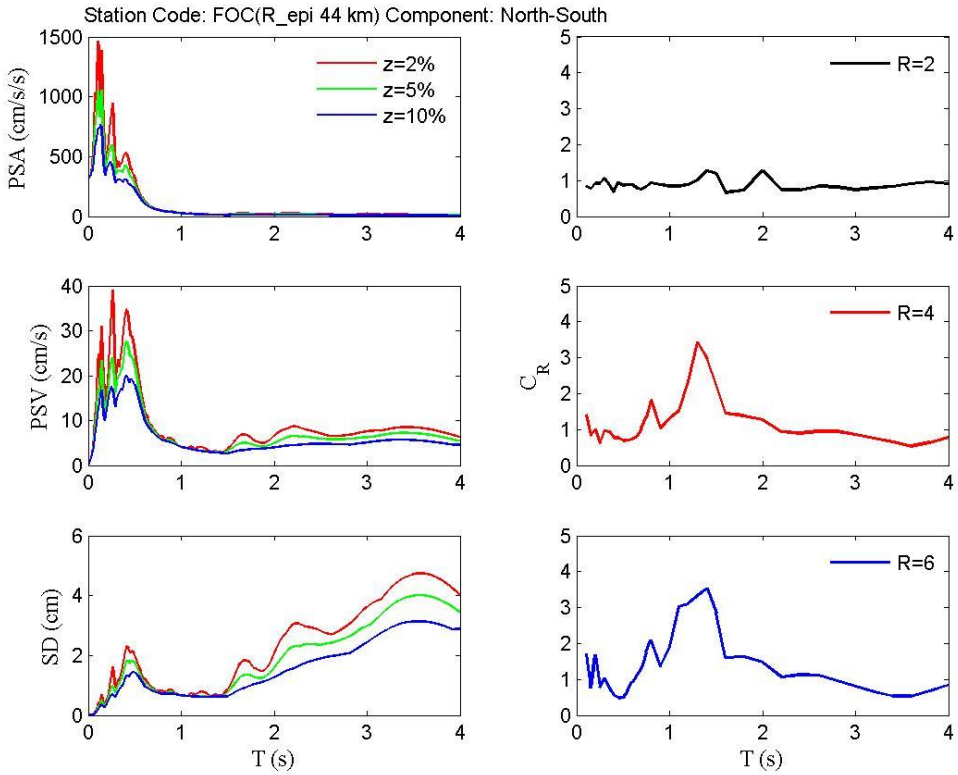
Station Code: FOC(R_epi 44 km) Component: North-South
PSA (cm/s/s)
PSV (cm/s)
SD (cm)
T (s)
z=2%
z=5%
z=10%
R=2
R=4
R=6
C_R

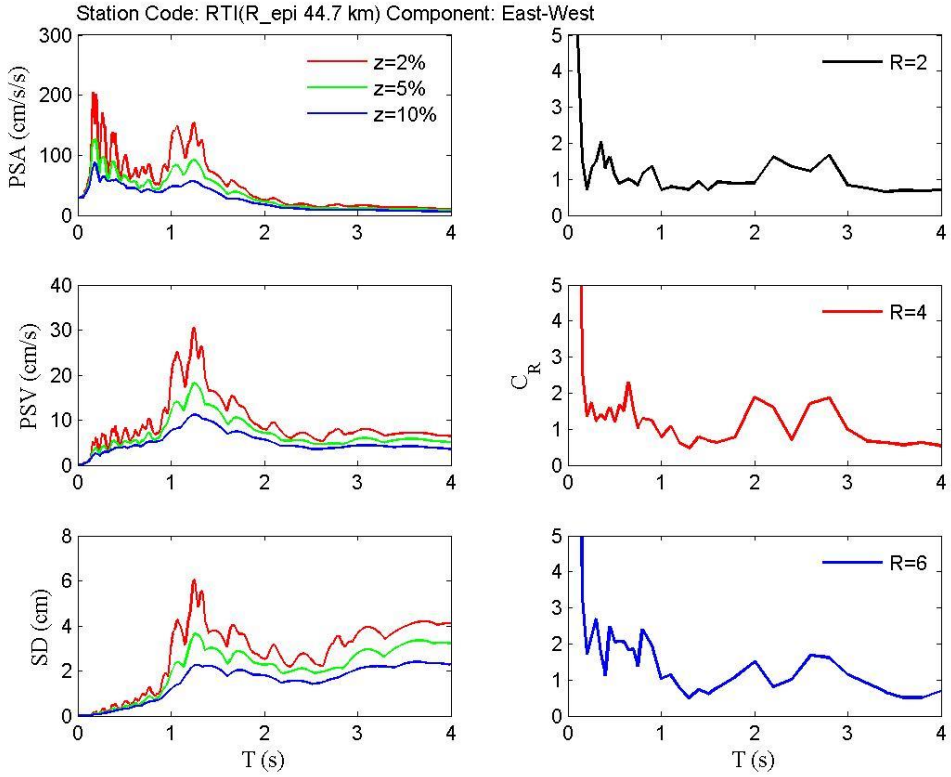
Station Code: RTI(R_epi 44.7 km) Component: East-West
PSA (cm/s/s)
PSV (cm/s)
SD (cm)
T (s)
z=2%
z=5%
z=10%
R=2
R=4
R=6
C_R

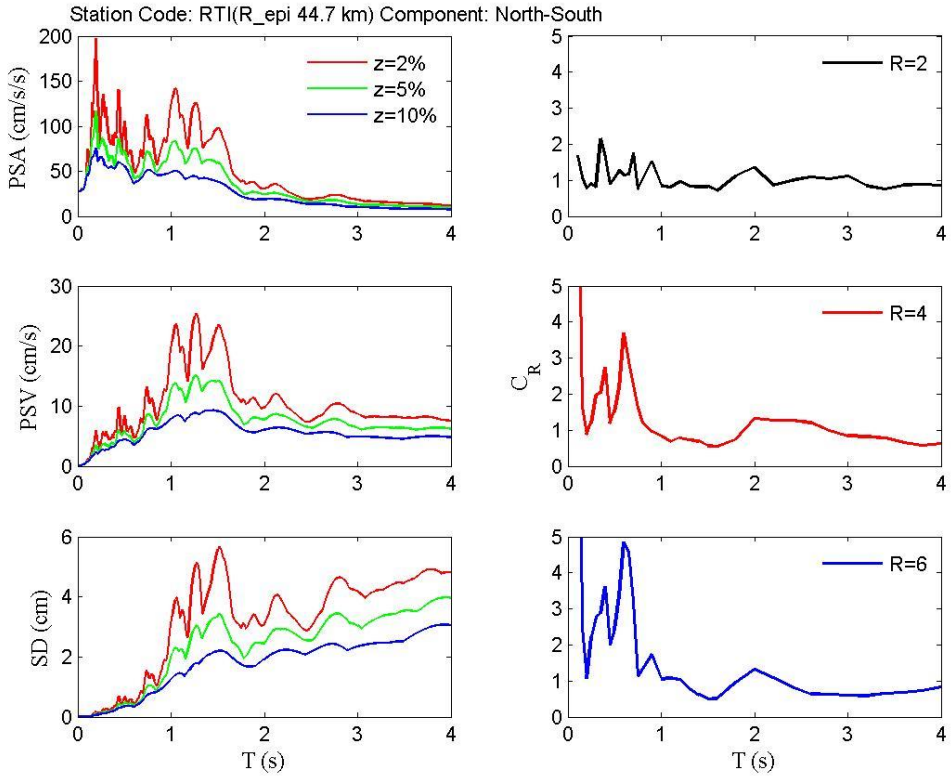
Station Code: RTI(R_epi 44.7 km) Component: North-South
PSA (cm/s/s)
PSV (cm/s)
SD (cm)
T (s)
z=2%
z=5%
z=10%
R=2
R=4
R=6
C_R

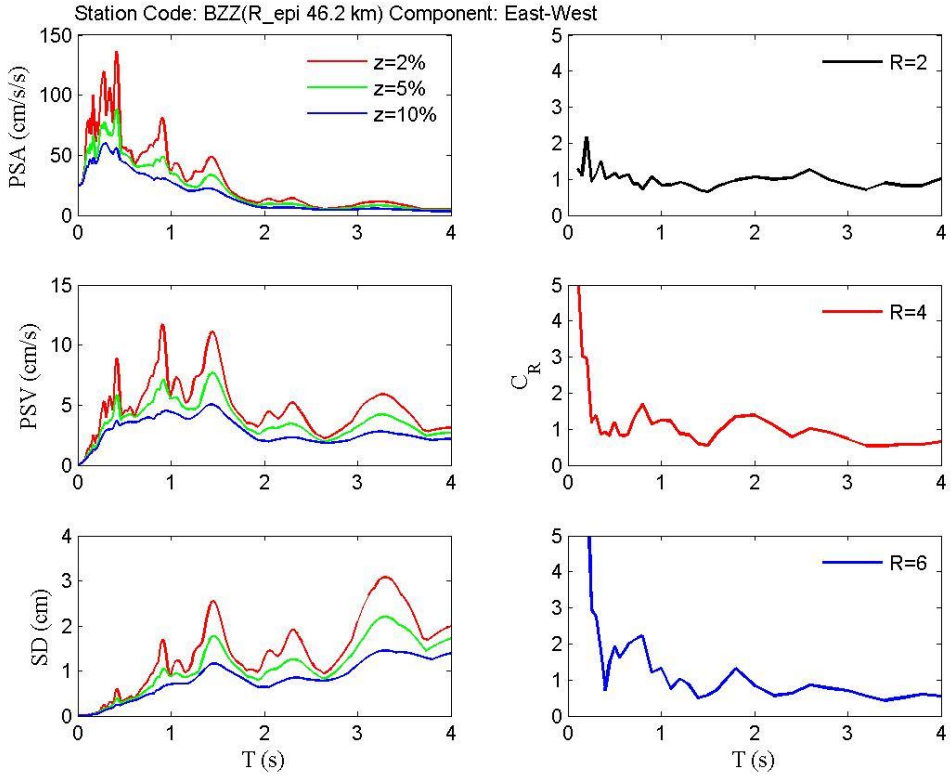
Station Code: BZZ(R_epi 46.2 km) Component: East-West
PSA (cm/s/s)
PSV (cm/s)
SD (cm)
T (s)
z=2%
z=5%
z=10%
R=2
R=4
R=6
C_R

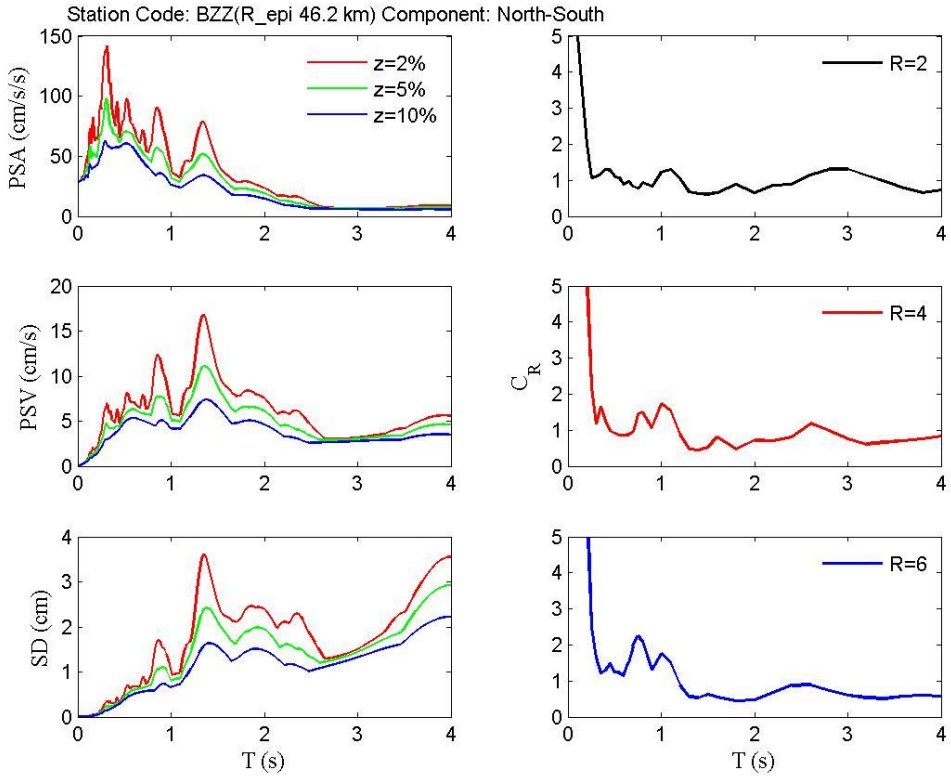
Station Code: BZZ(R_epi 46.2 km) Component: North-South
PSA (cm/s/s)
PSV (cm/s)
SD (cm)
T (s)
z=2%
z=5%
z=10%
R=2
R=4
R=6
C_R

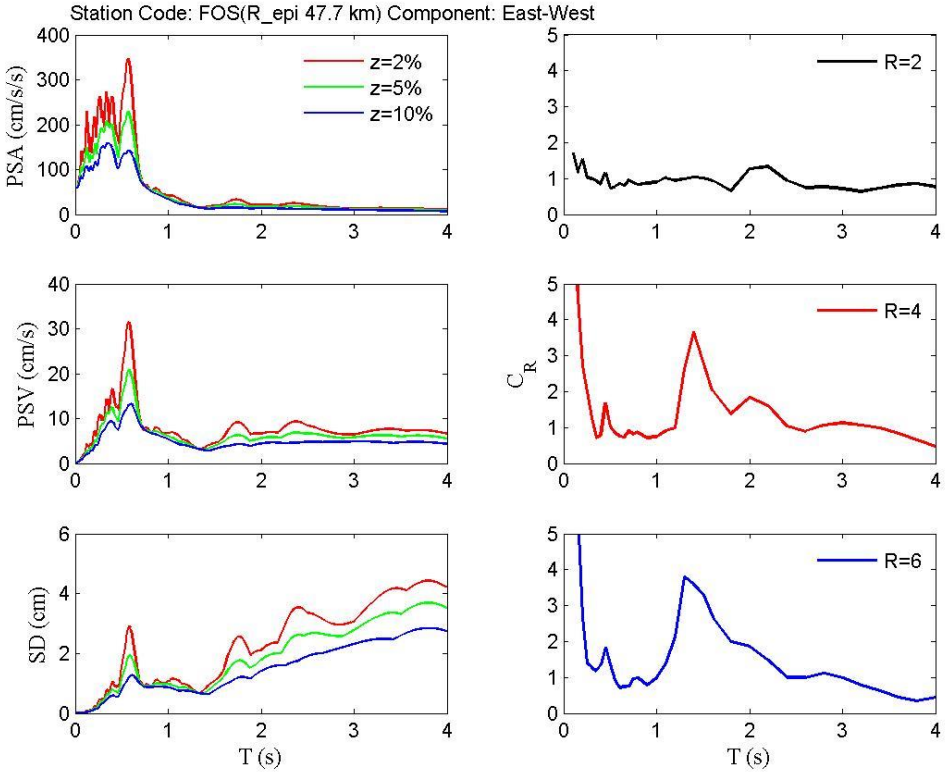
Station Code: FOS(R_epi 47.7 km) Component: East-West
PSA (cm/s/s)
PSV (cm/s)
SD (cm)
T (s)
z=2%
z=5%
z=10%
R=2
R=4
R=6
C_R

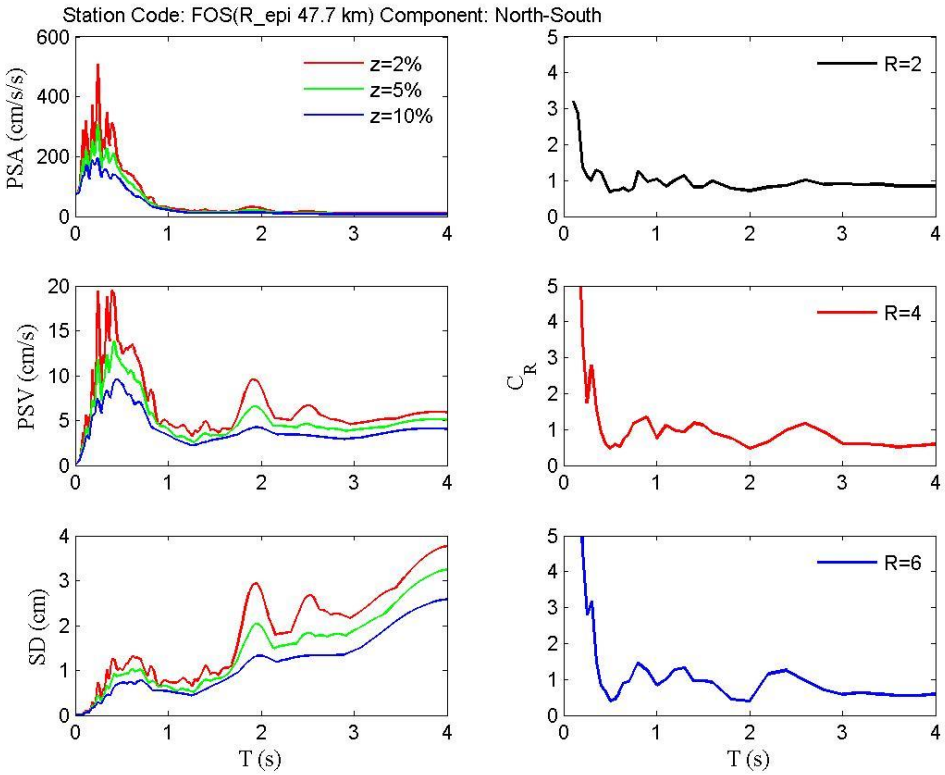
Station Code: FOS(R_epi 47.7 km) Component: North-South
PSA (cm/s/s)
PSV (cm/s)
SD (cm)
T (s)
z=2%
z=5%
z=10%
R=2
R=4
R=6
C_R

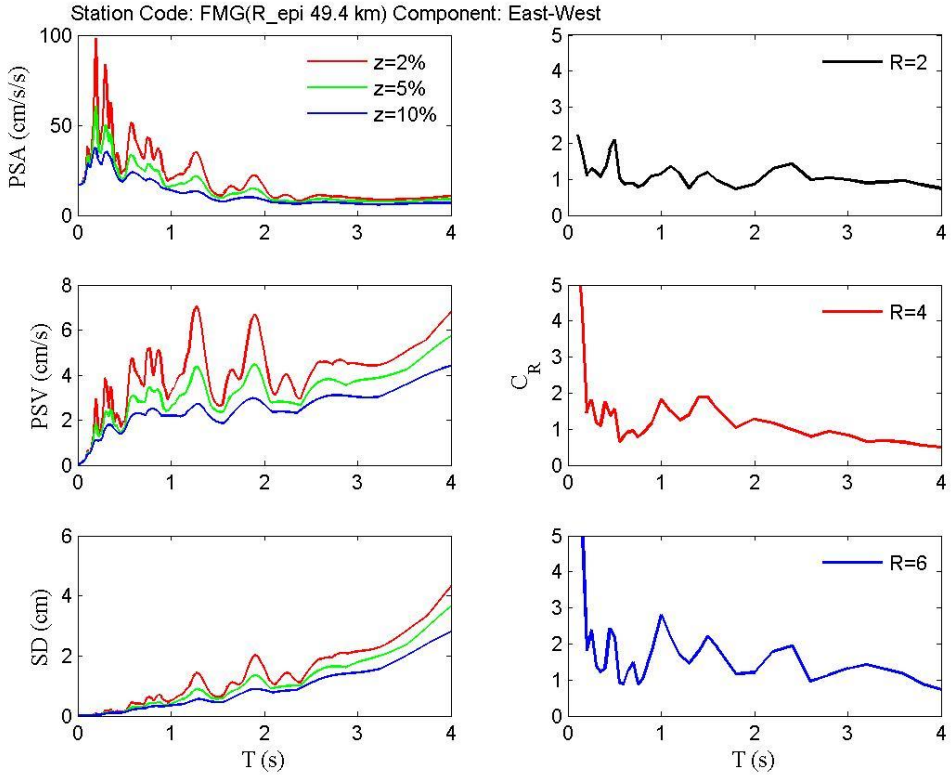
Station Code: FMG(R_epi 49.4 km) Component: East-West
PSA (cm/s/s)
PSV (cm/s)
SD (cm)
T (s)
z=2%
z=5%
z=10%
R=2
R=4
R=6
C_R

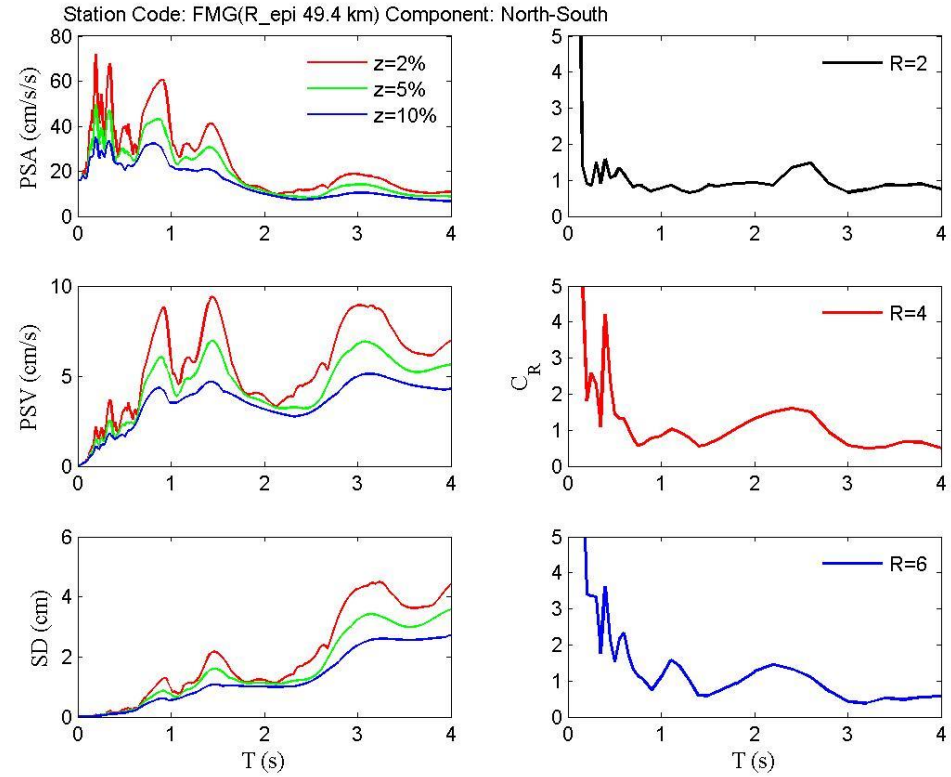
Station Code: FMG(R_epi 49.4 km) Component: North-South
PSA (cm/s/s)
PSV (cm/s)
SD (cm)
T (s)
z=2%
z=5%
z=10%
R=2
R=4
R=6
C_R

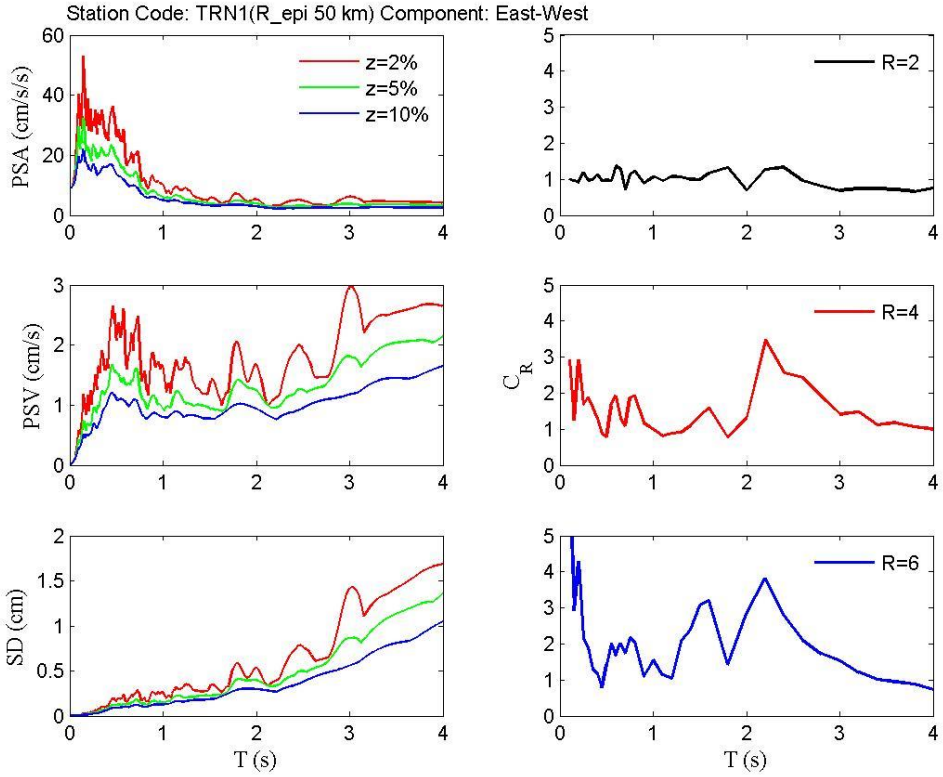
Station Code: TRN1(R_epi 50 km) Component: East-West
PSA (cm/s/s)
z=2%
z=5%
z=10%
PSV (cm/s)
SD (cm)
T (s)
R=2
R=4
R=6
C_R
T (s)

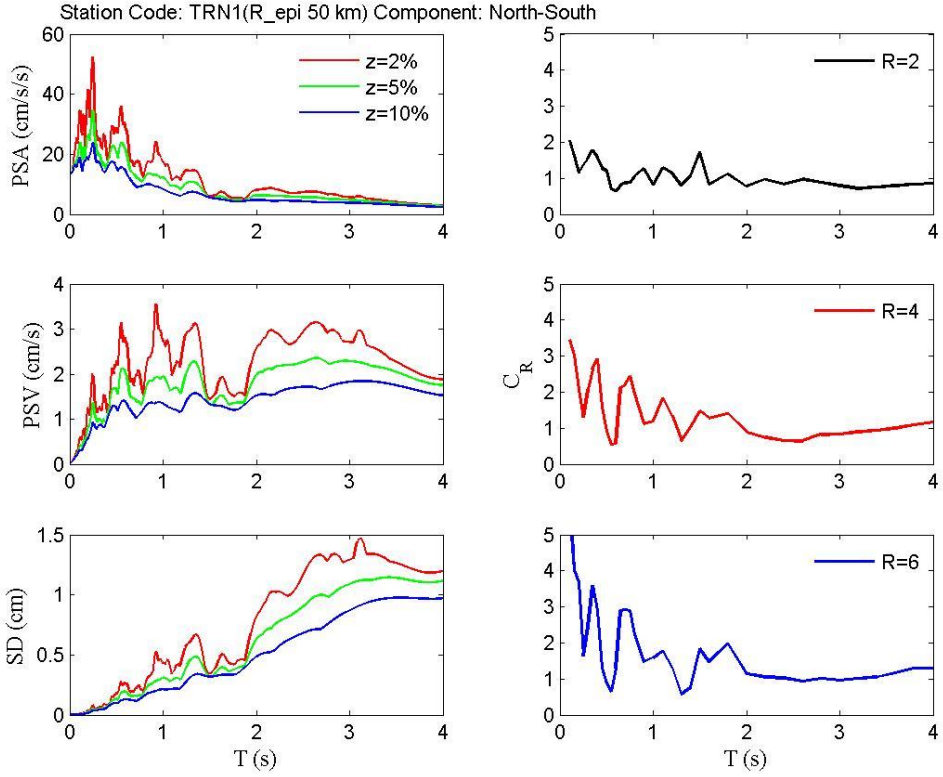
Station Code: TRN1(R_epi 50 km) Component: North-South
PSA (cm/s/s)
z=2%
z=5%
z=10%
PSV (cm/s)
SD (cm)
T (s)
R=2
R=4
R=6
C_R
T (s)

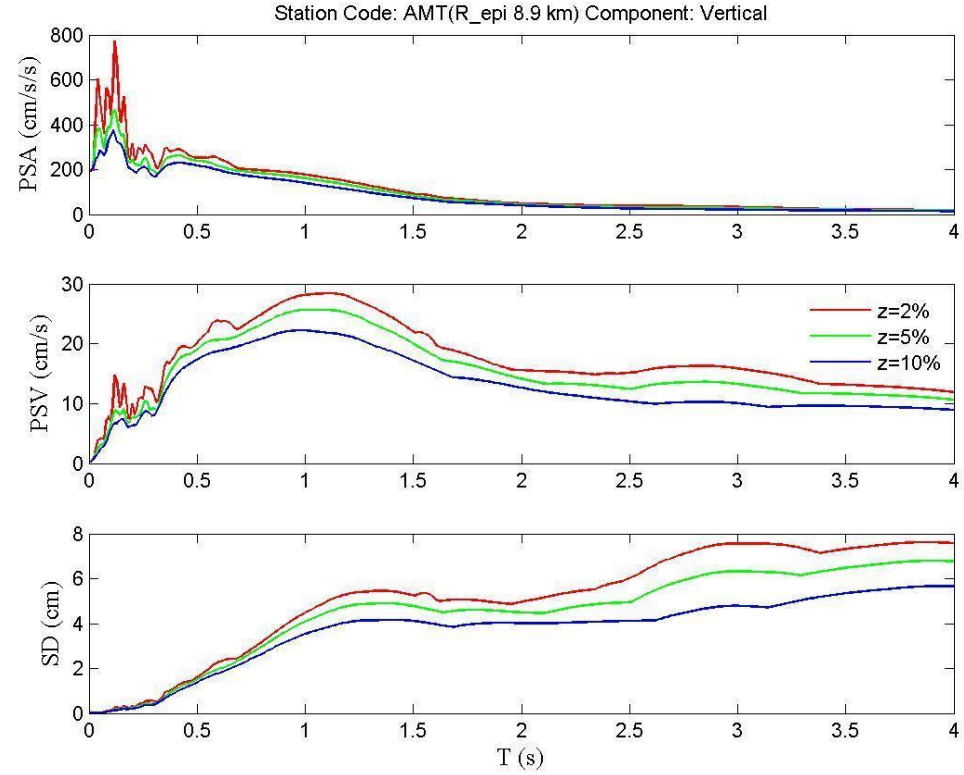
Station Code: AMT(R_epi 8.9 km) Component: Vertical
PSA (cm/s/s)
PSV (cm/s)
SD (cm)
z=2%
z=5%
z=10%
T (s)

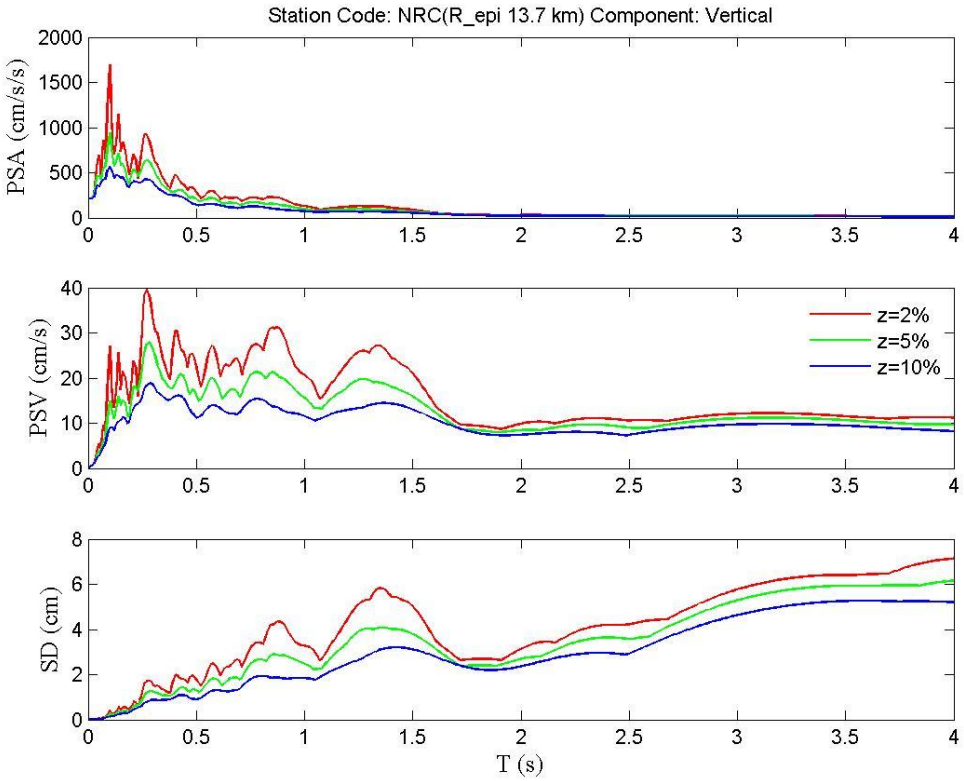
Station Code: NRC(R_epi 13.7 km) Component: Vertical
PSA (cm/s/s)
PSV (cm/s)
SD (cm)
z=2%
z=5%
z=10%
T (s)

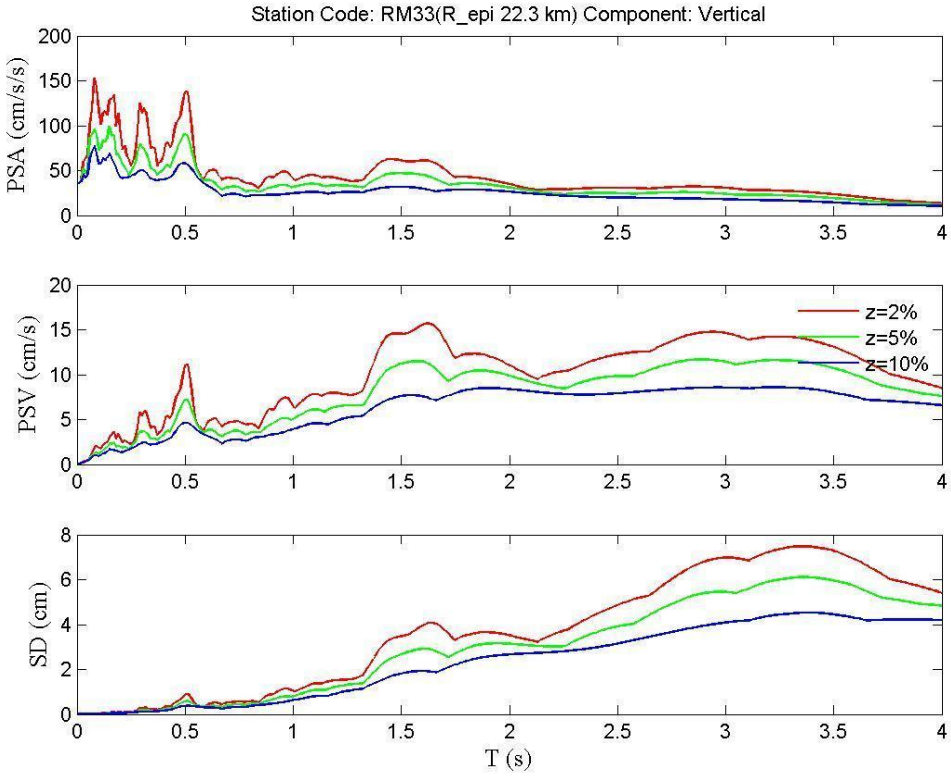
Station Code: RM33(R_epi 22.3 km) Component: Vertical
PSA (cm/s/s)
PSV (cm/s)
SD (cm)
z=2%
z=5%
z=10%
T (s)

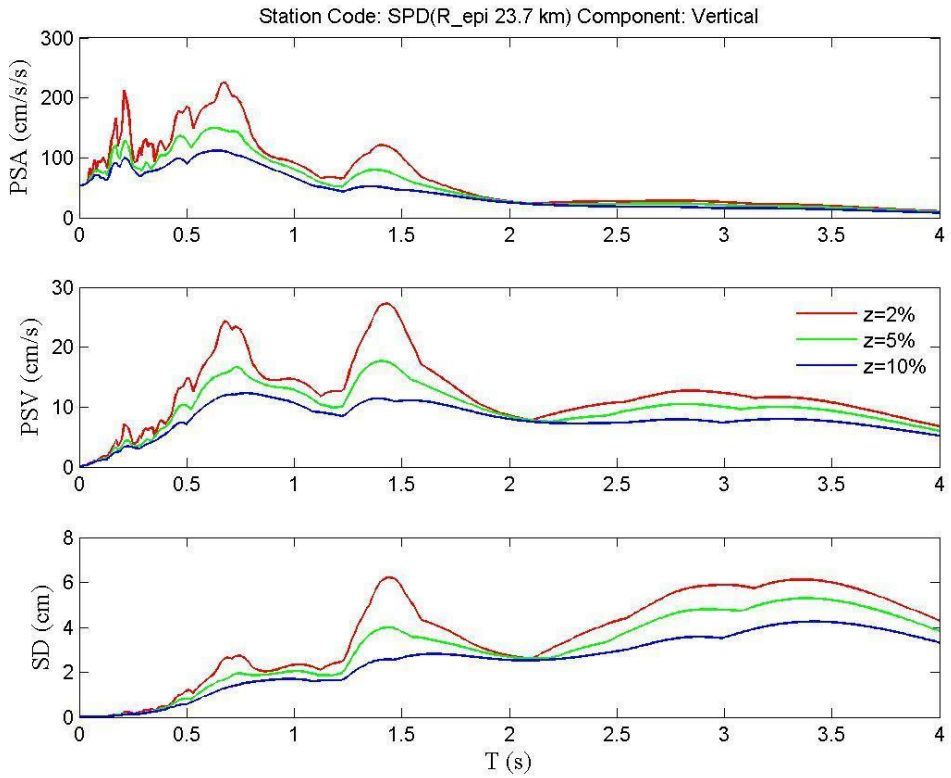
Station Code: SPD(R_epi 23.7 km) Component: Vertical
PSA (cm/s/s)
PSV (cm/s)
SD (cm)
z=2%
z=5%
z=10%
T (s)

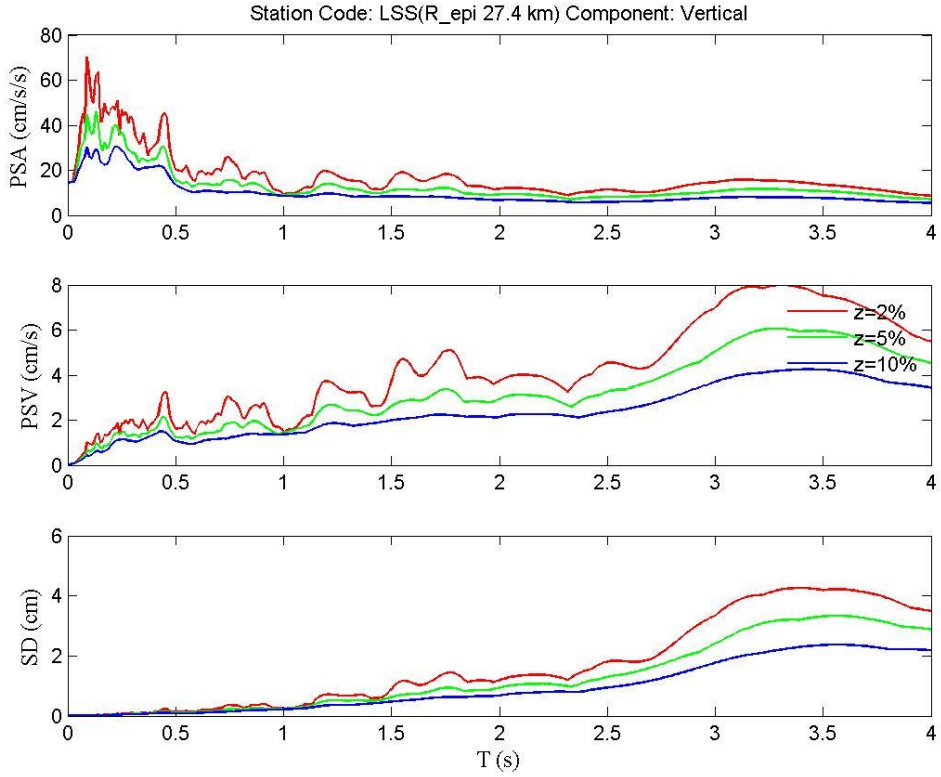
Station Code: LSS(R_epi 27.4 km) Component: Vertical
PSA (cm/s/s)
PSV (cm/s)
SD (cm)
z=2%
z=5%
z=10%
T (s)

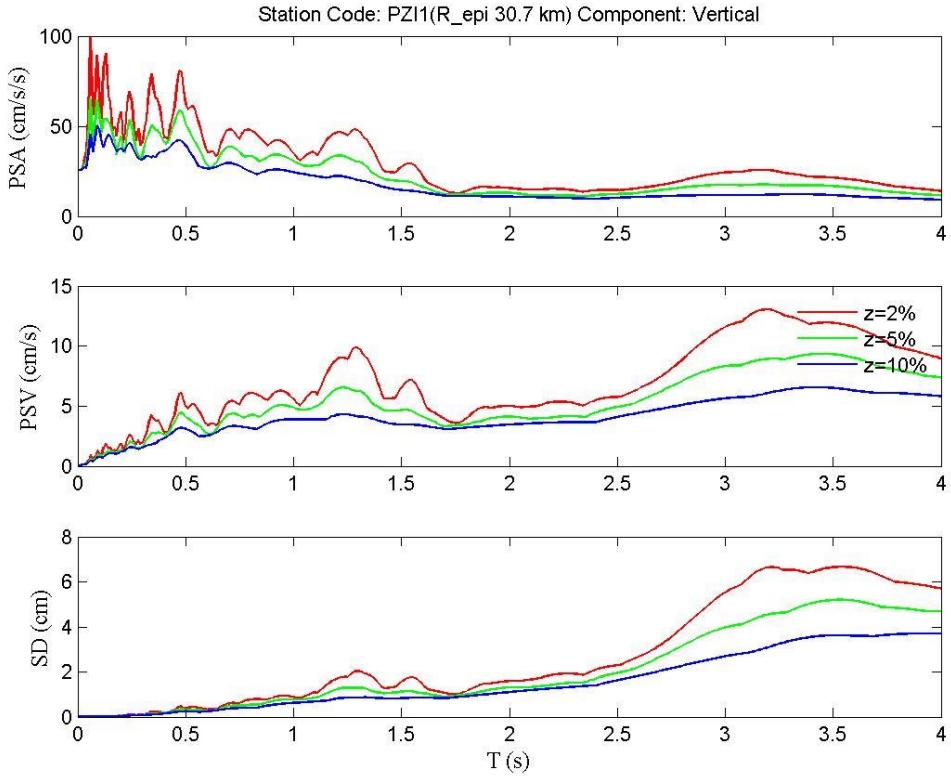
Station Code: PZI1(R_epi 30.7 km) Component: Vertical
PSA (cm/s/s)
PSV (cm/s)
SD (cm)
z=2%
z=5%
z=10%
T (s)

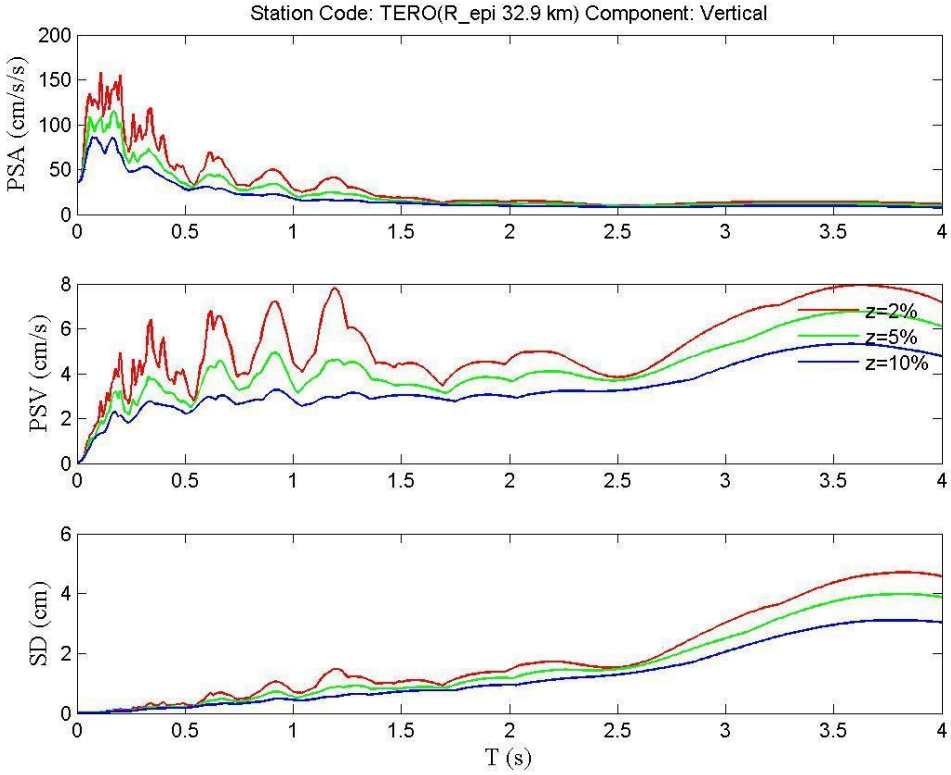
Station Code: TERO(R_epi 32.9 km) Component: Vertical
PSA (cm/s/s)
PSV (cm/s)
SD (cm)
T (s)
z=2%
z=5%
z=10%

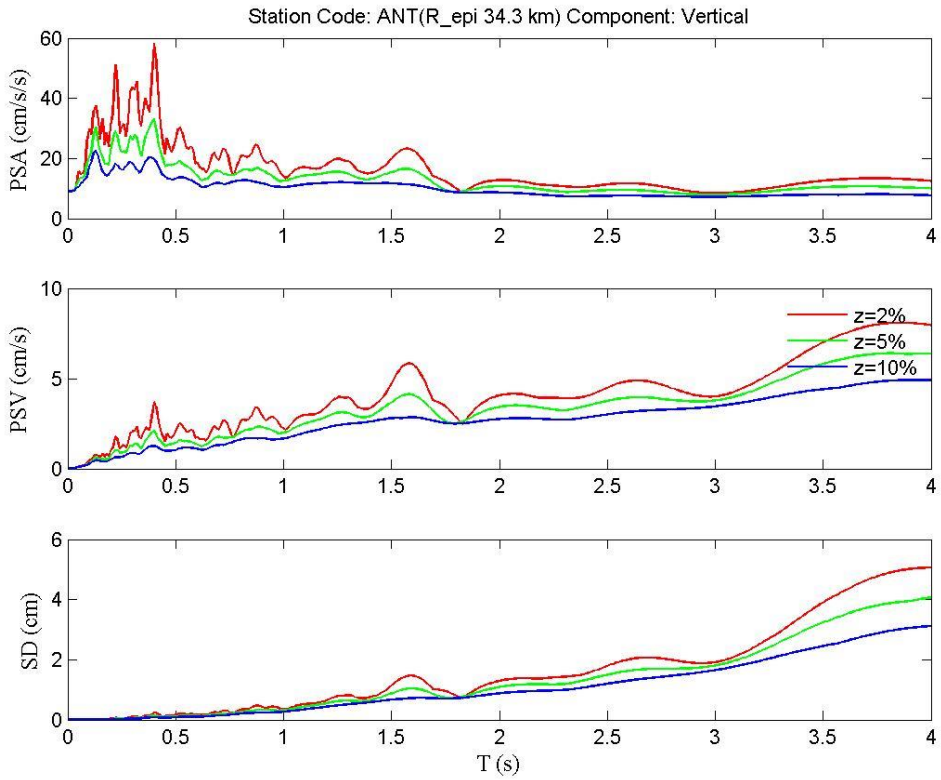
Station Code: ANT(R_epi 34.3 km) Component: Vertical
PSA (cm/s/s)
PSV (cm/s)
SD (cm)
T (s)
z=2%
z=5%
z=10%

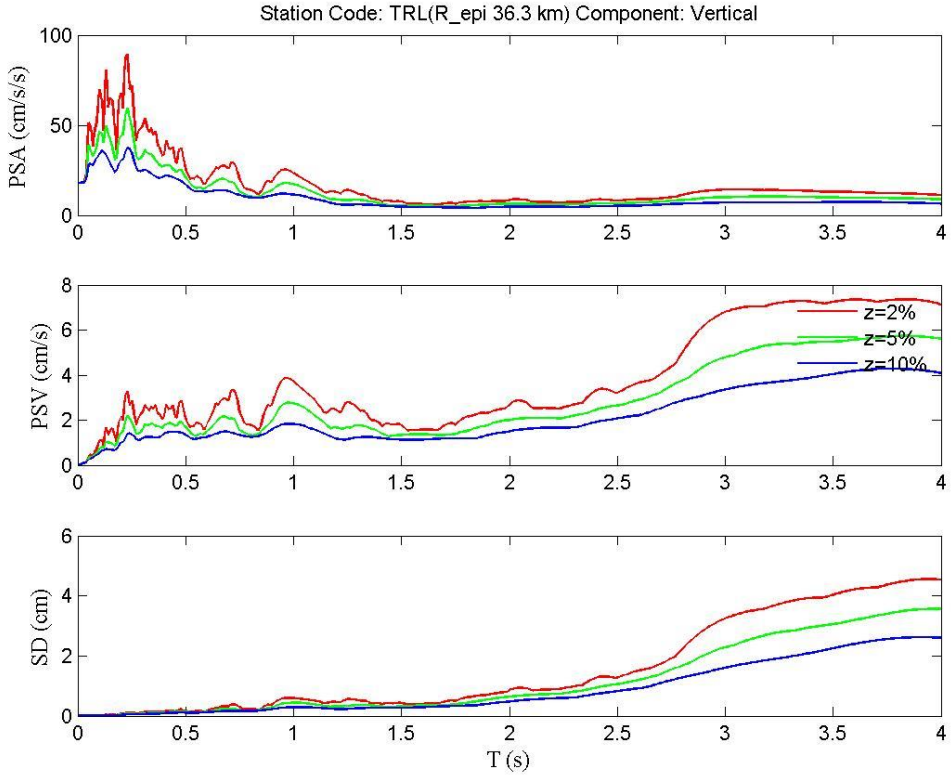
Station Code: TRL(R_epi 36.3 km) Component: Vertical
PSA (cm/s/s)
PSV (cm/s)
SD (cm)
z=2%
z=5%
z=10%
T (s)

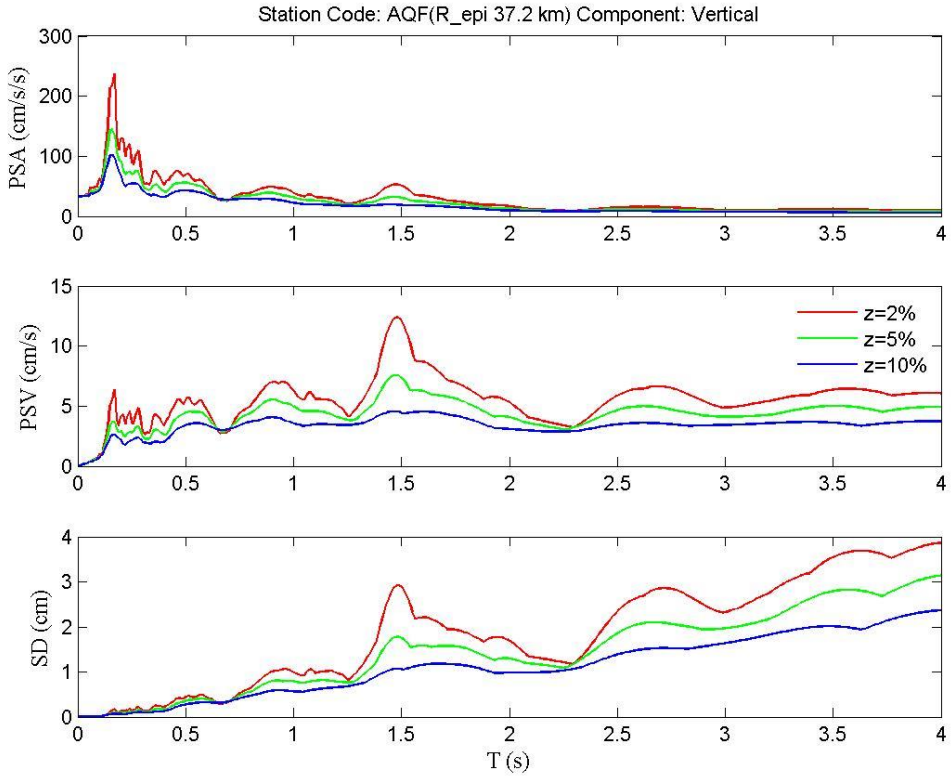
Station Code: AQF(R_epi 37.2 km) Component: Vertical
PSA (cm/s/s)
PSV (cm/s)
SD (cm)
z=2%
z=5%
z=10%
T (s)

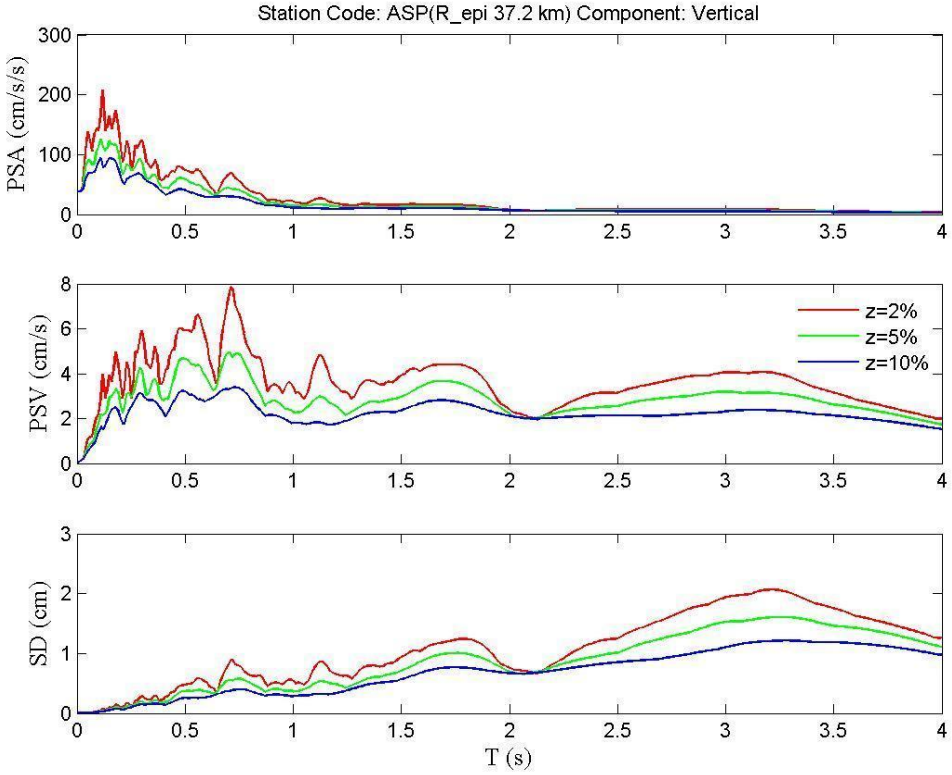
Station Code: ASP(R_epi 37.2 km) Component: Vertical
PSA (cm/s/s)
PSV (cm/s)
SD (cm)
z=2%
z=5%
z=10%
T (s)

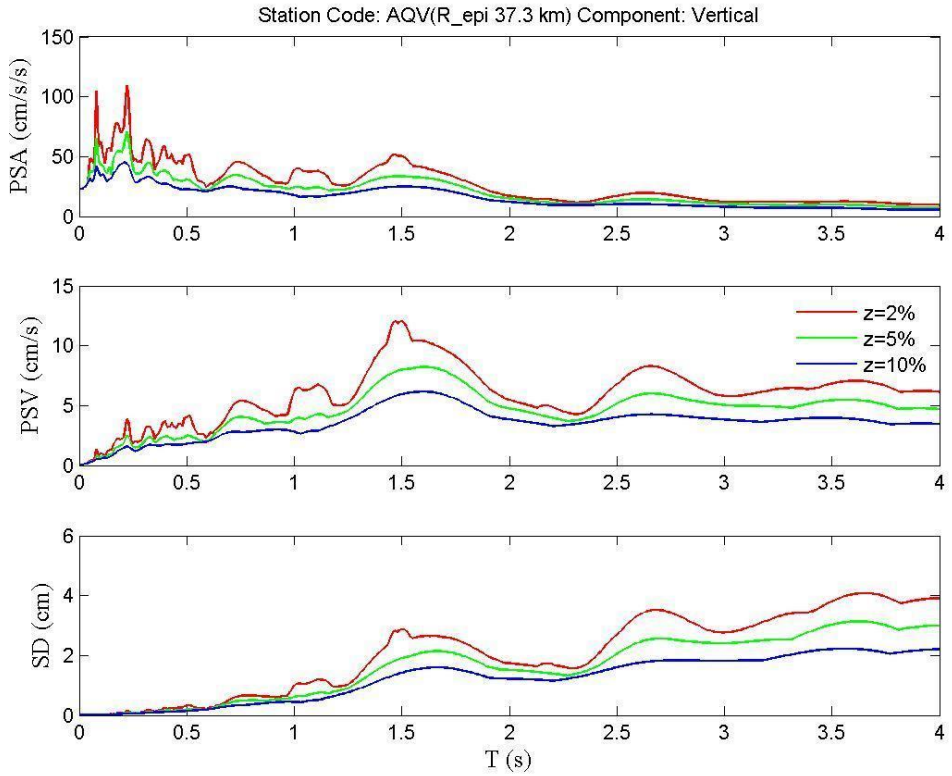
Station Code: AQV(R_epi 37.3 km) Component: Vertical
PSA (cm/s/s)
PSV (cm/s)
SD (cm)
z=2%
z=5%
z=10%
T (s)

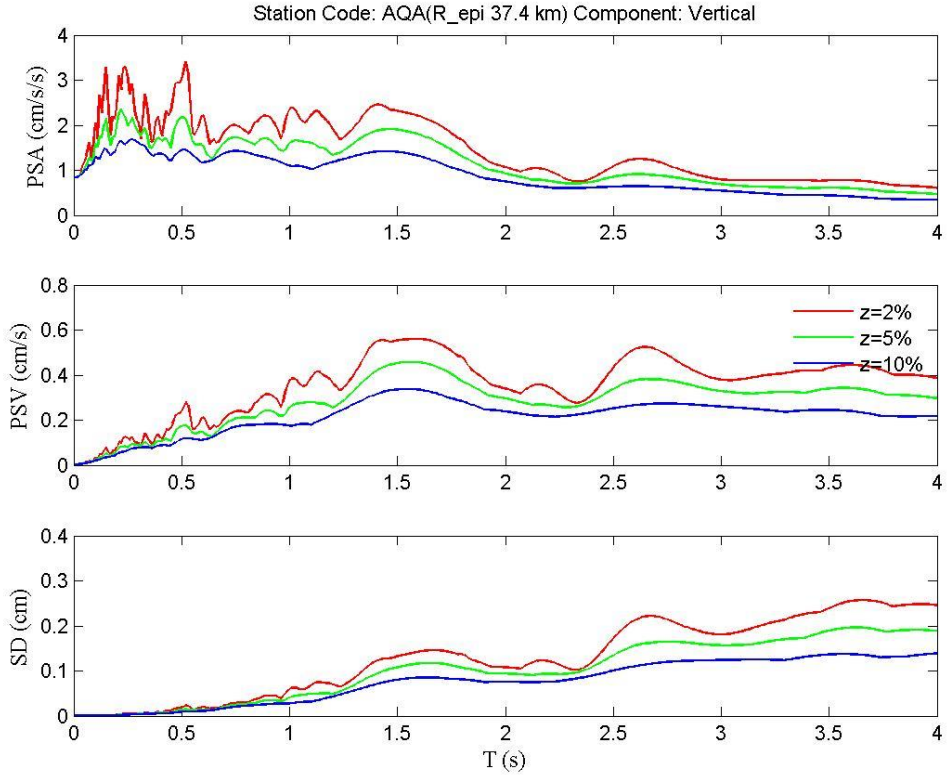
Station Code: AQA(R_epi 37.4 km) Component: Vertical
PSA (cm/s/s)
PSV (cm/s)
SD (cm)
z=2%
z=5%
z=10%
T (s)

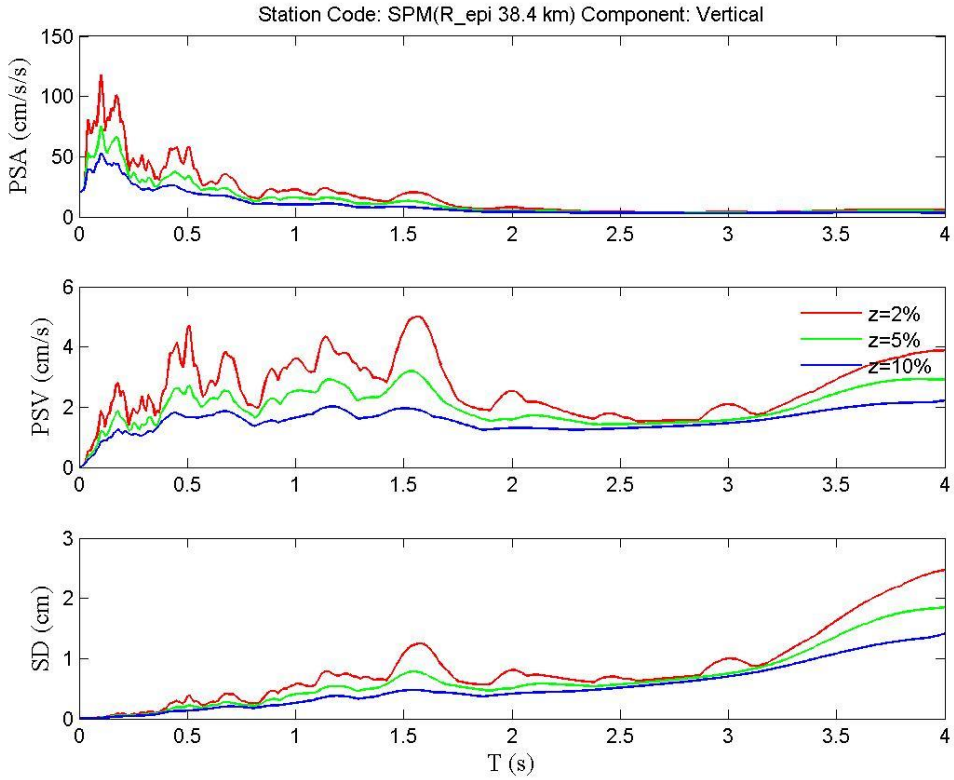
Station Code: SPM(R_epi 38.4 km) Component: Vertical
PSA (cm/s/s)
PSV (cm/s)
SD (cm)
z=2%
z=5%
z=10%
T (s)

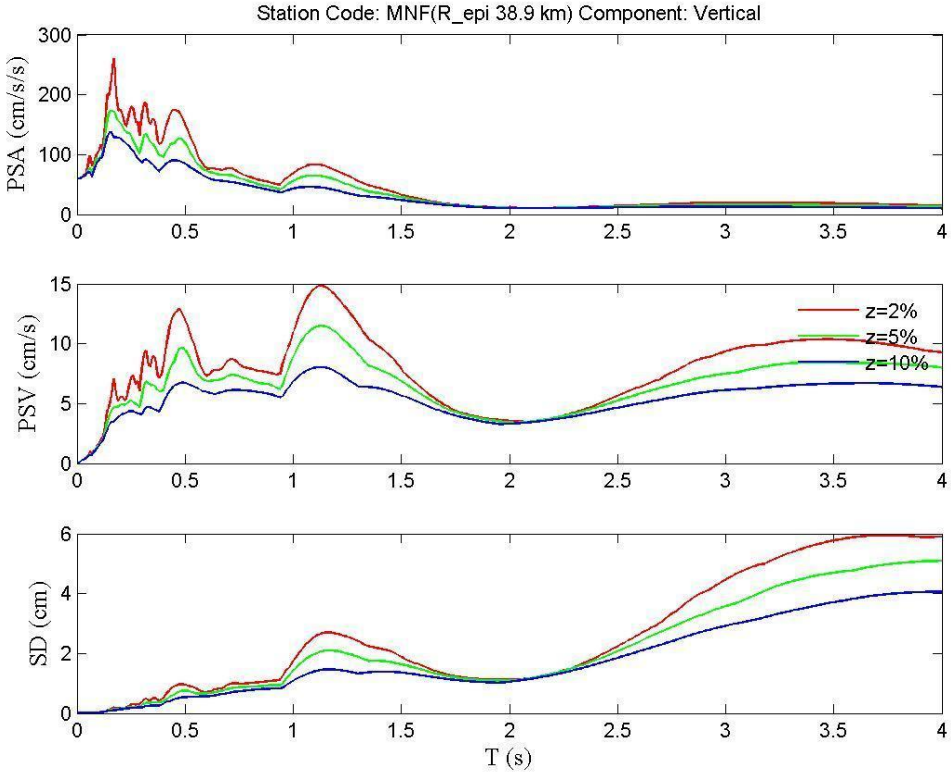
Station Code: MNF(R_epi 38.9 km) Component: Vertical
PSA (cm/s/s)
PSV (cm/s)
SD (cm)
T (s)
z=2%
z=5%
z=10%

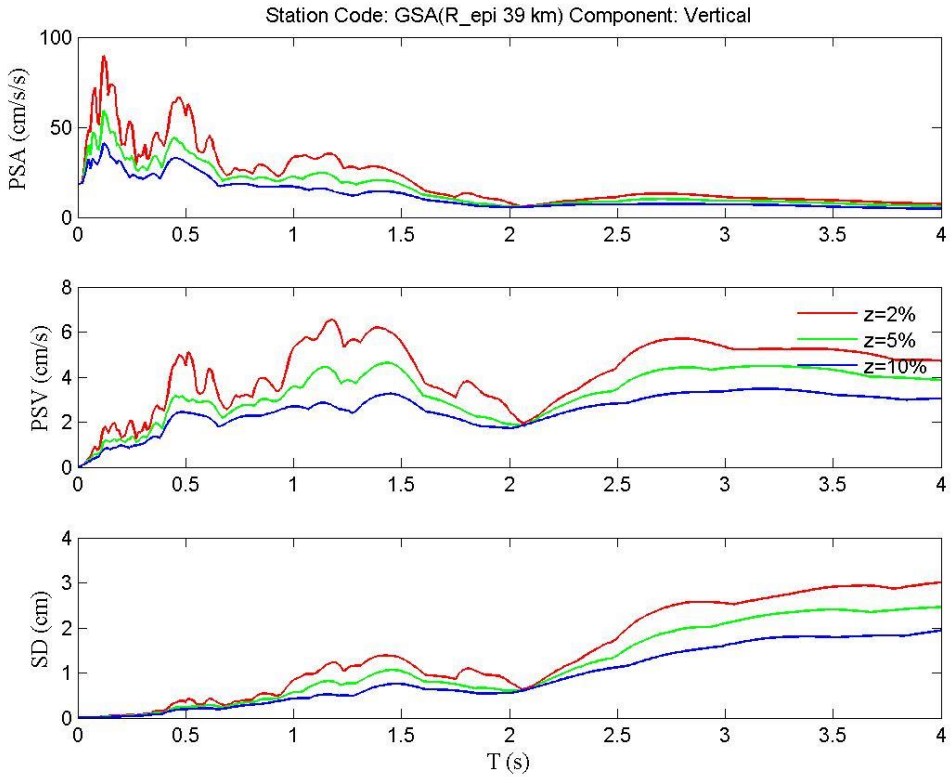
Station Code: GSA(R_epi 39 km) Component: Vertical
PSA (cm/s/s)
PSV (cm/s)
SD (cm)
T (s)
z=2%
z=5%
z=10%

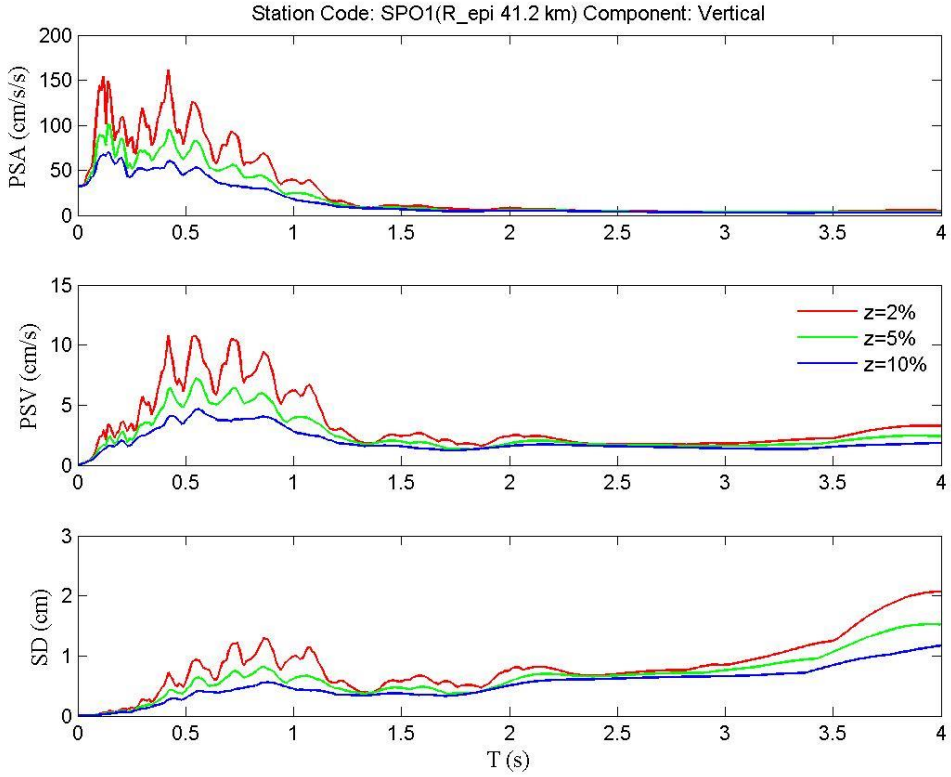
Station Code: SPO1(R_epi 41.2 km) Component: Vertical
PSA (cm/s/s)
PSV (cm/s)
SD (cm)
z=2%
z=5%
z=10%
T (s)

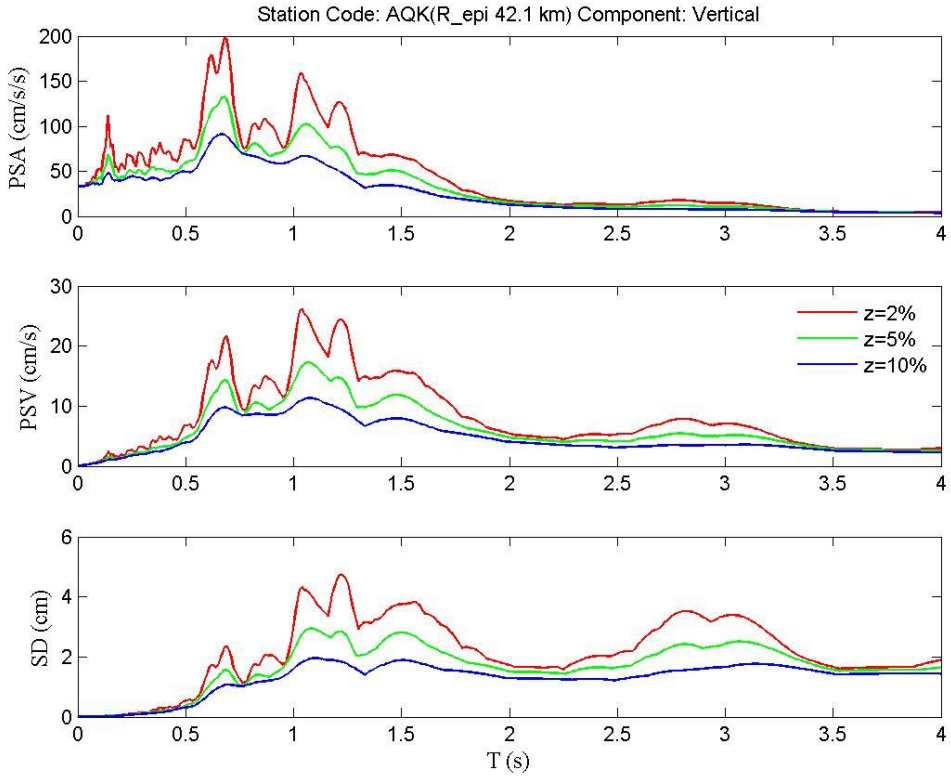
Station Code: AQK(R_epi 42.1 km) Component: Vertical
PSA (cm/s/s)
PSV (cm/s)
SD (cm)
z=2%
z=5%
z=10%
T (s)

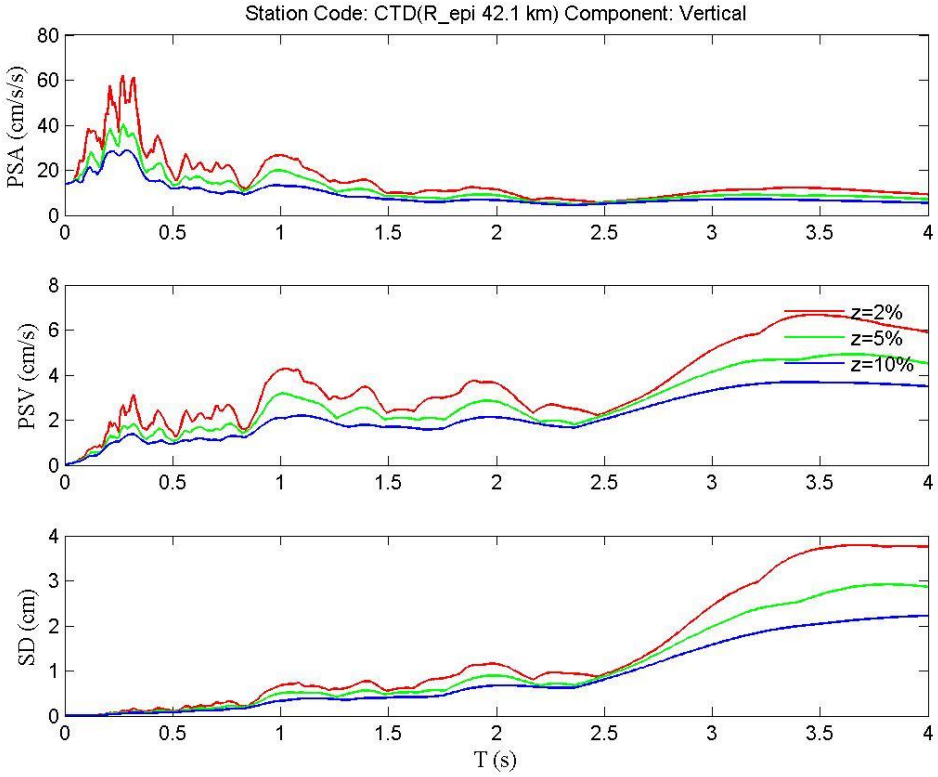
Station Code: CTD(R_epi 42.1 km) Component: Vertical
PSA (cm/s/s)
PSV (cm/s)
SD (cm)
z=2%
z=5%
z=10%
T (s)

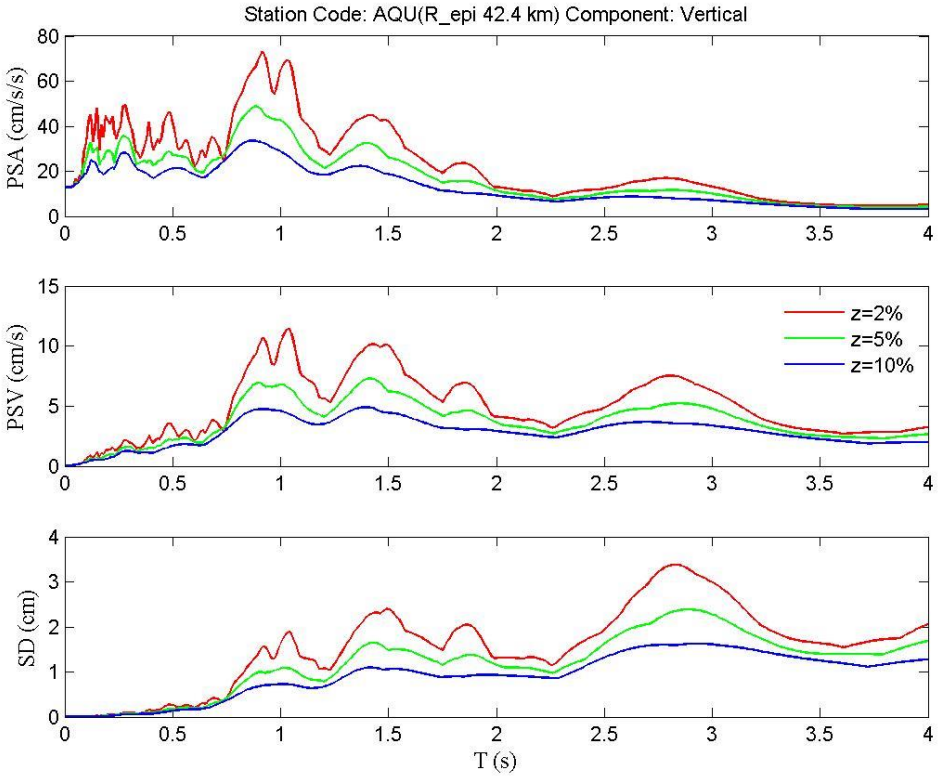
Station Code: AQU(R_epi 42.4 km) Component: Vertical
PSA (cm/s/s)
PSV (cm/s)
SD (cm)
z=2%
z=5%
z=10%
T (s)

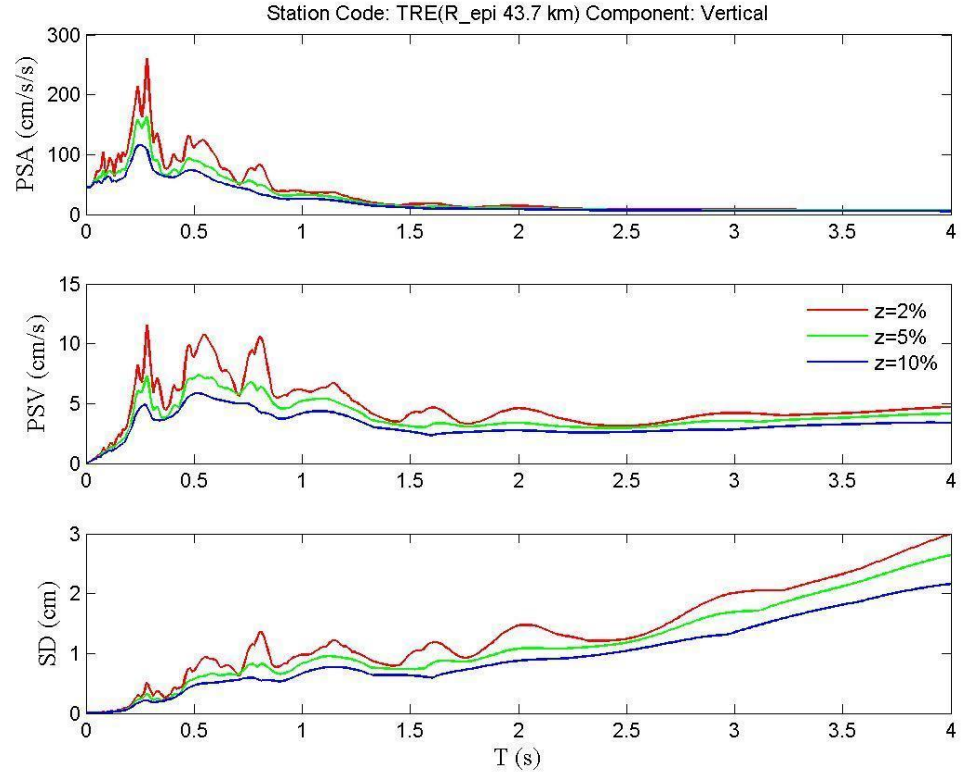
Station Code: TRE(R_epi 43.7 km) Component: Vertical
PSA (cm/s/s)
PSV (cm/s)
SD (cm)
z=2%
z=5%
z=10%
T (s)

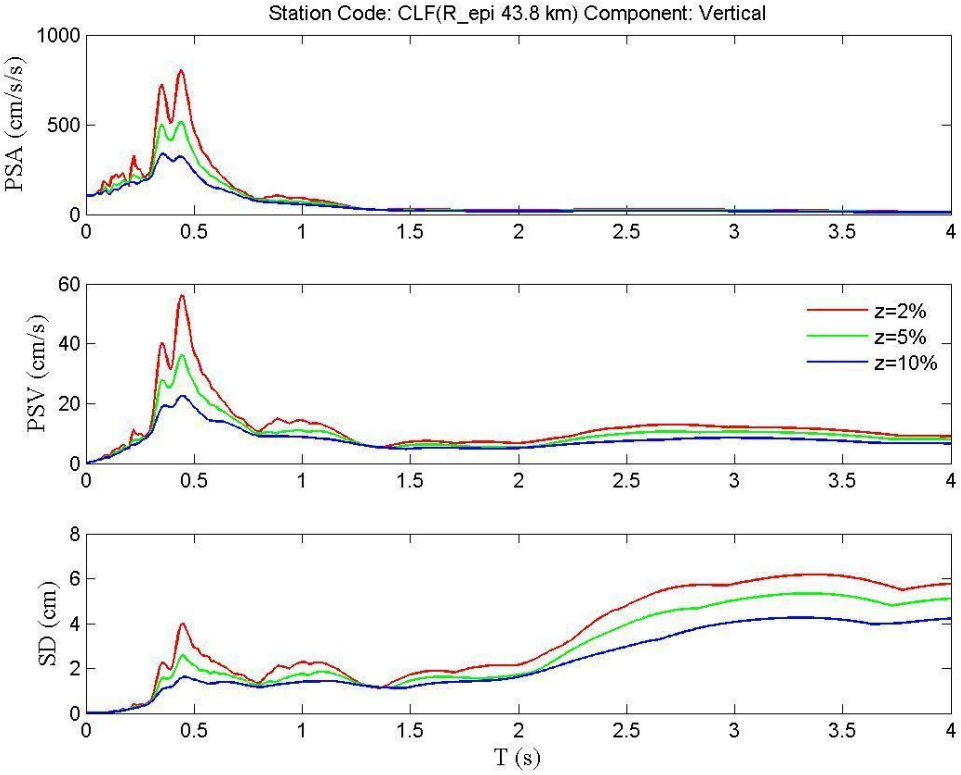
Station Code: CLF(R_epi 43.8 km) Component: Vertical
PSA (cm/s/s)
PSV (cm/s)
SD (cm)
z=2%
z=5%
z=10%
T (s)

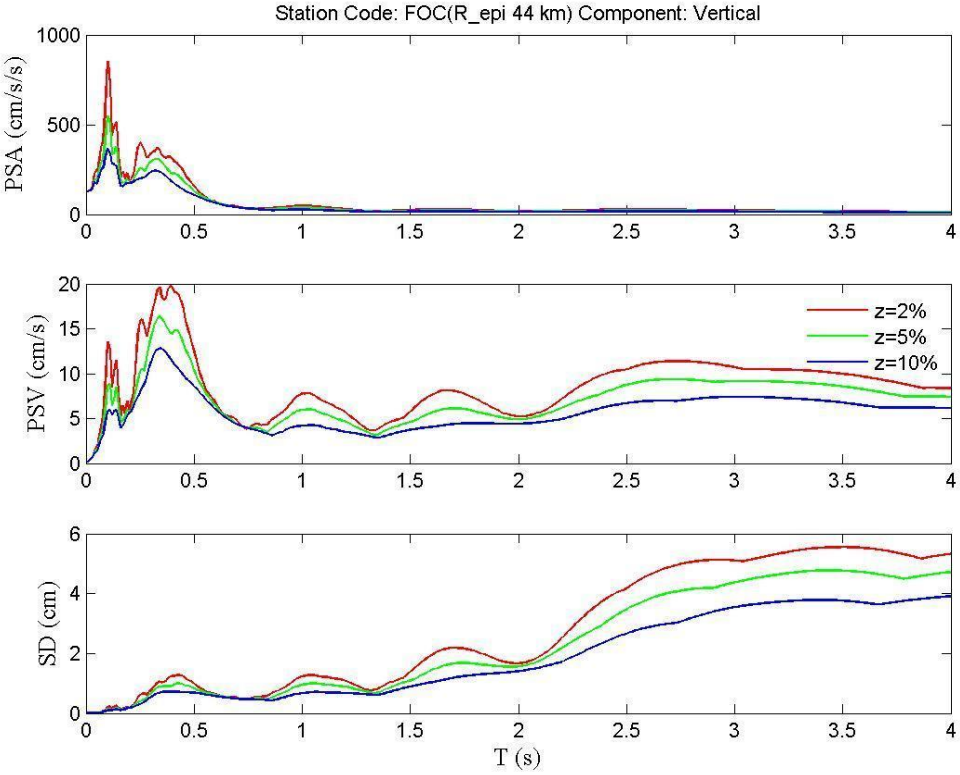
Station Code: FOC(R_epi 44 km) Component: Vertical
PSA (cm/s/s)
PSV (cm/s)
SD (cm)
z=2%
z=5%
z=10%
T (s)

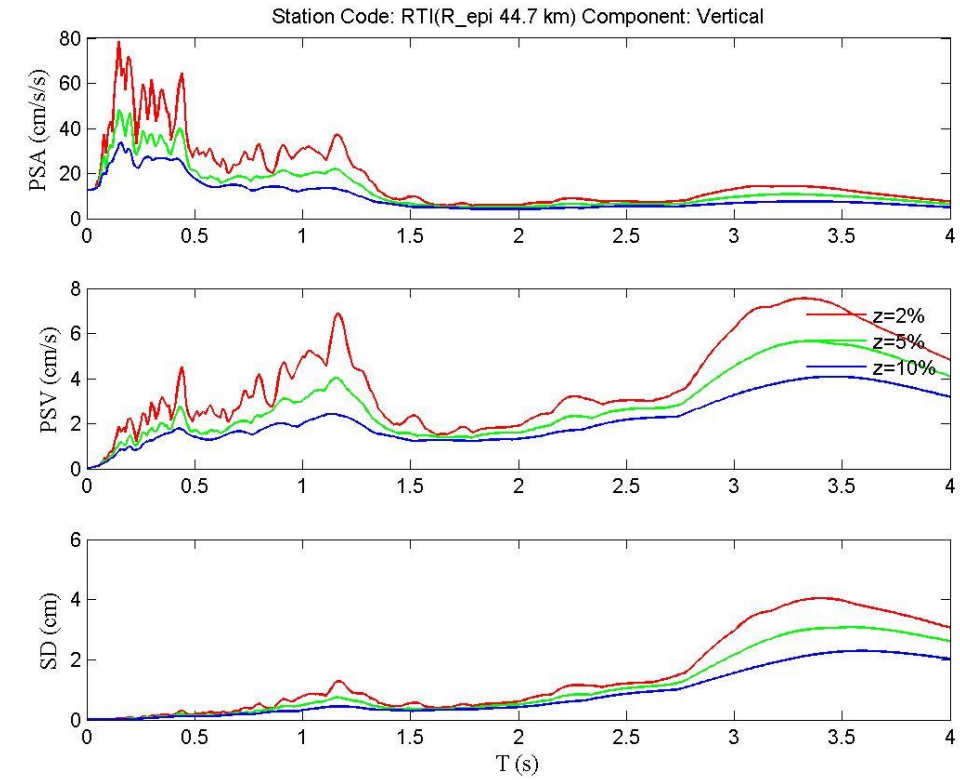
Station Code: RTI(R_epi 44.7 km) Component: Vertical
PSA (cm/s/s)
PSV (cm/s)
SD (cm)
z=2%
z=5%
z=10%
T (s)

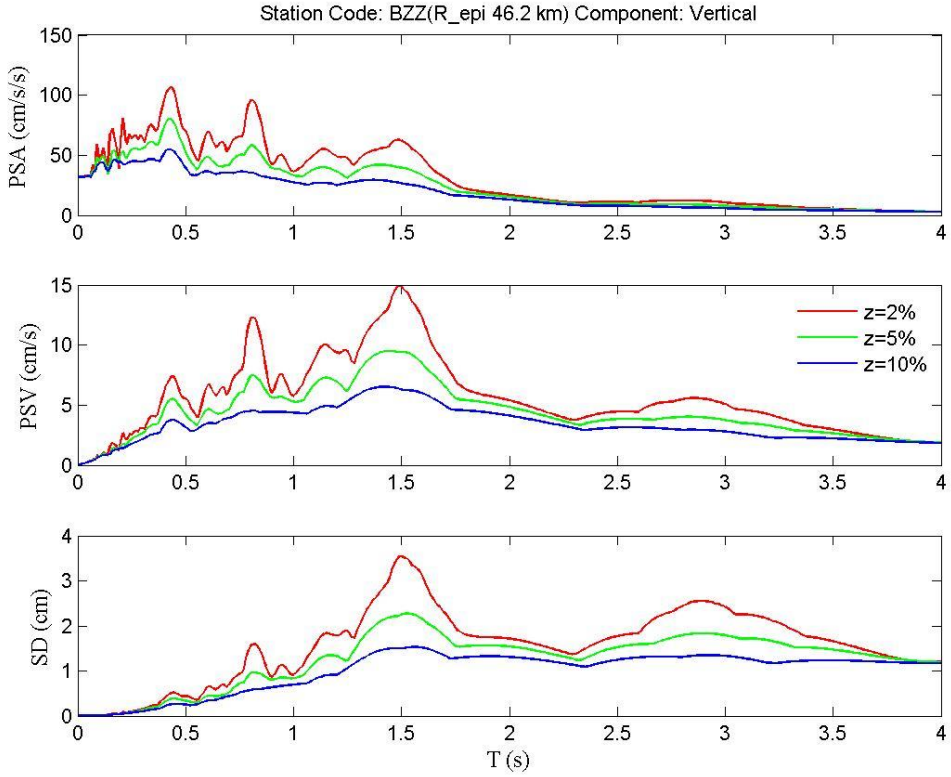
Station Code: BZZ(R_epi 46.2 km) Component: Vertical
PSA (cm/s/s)
PSV (cm/s)
SD (cm)
T (s)
z=2%
z=5%
z=10%

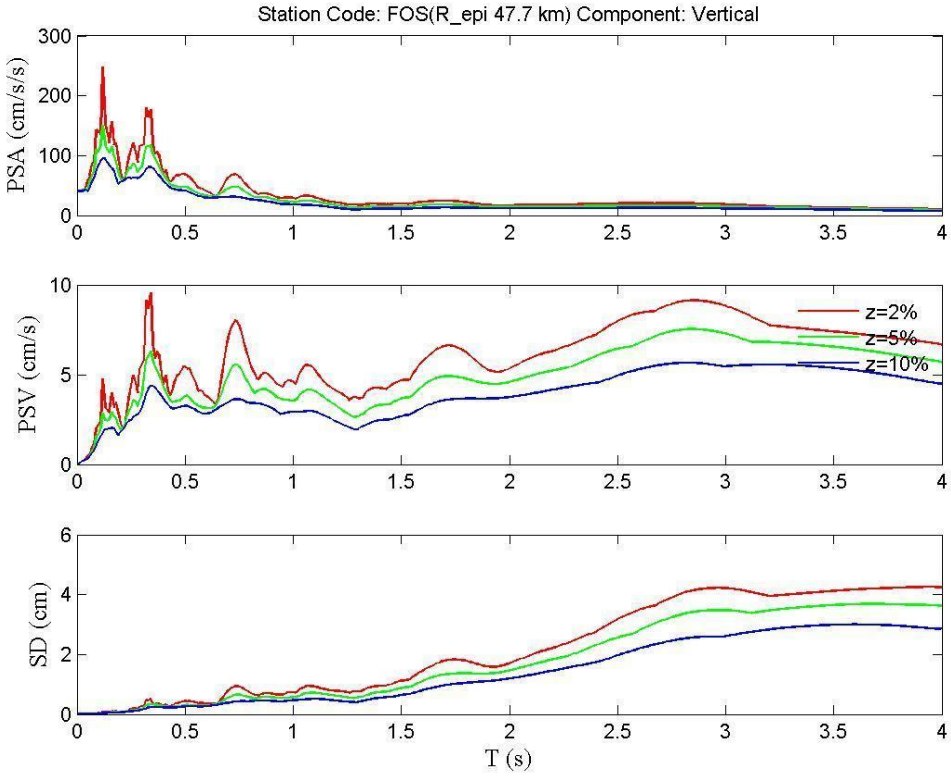
Station Code: FOS(R_epi 47.7 km) Component: Vertical
PSA (cm/s/s)
PSV (cm/s)
SD (cm)
T (s)
z=2%
z=5%
z=10%

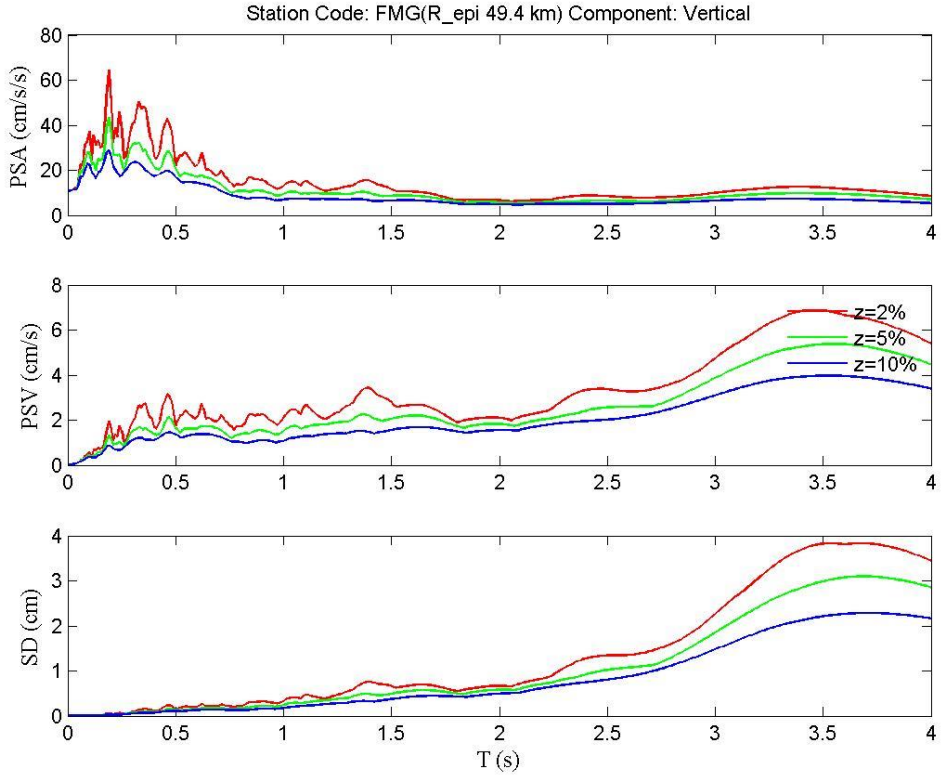
Station Code: FMG(R_epi 49.4 km) Component: Vertical
PSA (cm/s/s)
PSV (cm/s)
SD (cm)
z=2%
z=5%
z=10%
T (s)

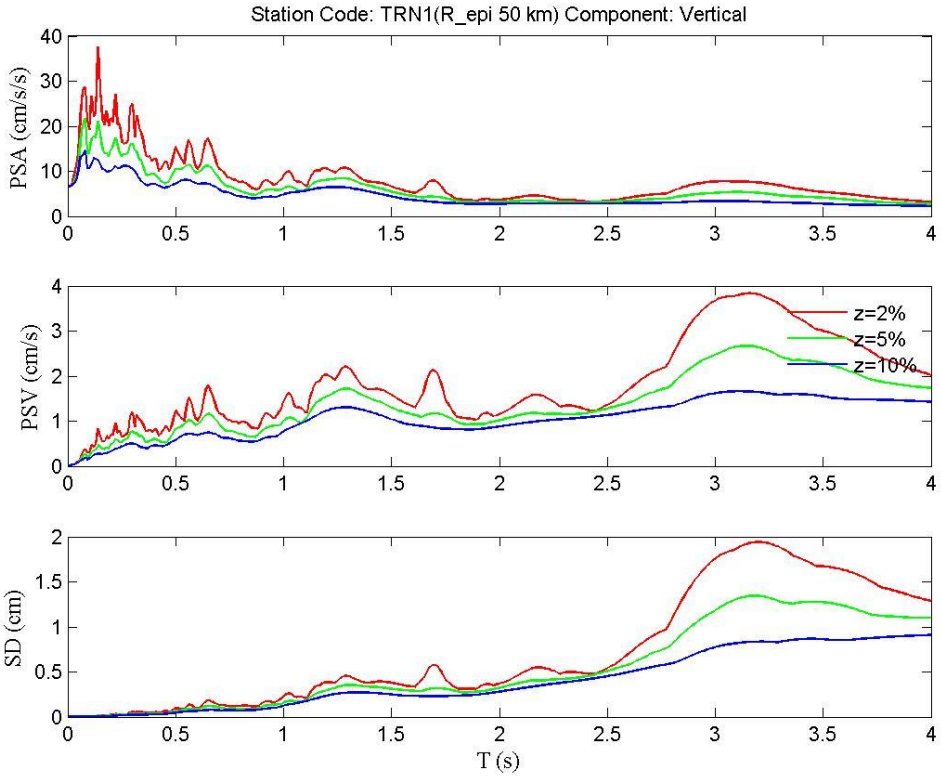
Station Code: TRN1(R_epi 50 km) Component: Vertical
PSA (cm/s/s)
PSV (cm/s)
SD (cm)
z=2%
z=5%
z=10%
T (s)

7. Comparison with the Italian seismic code

The pseudo-acceleration response spectra associated to the horizontal ground motions recorded by the four stations with lowest epicentral distance (AMT, NRC, RM33 and SPD) are compared with the elastic spectra provided by the Italian seismic code (NTC2008) at the corresponding sites for soil class provided in Appedix 1 and four different return periods (T_R): 50, 475, 975 and 2475 years. Note that comparison of individual earthquake recordings with probabilistic hazard is a delicate issue and no direct conclusions can be drawn to validate hazard (see Iervolino, 2013).

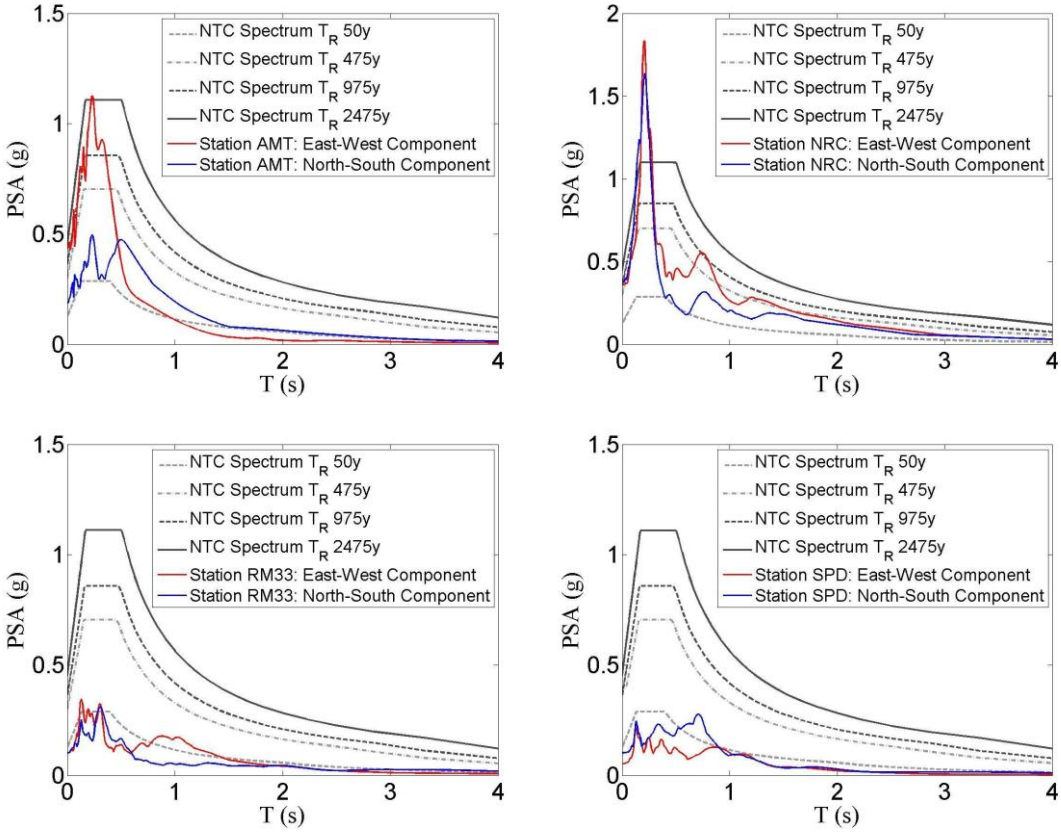

Figure 39. Comparison of the four closest-to-rupture stations' horizontal components PSA response spectra with the Italian code elastic response spectra at various return periods.

Referring to the geographical coordinates of the epicentre (42.70N; 13.24E), the hazard disaggregation (Iervolino et al., 2011) was computed for the PGA and for the pseudo-spectral acceleration at 1s vibration period, PSA(T=1s), for two T_R (475 and 2475 years) by means of REXEL v 3.5 (Iervolino et al., 2010), as shown in the following figures.

The disaggregations have a single modal value for both considered return periods. In the case of PGA and T_R=475 years, modal magnitude and distance are around 5.8 and 10 km, respectively. Increasing the return period to 2475 years, magnitude modal value increases to about 6.8 while the corresponding value of distance remains centred on 10 km. Similarly, for PSA(T=1s) and T_R=475 years, modal magnitude and distance are about 6.3 and 10 km, respectively. For T_R=2475 years, the magnitude of the mode increases to 6.8 while the distance remains equal to about 10 km. It is worth noting that, for a given return period, disaggregation of PSA(T=1s)

shows a non-negligible contribution of higher distances with respect to the case of the disaggregation of PGA. This is an expected result, see Iervolino et al. (2011), and is more evident for lower return periods. It may be concluded that, according to the hazard assessment of the area, exceedance of high-frequencies spectral accelerations corresponding to 475yr and 2475yr is most likely caused by a close moderate-magnitude earthquake, which is, in fact, compatible to what was observed.

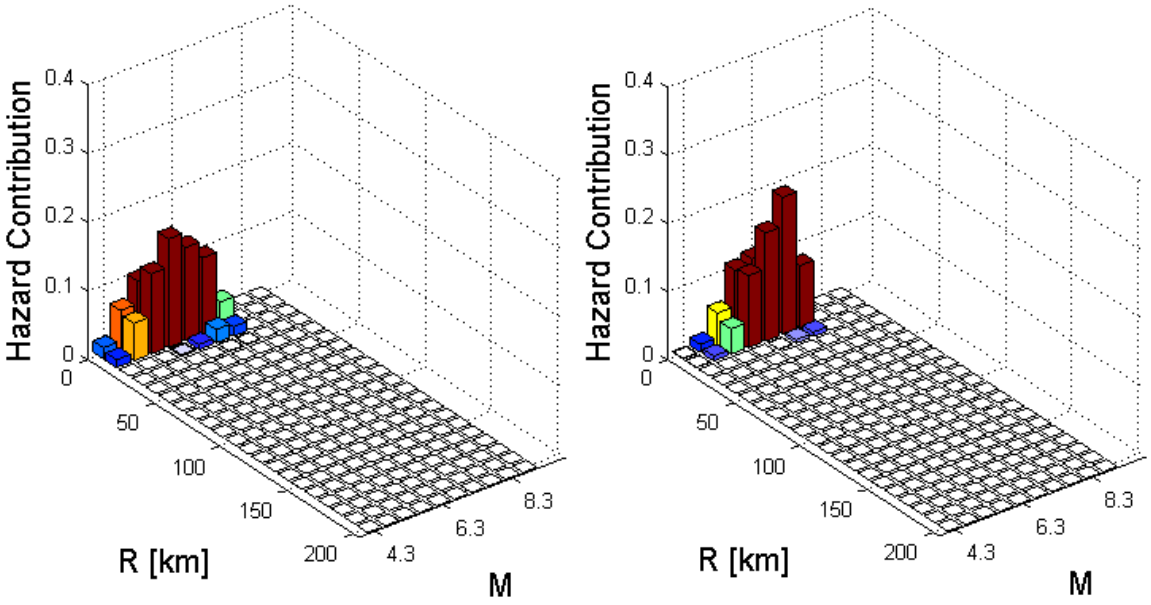

Figure 40. Disaggregation of PGA: T_R=475 years (sx) and 2475 years (dx)

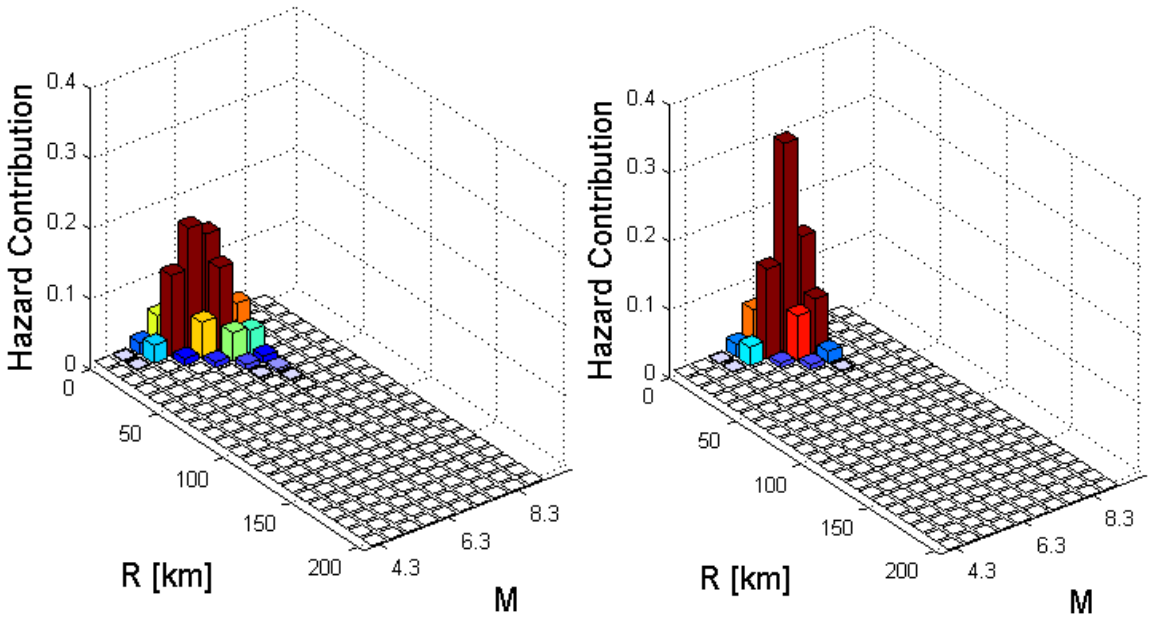

Figure 41. Disaggregation of PSA(T=1s): T_R=475 years (sx) and 2475 years (dx)

8. Pulse-like near-source ground motions

Pulse-like near-source ground motions may be the result of rupture directivity, a phenomenon that may lead seismic waves generated at different points along the rupture front to arrive at a near-source site simultaneously. This can lead to a constructive wave interference effect, which is manifested in the form of a double-sided velocity pulse that delivers most of the seismic energy early in the record (Somerville et al., 1997). Such impulsive behaviour of near-source ground motions has been probably found in Italian seismic events of normal faulting style before (e.g., L'Aquila 2009 M_w6.3 event – see Chioccarelli and Iervolino, 2010). In this preliminary investigation for such rupture directivity effects, the continuous wavelet transform algorithm suggested by Baker (2007) was implemented for all recordings (horizontal components) within an epicentral distance of 40km from the fault and for all orientations. The parameters of the preliminary finite-fault geometry used are available at http://esm.mi.ingv.it and for the time is being attributed to Tinti et al. (2016, personal communication by E.Tinti). The surface projection of the fault rupture plane is shown in Figure 42.

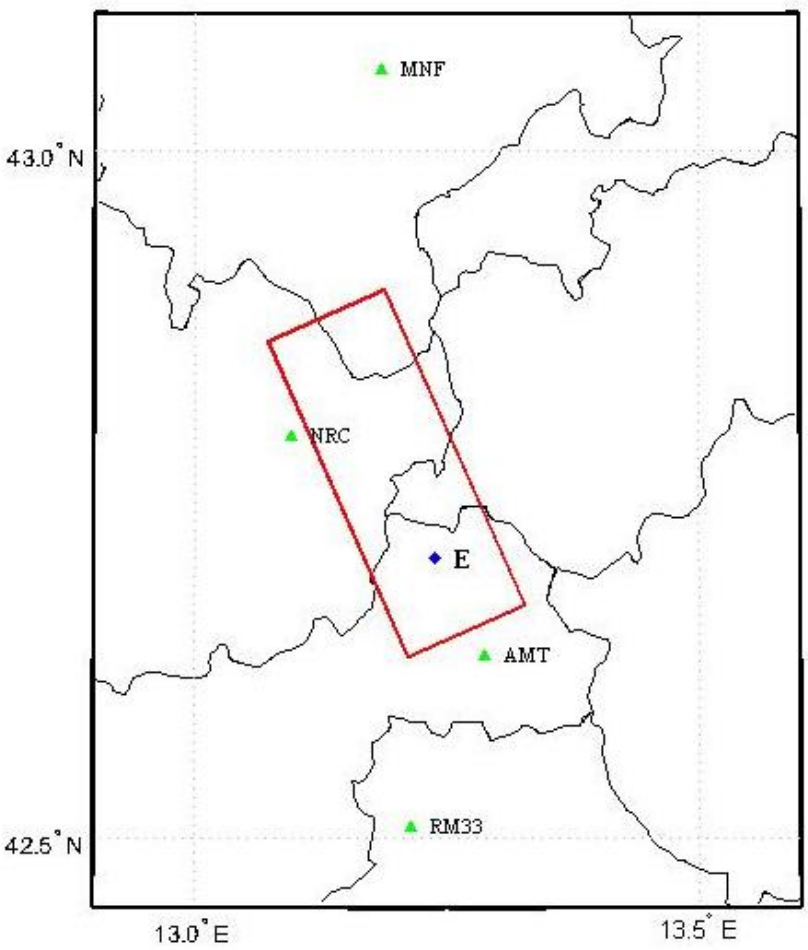

Figure 42. Surface projection of rupture plane; province borders and some NS stations shown on the map.

Out of all the main-shock records investigated, the four ground motions recorded at Amatrice (AMT), Norcia (NRC), Monterealle (RM33) and Fiastra (MNF) exhibited impulsive characteristics over a multitude of

orientations, as expressed by a Pulse Indicator (PI) score in excess of 0.85 (see Baker, 2007). The record at Amatrice revealed two distinct pulses, one being predominant in the fault-normal (FN) and the other longer pulse in the fault-parallel (FP) direction. The FN pulse has a pulse period T_p of 0.40s while the FP 0.98s. The Norcia record on the other hand was found to contain a 2.09s period pulse mostly towards orientations that lie between the FN and FP without being decidedly prevalent in any of the perpendicular/parallel directions to the strike. Note that some deviation of directivity pulses from the strictly FN orientation is not unheard of in dip-slip faulting. Finally, the ground motions recorded at the stations of Fiastra and Monterealle were found to contain pulses in the FN direction with T_p of 1.4s and 1.2s respectively, also hinting at rupture directivity effects, despite the lower velocity amplitude due to the greater distance from the fault and consequent attenuation.

In the Figures 43-47, a polar plot is presented for each station displaying the PI score per Azimuth as well as the velocity time histories at the most relevant directions (original signal, extracted pulse, residual signal).

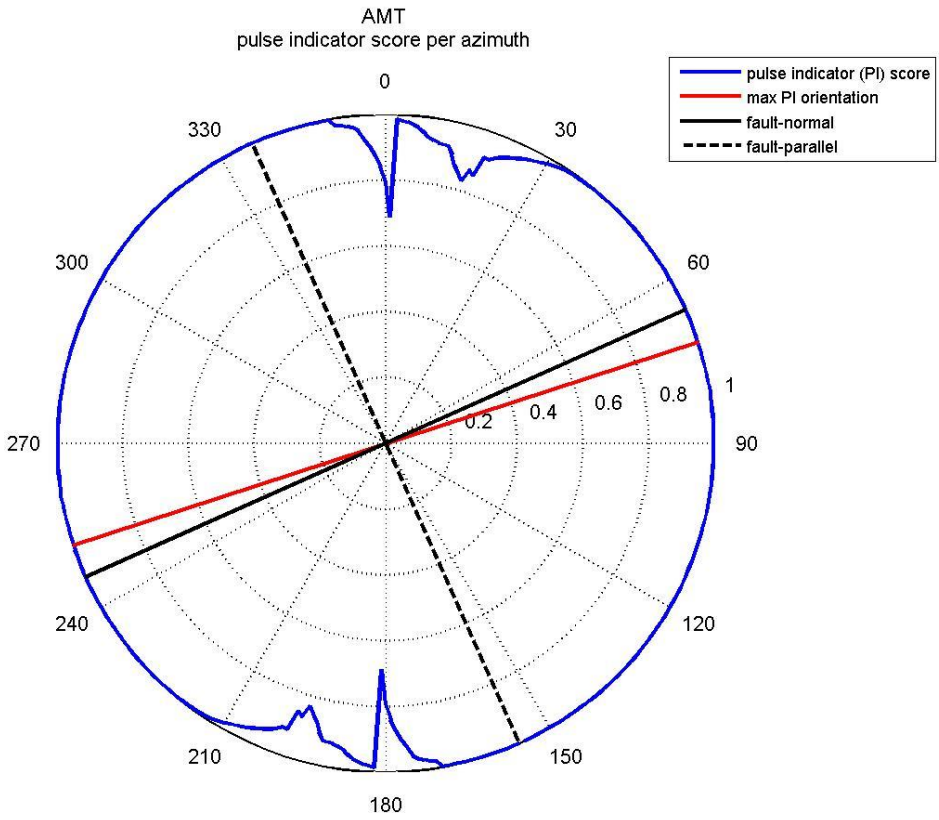

Figure 43. Polar plot of pulse indicator score per azimuth for the Amatrice record.

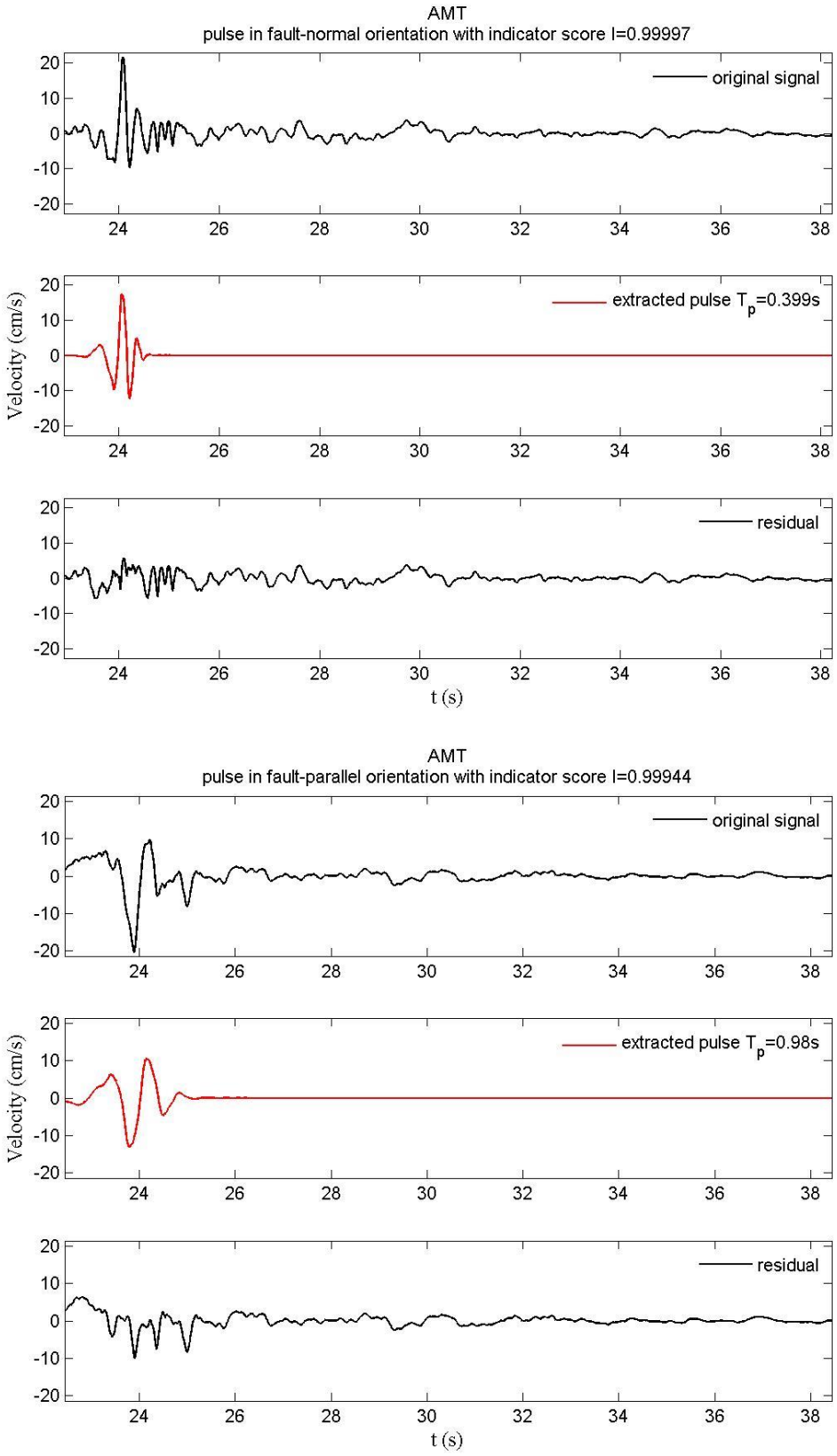

Figure 44. Original velocity time-history, CWT extracted pulse and residual signal for the fault-normal and fault-parallel components of the Amatrice record.

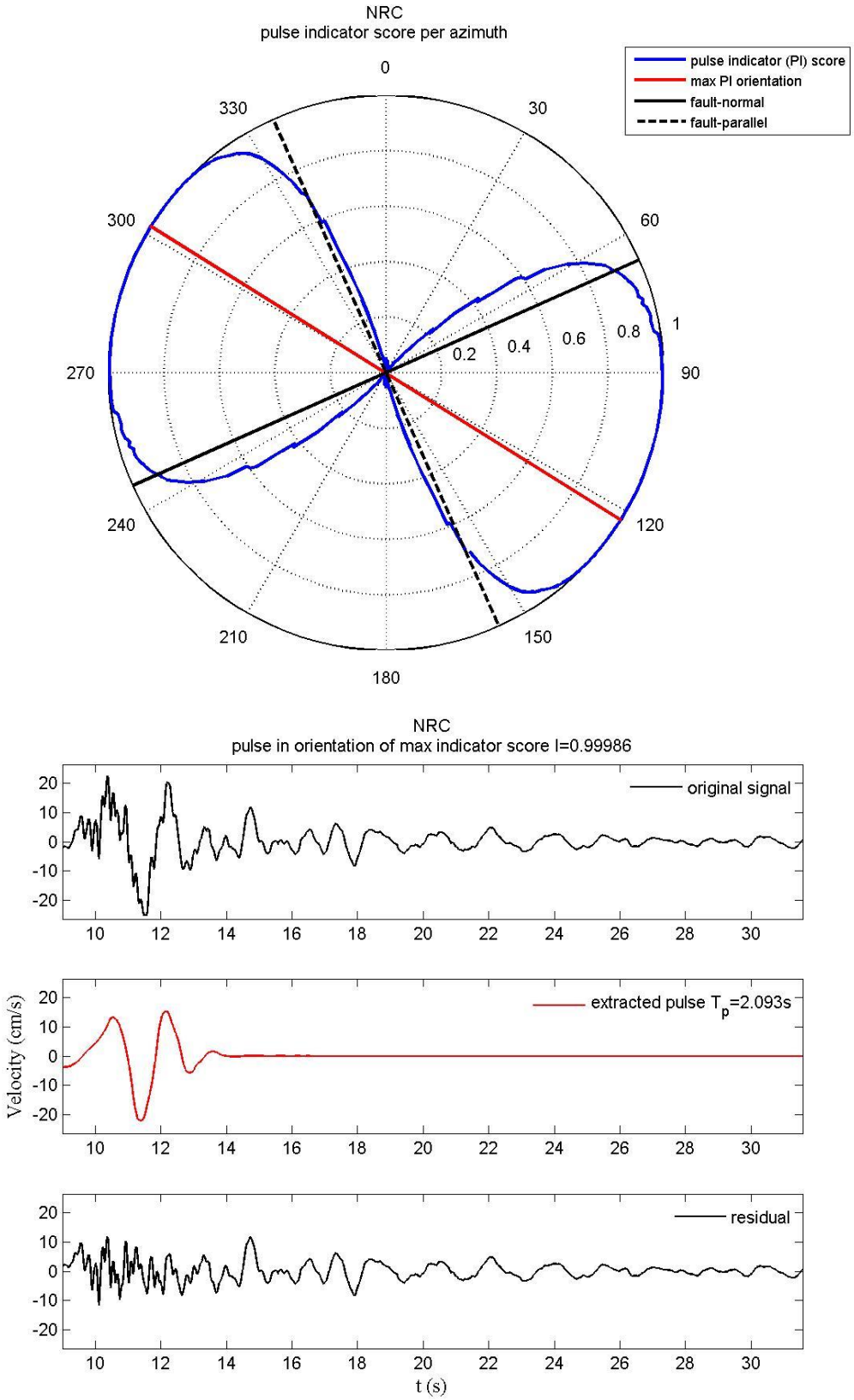

Figure 45. Polar plot of pulse indicator score per azimuth for the Norcia record, original velocity time-history, CWT extracted pulse and residual signal for the maximum PI component of the same record.

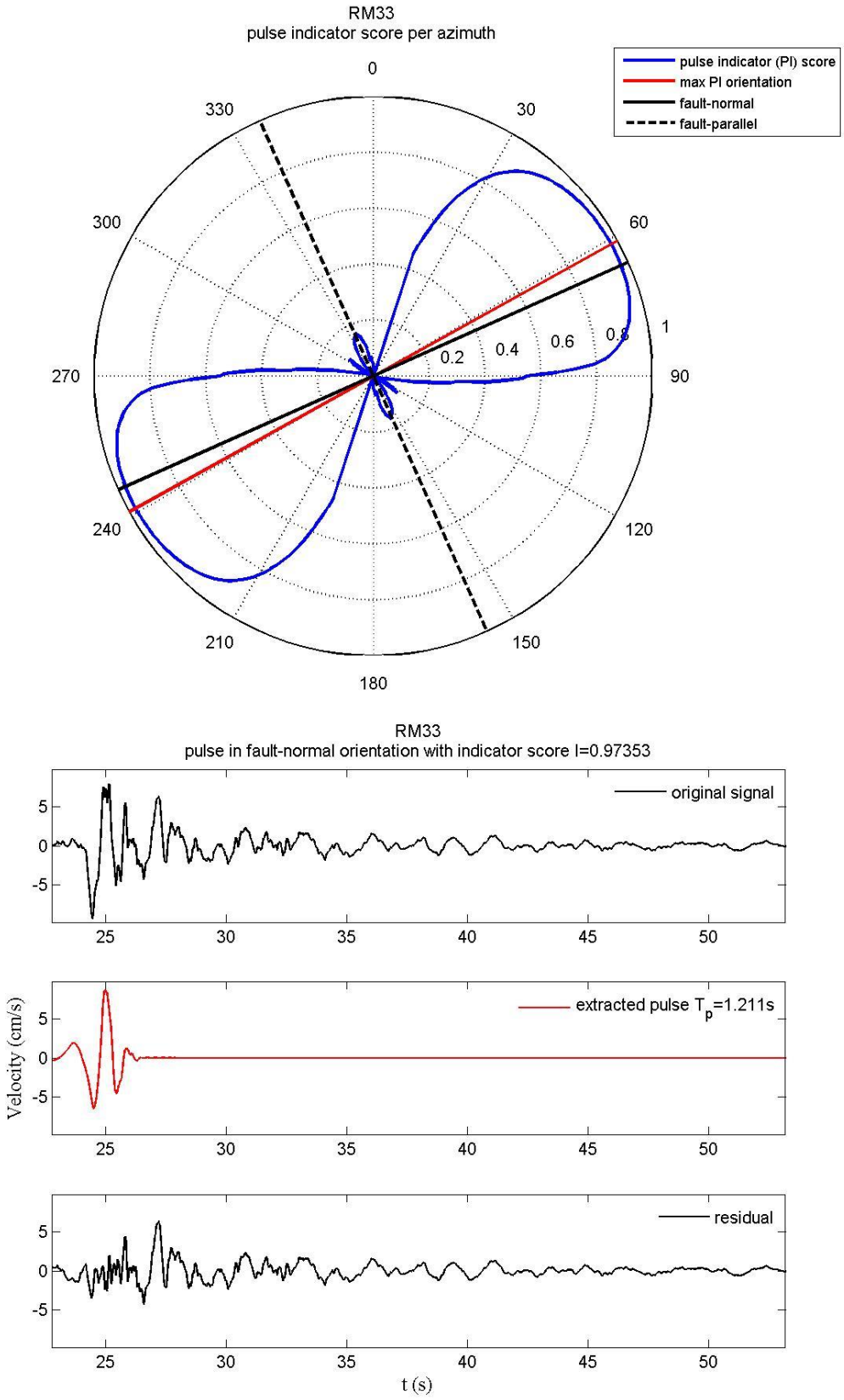

Figure 46. Polar plot of pulse indicator score per azimuth for the Fiastra record, original velocity time-history, CWT extracted pulse and residual signal for the fault-normal component of the same record.

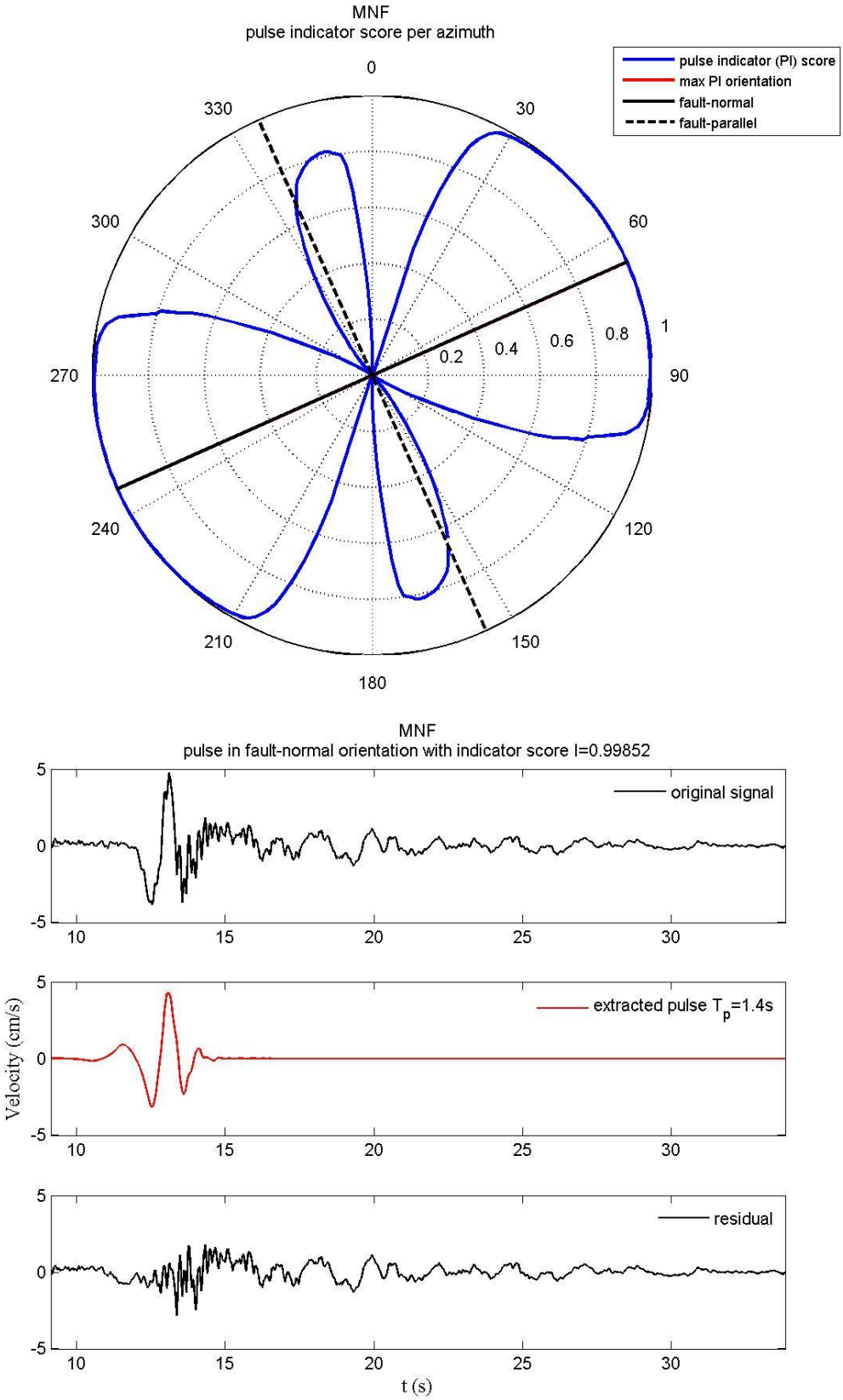

Figure 47. Polar plot of pulse indicator score per azimuth for the Montereale record, original velocity time-history, CWT extracted pulse and residual signal for the fault-normal component of the same record.

Finally, these findings are compared with existing empirical models for the probability of occurrence of an impulsive ground motion given rupture geometry (Iervolino and Cornell, 2008) and for pulse duration (Chioccarelli and Iervolino, 2010). The former is shown in Figure 47, while the latter corresponds to the regression model of Eq. (3) and is depicted in Figure 48.

$$\ln T_p = -6.19 + 1.07 \cdot M_w \ , \ \sigma_{\ln T_p} = 0.59 \tag{3}$$

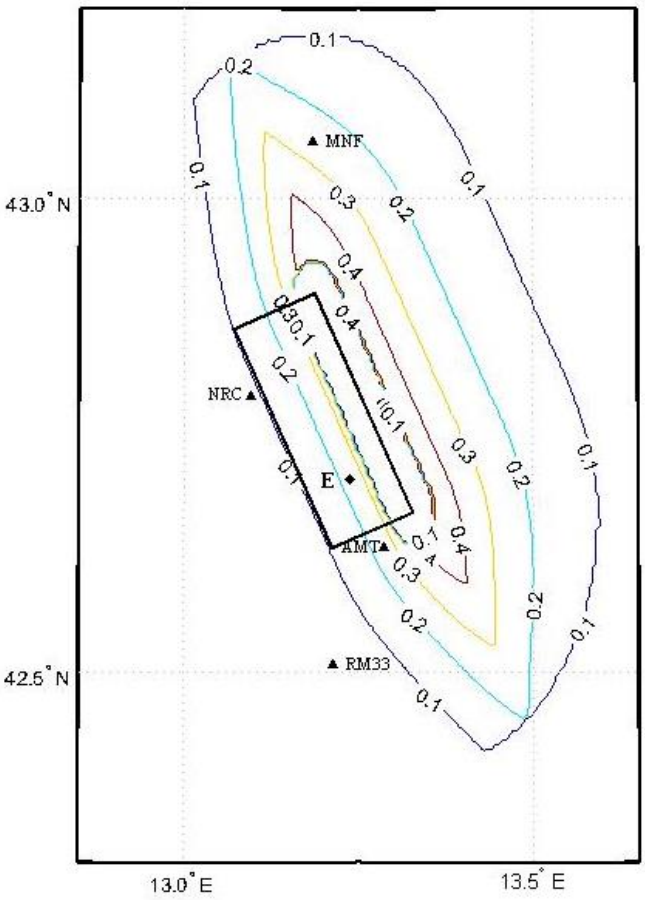

Figure 48. Equal probability of pulse occurrence contours according to the model of Iervolino and Cornell (2008), plotted against the surface projection of the rupture plane.

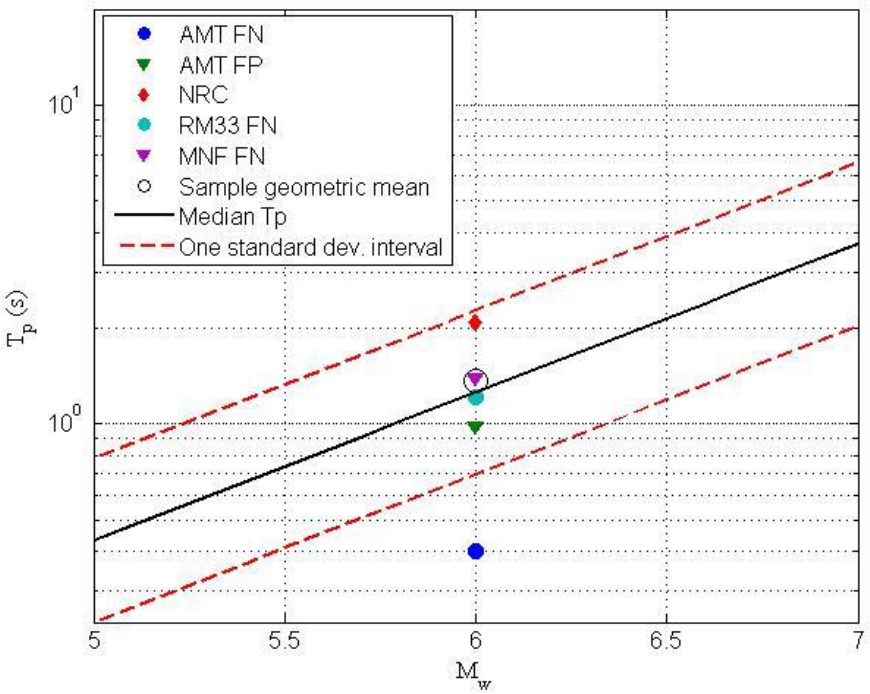

Figure 49. Extracted pulses' durations (periods T_p) shown against median prediction and $\pm\sigma$ interval (Chioccarelli and Iervolino, 2010 model).

Data and resources

Manually Processed and unprocessed strong-motion records
Engineering strong-motion database: http://esm.mi.ingv.ithttp://esm.mi.ingv.it/ http://esm.mi.ingv.it/
Automatically processed and raw strong-motion records
Rapid response Strong Motion database http://www.orfeus-eu.org/opencms/rrsm/http://www.orfeus-eu.org/opencms/rrsm/ http://www.orfeus-eu.org/opencms/rrsm/
Raw strong-motion records
European Integrated Data Archive http://www.orfeus-eu.org/data/eida/
Italian Department of Civil Protection: http://ran.protezionecivile.it/http://ran.protezionecivile.it/ http://ran.protezionecivile.it/
Shakemaps
Italy ShakeMaps http://shakemap.rm.ingv.it/http://shakemap.rm.ingv.it/ http://shakemap.rm.ingv.it/
Real time earthquake catalogue
ISIDe - Italian Seismological Instrumental and Parametric Database http://iside.rm.ingv.ithttp://iside.rm.ingv.it/ http://iside.rm.ingv.it/
Historical catalogue
Catalogo Parametrico dei Terremoti Italiani **http://emidius.mi.ingv.it/CPTI/**http://emidius.mi.ingv.it/CPTI/ http://emidius.mi.ingv.it/CPTI/
Macroseismic data
Database macrosismico Italiano http://emidius.mi.ingv.it/CPTI15-DBMI15/http://emidius.mi.ingv.it/CPTI15-DBMI15/

References

Baker J.W. (2007) Quantitative Classification of Near-Fault Ground Motions Using Wavelet Analysis. Bulletin of the Seismological Society of America, 97(5):1486–1501.

Bindi, D., F. Pacor, L. Luzi, R. Puglia, M. Massa, G. Ameri, and R. Paolucci (2011). Ground motion prediction equations derived from the Italian strong motion database, Bull. Earthq. Eng. 9, 1899–1920.

Chioccarelli E., Iervolino I. (2010). Near-Source Seismic Demand and Pulse-Like Records: a Discussion for L'Aquila Earthquake. Earthquake Engineering and Structural Dynamics. 39(9):1039–1062.

Iervolino I. (2013). Probabilities and fallacies: why hazard maps cannot be validated by individual earthquakes. Earthquake Spectra, 29(3): 1125–1136.

Iervolino I., Cornell C.A. (2008). Probability of occurrence of velocity pulses in near-source ground motions. Bulletin of the Seismological Society of America, 98(5): 2262-2277.

Iervolino I., Chioccarelli E., Convertito V. (2011). Engineering design earthquakes from multimodal hazard disaggregation, Soil Dynamics and Earthquake Engineering, 31, 1212-1231.

Iervolino I., Galasso C., Cosenza E. (2010). REXEL: computer aided record selection for code based seismic structural analysis, Bulletin of Earthquake Engineering, 8, 339-362.

Michelini, A., Faenza, L., Lauciani, V., & Malagnini, L. (2008). ShakeMap implementation in Italy. Seismological Research Letters, 79(5), 689–698. http://doi.org/10.1785/gssrl.79.5.689

Paolucci, R., F. Pacor, R. Puglia, G. Ameri, C. Cauzzi, and M. Massa (2011). Record processing in ITACA, the new Italian strong motion database, in Earthquake Data in Engineering Seismology, Geotech- nical, Geological and Earthquake Engineering Series, S. Akkar, P. Gulkan, and T. Van Eck (Editors), Vol. 14(8), 99–113.

Somerville P.G., Smith N.F., Graves R.W., Abrahamson N.A. (1997) Modification of empirical strong ground motion attenuation relations to include the amplitude and duration effects of rupture directivity. Seismological Research Letters, 68:199–222.

Appendix 1

Stations highlighted in gray are not used in the analysis; asterisk following EC8 site classification indicates that the classification is based on inferred, rather than measured, $V_{s,30}$.

Net code	Station code	EC8 class.	Station latitude	Station longitude
BA	PZUN	B*	40.6458	15.807
FR	SMPL	A*	42.094	9.285
IT	0CAN		43.4723	12.6308
IT	AMT	B*	42.63246	13.28618
IT	ANB	B*	43.59229	13.50741
IT	ANT	A*	42.41811	13.0786
IT	AQF	B*	42.38054	13.35474
IT	AQK	B	42.34497	13.40095
IT	AQV	B	42.37722	13.34389
IT	ASP	C*	42.848	13.6479
IT	ATN	A*	41.62032	13.80115
IT	AVL	C*	40.92283	14.78704
IT	AVZ	C	42.02746	13.42593
IT	BCN	C*	40.63435	15.38238
IT	BGR	B*	43.88951	11.99129
IT	BNE	C*	41.12756	14.78488
IT	BRS	A*	42.32427	13.59007
IT	BSS	B*	42.19173	13.84527
IT	BTT2	D	41.99833	13.54306
IT	BVG	C	42.93237	12.61107
IT	BZZ	B	42.33703	13.46858
IT	CCT	C*	43.3683	12.2346
IT	CER	B*	41.2595	15.9102
IT	CLF	D	43.03671	12.92043
IT	CLN	B*	42.08522	13.52072
IT	CMB	B*	41.5628	14.6523
IT	CME	A*	43.9543	10.3012
IT	CPS	B	42.27162	13.7583
IT	CRP	C*	44.7823	10.8703
IT	CSA	C*	43.00802	12.5906
IT	CSD	B	42.75405	12.00354
IT	CSN	B	44.13701	12.24141
IT	CSO1	B*	42.10093	13.08804
IT	CSS	B	41.48579	13.82309
IT	CTD	B*	42.38837	12.9477
IT	CTS	C*	43.49199	12.2234
IT	CVM	A*	42.99409	11.28231
IT	DUR	B*	41.6611	14.4565
IT	FAZ	C	44.29802	11.89075
IT	FBR	C*	43.3436	12.9119
IT	FIE	B*	43.80725	11.29439
IT	FMG	A*	42.26803	13.11722

IT	FOC	C*	43.0263	12.89651
IT	FOS	B*	43.01459	12.83513
IT	FRT		41.6926	13.255
IT	FSS	C*	43.69048	12.81007
IT	GBB	B*	43.35697	12.59725
IT	GBP	C	43.31381	12.58949
IT	GNU	A*	42.80382	12.57015
IT	GRN	A*	41.81346	13.31699
IT	GSA	B	42.42069	13.51936
IT	LSS	A	42.55824	12.96889
IT	MCR	C*	43.79989	12.44751
IT	MCS	B*	43.99437	12.10744
IT	MLF	B	40.9944	15.6527
IT	MMP1	B*	42.24923	12.74832
IT	MNF	A*	43.05968	13.18447
IT	MNG	A*	41.70354	15.95803
IT	MNT	A*	43.1397	11.18279
IT	MTL	B	43.24944	13.00834
IT	NAP	C*	40.79926	14.17961
IT	NCR	E	43.11158	12.78467
IT	NRC	B	42.79254	13.09648
IT	NRN	A*	42.51556	12.51944
IT	ORP	B	41.27923	15.26506
IT	PAN	B*	43.00581	12.14362
IT	PGG	B*	42.32287	13.53945
IT	PNC	B*	42.84745	11.6936
IT	PNN	C	43.81816	12.26285
IT	PSC	A	41.81204	13.7892
IT	PTI	B*	43.06657	13.65708
IT	PTL	B*	43.42733	12.4486
IT	PVF	B*	44.3331	10.82523
IT	PZI1	B*	42.4356	13.3262
IT	RDG	A*	41.9264	15.8792
IT	RQT	B*	42.81309	13.31103
IT	RTI	D	42.43028	12.8291
IT	SAG	A*	40.93156	15.18763
IT	SBC	A	41.91316	13.10552
IT	SCF	B*	42.26512	13.99849
IT	SDM	A*	42.28971	13.55765
IT	SGMA	B*	41.6845	14.9644
IT	SGPA	B	41.6876	14.9629
IT	SGPA	B	41.6876	14.9629
IT	SGSC	B*	41.6892	14.9581
IT	SGSC	B*	41.6892	14.9581
IT	SIG	C*	43.3308	12.7408
IT	SNG	C	43.68558	13.22616
IT	SNI	B*	42.632	12.5536
IT	SNM	B*	43.93433	12.44929
IT	SNS1	C*	43.5735	12.1312
IT	SOR		41.7203	13.6136
IT	SPD	B*	42.51514	13.37104
IT	SPM	A*	42.72324	12.75127
IT	SPO1		42.7344	12.7363
IT	SSC	E	42.87473	11.87679
IT	SSG	B*	43.56986	12.14632
IT	SSO		43.5715	12.154

IT	STF	B*	43.90811	11.79446
IT	SUL	A*	42.089	13.934
IT	SULA	C*	42.0734	13.9166
IT	SULC	C*	42.068	13.909
IT	SULP	B*	42.085	13.9274
IT	TLN	B*	43.2159	13.25838
IT	TOD	A*	42.73817	12.38728
IT	TRE	C*	42.8765	12.7358
IT	TRL	A*	42.46131	12.93231
IT	TRN1	D*	42.5582	12.6461
IT	TRV	B*	41.78294	14.55071
IT	TSC	A*	42.42261	11.8696
IT	TVL	B*	41.89302	12.77322
IT	UMB	B*	43.25444	12.2556
IT	VAL	B*	43.1593	12.6017
IT	VLL	B*	41.67047	12.77267
IT	VLN	C*	43.14273	11.89472
IT	VNF1	C*	41.4805	14.0501
IT	VSE	B*	42.12218	14.70719
IV	ACER	B*	40.7867	15.9427
IV	APEC	B*	43.55846	12.41991
IV	APRC		41.75738	15.54308
IV	ASOL	A*	45.8003	11.9023
IV	ATCC	B*	43.18514	12.63994
IV	ATFO	B*	43.3666	12.5715
IV	ATLO	B*	43.3152	12.4073
IV	ATPC	B*	43.4807	12.457
IV	ATTE	A*	43.1979	12.3536
IV	ATVO	B*	43.38211	12.40663
IV	BDI	B*	44.0624	10.597
IV	BIOG	B*	41.1999	15.13263
IV	BOB	B*	44.7679	9.4478
IV	BRIS	B*	44.2245	11.7666
IV	BSSO	A*	41.5461	14.5938
IV	CADA	B*	43.1942	13.7614
IV	CAFE	A*	41.028	15.2366
IV	CDCA	C*	43.4584	12.2336
IV	CERA	A*	41.5978	14.0183
IV	CIMA	B*	43.3053	13.67009
IV	CMPO	C*	44.5808	11.8056
IV	COR1	B*	43.6318	13.0003
IV	CPGN	B*	43.8011	12.3205
IV	CRMI	B*	43.7956	10.9795
IV	CRND	C*	45.8361	12.0131
IV	CTL8	C*	45.2755	9.7621
IV	FAEN	C*	44.2895	11.877
IV	FERS	C	44.9035	11.5406
IV	FIU1	B*	43.18856	12.9316
IV	FOSV	B*	43.29483	12.76117
IV	FRE8	A*	46.015	12.3552
IV	GAG1	B*	43.2381	13.0674
IV	GATE	B*	41.51315	14.9102
IV	GUMA	B*	43.0627	13.3352
IV	IMOL	C*	44.35955	11.74248
IV	LEOD	C*	45.4582	10.1234
IV	MCEL	A*	40.3249	15.8019

IV	MDAR	B*	43.1927	13.1427
IV	MELA	A*	41.7059	15.127
IV	MGAB	A*	42.91263	12.11214
IV	MGR	B*	40.1376	15.5535
IV	MNTV	C*	45.1495	10.7897
IV	MOCO	B*	41.37	15.158
IV	MODE	C*	44.6297	10.9492
IV	MRB1	B*	41.1227	14.96815
IV	MRLC	B*	40.7564	15.48892
IV	MSAG	A*	41.712	15.9096
IV	MTRZ	B*	44.3128	11.4248
IV	MURB	B*	43.263	12.5246
IV	NDIM	C*	44.8873	10.8987
IV	NEVI	B*	44.5834	10.3163
IV	NRCA	B*	42.83355	13.11427
IV	OPPE	C*	45.3082	11.1724
IV	ORZI	C*	45.4056	9.9307
IV	OSSC	B*	43.5236	11.2458
IV	PAOL	A*	41.03121	14.56749
IV	PCRO	B*	43.6077	13.5323
IV	PIEI	A*	43.53567	12.535
IV	PIGN	A*	41.2	14.17989
IV	POFI	A*	41.71743	13.71202
IV	PP3	C*	43.3778	13.6095
IV	PTRJ	A*	41.3641	14.529
IV	RM33	B*	42.509	13.2145
IV	RNI2	A*	41.70328	14.1524
IV	ROM9	B*	41.82842	12.51553
IV	ROVR	A*	45.6468	11.0721
IV	SACS	B*	42.84906	11.90967
IV	SALO	A*	45.6183	10.5243
IV	SANR	C*	45.64	11.6099
IV	SBPO	C*	45.0511	10.9199
IV	SERM	C*	45.01	11.2958
IV	SGG	A*	41.38667	14.37917
IV	SGTA	B*	41.135	15.365
IV	SIRI	B*	40.1821	15.8675
IV	SNAL	A*	40.9254	15.2091
IV	SNTG	A*	43.255	12.9406
IV	SSFR	A*	43.4363	12.7822
IV	SSM1	B*	43.22878	13.17696
IV	STAL	B*	46.2601	12.7104
IV	TERO	B*	42.62279	13.60393
IV	TRE1	B*	43.3112	13.31285
IV	TREG	C*	45.523	11.1606
IV	TRIV	B*	41.7666	14.5502
IV	VAGA	A*	41.4154	14.2342
IV	VENL	D*	45.4167	12.3765
IV	VITU	A*	41.18326	14.63015
IV	VOBA	C*	45.6429	10.504
IV	VULT	B*	40.9549	15.6163
IV	ZCCA	B*	44.35085	10.9765
IV	ZEN8	A*	45.6378	10.7319
IV	ZOVE	B*	45.4536	11.4876
MN	AQU	B*	42.35388	13.40193
MN	BLY		44.7488	17.1839

MN	CUC	A*	39.9938	15.8155
MN	VLC	A*	44.1594	10.3864
OX	ACOM		46.548	13.5137
OX	AGOR		46.2329	12.0472
OX	CGRP		45.8806	11.8047
OX	CIMO		46.3116	12.4448
OX	CLUD		46.4569	12.8814
OX	MPRI		46.2408	12.9877
OX	SABO	B*	45.9875	13.6336
OX	VARN		45.9922	12.1051
OX	ZOU2		46.5584	12.9729
ST	DOSS		45.8808	11.1884
ST	VARA	A*	45.826	10.8965